Earth-Science Reviews 275 (2026) 105411

Contents lists available at ScienceDirect

Earth-Science Reviews

journal homepage: www.elsevier.com/locate/earscirev

Innovations in underground hydrogen storage with multiphysics simulations, optimization, and monitoring: A review

Yue Zhang [a,b], Zhenxue Dai [a,b,c,*], Hung Vo Thanh [d,e], Mingxu Cao [a,b], Lulu Xu [a,b], Xiaoying Zhang [a], Bicheng Yan [f], Philip H. Stauffer [g], Huichao Yin [h], Kenneth C. Carroll [h], Mohamad Reza Soltanian [i]

[a] State Key Laboratory of Deep Earth Exploration and Imaging, College of Construction Engineering, Jilin University, Changchun 130026, China
[b] Institute of Intelligent Simulation and Early Warning for Subsurface Environment, Jilin University, Changchun 130026, China
[c] School of Environmental and Municipal Engineering, Qingdao University of Technology, Qingdao 266033, China
[d] Faculty of Science and Engineering, Waseda Research Institute for Science and Engineering, Waseda University, 3-4-1 Okubo, Shinjuku-ku, Tokyo 169-8555, Japan
[e] Faculty of Science and Engineering, School of Creative Science and Engineering, Waseda University, 3-4-1 Okubo, Shinjuku-ku, Tokyo 169-8555, Japan
[f] Physical Sciences and Engineering Division, King Abdullah University of Science and Technology, 23955-6900 Thuwal, Saudi Arabia
[g] Los Alamos National Laboratory, Los Alamos, NM, USA
[h] Plant & Environmental Sciences Department, New Mexico State University, Las Cruces, NM, USA
[i] Departments of Geosciences and Environmental Engineering, University of Cincinnati, Cincinnati, OH 45220, USA

ARTICLE INFO

Keywords:
Underground Hydrogen Storage (UHS)
Geomechanics
Multiphysics-coupled numerical simulation
Machine learning
Multi-objective optimization (MOO)

ABSTRACT

Underground Hydrogen Storage (UHS) is a promising solution for large-scale energy storage and a critical component in advancing low-carbon energy system. Ensuring the safety and efficiency of UHS necessitates a comprehensive understanding of multiphysical interactions driven by cyclic pore fluid pressure fluctuations and coupled physicochemical processes. This review examines the key geomechanical responses in UHS, including rock property variations under cyclic loading, fracture evolution and propagation, reservoir stress sensitivity, and fault stability. It also explores the impact of geochemical and microbial reactions on geomechanical characteristics. We provide an in-depth analysis of Thermal-Hydraulic-Mechanical-Chemical (THMC) coupled numerical simulations, highlighting their potential for future multi-scale modeling. Limitations of current machine learning (ML) approaches in addressing UHS challenges are highlighted, emphasizing the need for innovative ML-based methodologies. Operational strategies for hydrogen injection and production are reviewed, focusing on safety, efficiency, and economic viability. The necessity for multi-objective optimization (MOO) to balance storage efficiency, risk mitigation, and cost-effectiveness is also discussed. Current monitoring technologies are evaluated to ensure safe and efficient UHS operations. Finally, this review identifies critical knowledge gaps and underscores the importance of advancing geomechanical understanding under multiphysics-coupling. We highlight the need for ML-driven multiphysics theories, enhanced modeling techniques, and robust optimization strategies to improve UHS performance. This study serves as a comprehensive reference for future research and the large-scale implementation of UHS systems.

Contents

* Corresponding author at: College of Construction Engineering, Jilin University, State Key Laboratory of Deep Earth Exploration and Imaging, Changchun 130026, China.
E-mail address: dzx@jlu.edu.cn (Z. Dai).

https://doi.org/10.1016/j.earscirev.2026.105411
Received 4 April 2025; Received in revised form 22 January 2026; Accepted 26 January 2026
Available online 28 January 2026

1. Introduction

The rapid growth of population and industrialization have significantly increased fossil fuel consumption, exacerbating global climate challenges (Zhang et al., 2020; Lee et al., 2023). Atmospheric carbon dioxide (CO_2) concentration reached 420 ppm by January 2024 (51% above pre-industrial levels) (WMO, 2024). Global surface temperatures reached 1.54 °C above pre-industrial levels by September 2024, capping the warmest decade (2014–2024) in recorded history (Kennedy et al., 2024). In response to climate change, energy strategies such as development of renewable energy sources, and the exploration of alternative energy carriers have been emphasized by many major energy consumers (Du et al., 2024). Renewable energy sources such as hydrogen based energy, solar and wind are gradually replacing traditional fossil fuels and are expected to reach 45% by 2050 (İlkiliç and Türkbay, 2010). with hydrogen emerging as a versatile energy carrier due to its high energy density (142 MJ/kg) and carbon-free combustion. As a key enabler for decarbonization and grid-scale energy storage, hydrogen is projected to dominate the global energy landscape by 2150 (Sun et al., 2025).

As the share of hydrogen energy in renewable energy increases, renewable sources provide a new pathway for hydrogen production. While renewable-powered hydrogen production can utilize surplus energy, its intermittent nature complicates storage coordination. Meanwhile, global natural hydrogen reserves could theoretically meet energy demands for millennia, but their exploitation requires parallel storage innovations (Hand, 2023). Gaseous, liquid and solid-state hydrogen storage methods have limitations (Han et al., 2020). For example, gaseous hydrogen storage requires high-pressure tanks (Miocic et al., 2022), liquid hydrogen storage requires extremely low temperatures (Zhao et al., 2019), and solid-state hydrogen storage relies on specific materials (*e.g.,* metal hydrides) (Singh et al., 2020). The immaturity of these technologies, together with their limited storage capacity and reduced safety, limits the large-scale application and use of hydrogen (Panfilov, 2016). To overcome these limitations, UHS is the optimal solution for large-scale hydrogen storage and utilization to meet seasonal energy demand (Heinemann et al., 2021a). It offers advantages such as low cost and high safety (Tarkowski, 2019), with capacities ranging from millions to hundreds of millions of cubic meters (Cai et al., 2022), UHS systems are geographically widespread, enabling decentralized storage (Aftab et al., 2022). Countries such as the United States and the United Kingdom have implemented underground hydrogen storage projects, integrating local solar photovoltaics and other low carbon energy facilities to achieve zero or low-carbon emissions (Fig. 1) (Heinemann et al., 2018; Schöpping and Rossen, 2019; Scafidi et al., 2021).

UHS in porous media faces critical challenges from hydrogen's low density, high reactivity, and reservoir heterogeneity (Kabuth et al., 2016; Jahanbakhsh et al., 2024). These factors complicate the balance between safety and economics, particularly in terms of geomechanical stability and microbial interactions. Current studies focus on three length scales: (1) pore-scale interfacial phenomena (Braid et al., 2024), (2) site-scale caprock integrity (Silverii et al., 2021; Bai and Tahmasebi, 2022; Wen et al., 2024a), and (3) reservoir-scale storage efficiency (Aftab et al., 2022). However, four interdependent barriers hinder progress. Efficient THMC multiscale numerical simulation is a key challenge, pore-scale models frequently neglect site-scale geomechanical feedback, while reservoir-scale analyses oversimplify microscale fluid-rock interactions. This disconnect leads to an

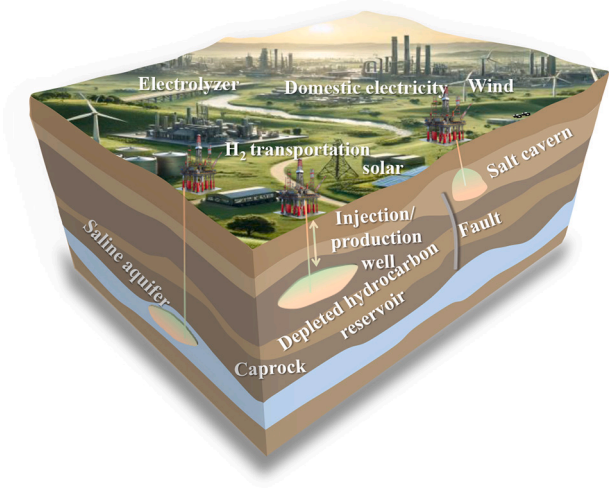

Fig. 1. Schematic of UHS integrated with low-carbon energy sources. Figure modified from (Mao et al., 2024).

overemphasis on economic strategies at the expense of geomechanical safety assessments. Second, the coupled THMC processes governing hydrogen migration and trapping remain poorly quantified, largely due to insufficient experimental data for calibrating constitutive models under *in situ* conditions. Third, existing numerical frameworks often overlook the design of UHS monitoring networks. Finally, reliance on costly and time-consuming laboratory experiments limits the exploration of operational parameter spaces (*e.g.,* injection rates, cushion gas ratios), resulting in sluggish advancements in optimizing storage efficiency under multiple objectives (Yang et al., 2024a). These interconnected gaps escalate UHS development costs and risks, underscoring the urgency of adopting machine learning-driven multiscale frameworks to unify THMC-coupled simulations and monitoring network design.

Computer-Aided Engineering (CAE) tools address multiscale UHS challenges, such as seepage mechanics, microbial-geochemical interactions, and geomechanical deformation (Malki et al., 2024). They can integrate fundamental physics, molecular dynamics (MD), and pore-scale analysis to simulate hydrogen migration and stability. For, example, Fundamental physical laws (*e.g.,* Darcy's law, thermodynamic principles) and elastoplastic constitutive models are integrated into CAE frameworks to simulate hydrogen migration and reservoir-caprock-fault stability (Ramesh Kumar et al., 2023). MD simulations quantify hydrogen diffusion coefficients and interfacial tension dependencies on temperature/pressure/cushion gas type/salinity (Zhang et al., 2023a; Doan et al., 2024; Kalati et al., 2024), while pore-scale models resolve microscale fluid dynamics (*e.g.,* wettability hysteresis) (Zaid et al., 2023). However, CAE's dependency on *in situ* data (*e.g.,* salinity, mineral composition) underscores the need for ML (Hassanpouryouzband et al., 2022; Dabbaghi et al., 2024; Limaluka et al., 2024; Mu et al., 2024). ML algorithms like random forest (RF) enable efficient analysis of multiscale datasets to uncover hidden correlations between operational parameters and storage efficiency, thereby reducing reliance on costly experimental campaigns (Ansari et al., 2022; Kanaani et al., 2023; Vo Thanh et al., 2024b). Hybrid CAE-ML frameworks uniquely address these gaps, CAE ensures physical consistency while ML enhances prediction speed and optimization accuracy, enabling MOO of storage efficiency and safety.

Existing reviews focus narrowly on geochemical reactions, geomechanics (Navaid et al., 2023), experimental and numerical simulations (Wang et al., 2023a), and machine learning (Saeed and Jadhawar, 2024a), neglecting multiscale and multiphysics-coupling in UHS, particularly in monitoring technologies. In contrast to previous work, we prioritize three underexplored synergies: (1) multiscale analysis under THMC coupling based on geomechanical responses, (2) ML-driven numerical simulations integrated with MOO strategies, and (3) ML data-driven monitoring network optimization under THMC coupling. These approaches collectively bridge the gap between theoretical UHS models and site-scale implementation.

This review is built upon the foundation of geomechanical responses, introducing and discussing the latest advancements in analyzing UHS through multiphysics-coupling theories and computational methods, while providing a concise outlook on future developments. Specifically, this review is divided into seven sections. Section 2 provides an overview of geomechanical responses across different scales, with a brief description of the experimental methods and techniques employed. Section 3 emphasizes the long-term effects of biogeochemical reactions on geomechanics at the pore-laboratory scale. Section 4 explores the theories and methods of Multiphysics-coupling simulations, highlighting the potential applications of ML techniques in UHS at various scales. Section 5 emphasizes that future research on UHS monitoring network optimization should focus on integrating real-time geophysical imaging and advanced inversion techniques to optimize UHS production strategies. Section 6 discusses the trade-offs between subsurface structural safety and economic feasibility induced by hydrogen migration and injection-extraction behaviors, emphasizing the importance of MOO. Section 7 provides a comprehensive summary of the current state of research on multiphysics-coupling numerical simulations and machine learning-inspired studies in the context of UHS, highlighting key advancements and offering valuable insights into future directions. This review serves as a valuable resource for researchers in academia and industry to stay abreast of the latest advances in UHS.

2. Geomechanic responses in UHS

Numerous laboratory-scale studies have investigated the stress and strain behavior of rocks under various loading conditions. Hydrogen injection induces multiple cycles of pore pressure fluctuations, essential

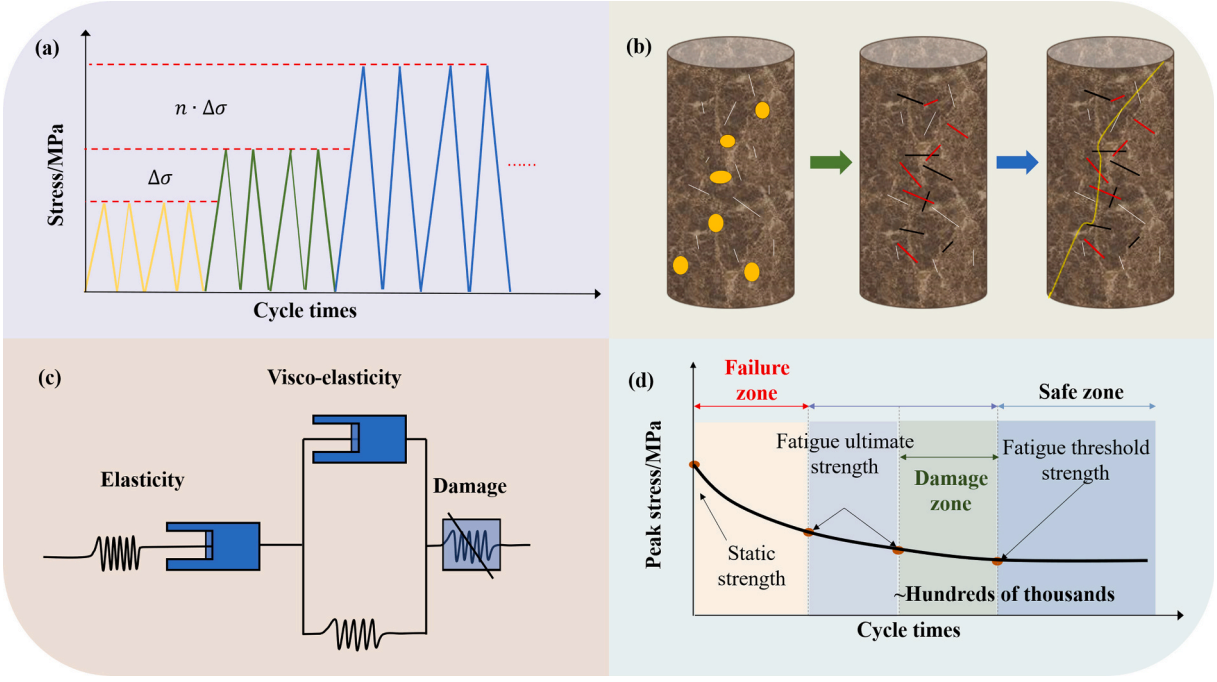

Fig. 2. The geomechanical response mechanism in geological systems. (a) cyclic stress and strain response. (b) microscopic damage mechanisms in rock. (c) viscoelasticity and damage models. (d) fatigue zone and strength evolution. Figure modified from (Tian et al., 2024).

for maintaining formation pressure. These cycles can induce mechanical phenomena such as fatigue damage and induce fractures in the rock, potentially compromising the stability of the reservoir, caprock and fault systems while increasing stress sensitivity. A preliminary assessment of the geomechanical consequences is essential to ensure safe storage operations.

2.1. Variable amplitude cyclic loading and unloading of rock

In the hydrogen storage process within porous media, similar to energy extraction and utilization processes such as deep coal mining, underground gas storage (UGS), and compressed air energy storage (CAES) (Liu et al., 2014; Jiang et al., 2017), the rock undergoes multi-stage, non-constant loading. This long-term cyclic loading, lasting for decades or even centuries, significantly affects the rock's fatigue life and damage strength. The mechanical properties of the rock exhibit nonlinear variations (Li et al., 2024), with increased fracture severity and higher dissipated energy (Xue et al., 2024), which directly influence the rock fatigue life and damage strength. Understanding the rock performance under maximum loading cycles (fatigue life) and the maximum applied stress it can withstand (fatigue strength) is crucial for ensuring the stability and safety of underground hydrogen storage (Singh, 1989; Suresh, 1998).

The gradual damage of rocks under cyclic loading is influenced by various factors, the maximum stress and amplitude are the primary factors affecting fatigue strength and deformation (Liu and He, 2012; Ma et al., 2013; Zhou et al., 2020). Increased in upper stress limit, enhanced stress amplitude, loading frequency, and loading rate will lead to a reduction in the fatigue life of rock (Nejati and Ghazvinian, 2014), typically represented by the “stress-number of cycles curve of rock” curve (Fig. 2(d)) (Liu et al., 2017), upon entering variable amplitude cyclic loading and unloading, the stress-strain curve gradually deviates from its initial linear state, with a reduction in the rate of cumulative deformation that accelerates toward the end of the cycle, resulting in a significant lag. Cumulative damage from cyclic loading and unloading reduces rock strength compared to its conventional compressive strength. There exists a threshold for rock fatigue failure, when the cyclic upper stress remains below the threshold (Zhang et al., 2019). When the maximum stress exceeds a threshold, additional damage accumulates, residual deformation increases with each cycle and irreversible deformation rises. At high-stress levels significantly greater than at low-stress levels, deformation follows a nonlinear growth trend (Cerfontaine and Collin, 2018).

During the cyclic injection and production of hydrogen, the damage evolution of the rock can be divided into four stages: the elastic stage, the stable crack propagation stage, the accelerated crack propagation stage, and the post-peak failure stage. In the initial elastic stage, lateral strain increases faster than axial strain (Wang et al., 2023c). Under cyclic loading, damage density exhibits an exponential dependence on the cyclic stress upper limit ratio, accelerating crack propagation and higher damage density compared to monotonic loading (Liu et al., 2023). The damage accumulation caused during the unloading phase leads to rock instability, with significant lateral expansion of the rock resulting in drastic plastic deformation. The elastic and secant moduli decrease overall, while higher loading rates lead to greater plastic strain and lower residual strength (Wang et al., 2022c). For a given confining pressure, residual strain increases as the upper limit cyclic stress ratio increases (Liu et al., 2023), the irreversible residual strain increases with stress and its deforming rate gradually accelerates (Li et al., 2019). At low-to-medium stresses, cyclic loading induces compaction-dominated volumetric strain (Jia et al., 2018), while high stress triggers dilation, exacerbating irreversible deformation with larger load amplitudes (Liu et al., 2014). Concurrently, wave velocity will decrease as the number of cycles increases (Jia et al., 2019), the energy dissipation and cumulative acoustic emission (AE) counts increase with the number of cycles (Meng et al., 2018).

Mechanistically, damage evolution spans multi-scale interactions (Fig. 3). Microscopic damage (nm to μm) is analyzed using MD, scanning electron microscopy (SEM) to quantify molecular bond fracture and interface rupture (Tang, 2020). Mesoscopic damage (μm to mm) is characterized by x-ray computed tomography (X-CT), nuclear magnetic resonance (NMR), and AE for crack extension and surface cementation (Hu and Yang, 2020). Macroscopic damage analysis can be performed using ultrasonic testing and digital image correlation (DIC) in combination with mechanical parameters (Tabiai, 2018).

Establishing a quantitative relationship between multi-scale damage and its effects. By using SEM imaging, the variation patterns of rock surface porosity are obtained. Based on Kachanov's classical damage theory, a rock damage factor is established using rock surface porosity as a parameter. The relationships between rock surface porosity, volumetric porosity, and plastic deformation are analyzed (Jia et al., 2017), or by developing a damage model using the fractal dimension of

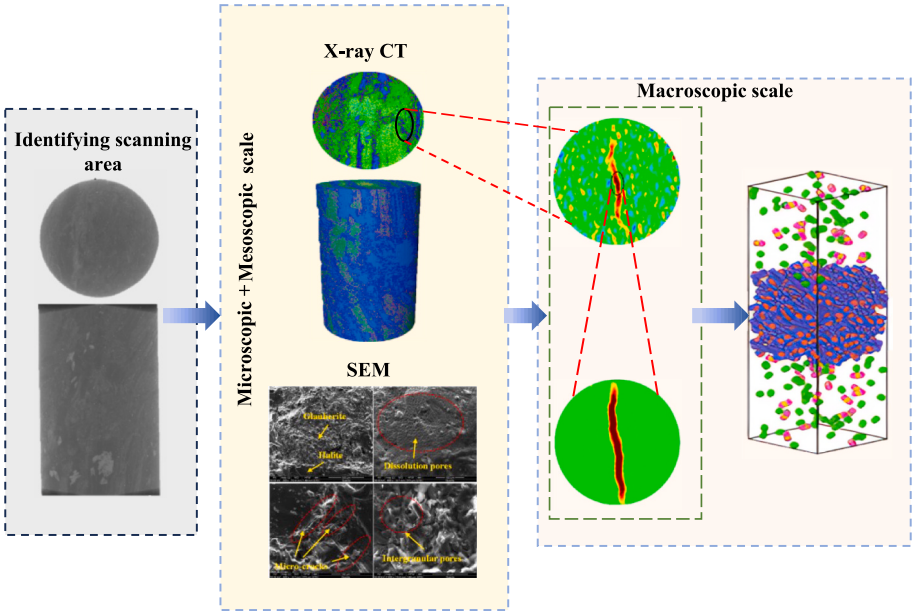

Fig. 3. Research on multi-scale damage identification of rocks (Sharafisafa et al., 2018; Doan et al., 2024; Song et al., 2024).

mesoscopic cracks as a variable (Yin et al., 2024). The identification information of multi-scale rock damage can be categorized into two types: image-based and numerical (Yang et al., 2018), identifying and analyzing these multidimensional and multi-scale data poses significant challenges, and traditional methods often struggle to fully extract effective information. ML methods are being used to address these issues (Ren et al., 2023), an integrated Back propagation neural network (BP neural network) was used to extract AE signal features (Ding et al., 2022), high-quality three-dimensional (3D) rock modeling is achieved by using a deep convolutional neural network (CNN) to pre-process noisy micro-computed tomography (micro-CT) images (Sidorenko et al., 2021), the Transformer algorithm is used to repair DIC images and extract damage regions from the complete strain field (Xu et al., 2024). Micro-damage in rock can be used as a variable to analyze the multi-scale damage quantity-effect relationship of rock using statistical analysis, fractal theory, numerical simulation, and artificial intelligence (AI) algorithms (Zhou et al., 2020).

Variable-amplitude cyclic loading and unloading experiments reveal that high frequency and amplitude stress paths significantly accelerate rock damage accumulation. The critical stress ratio provides a threshold condition for microcrack network formation. This multi-scale rock damage mechanism directly governs the initial defect distribution for fracture propagation, establishing experimental and theoretical boundaries for analyzing dynamic fracture evolution. This behavior is influenced by both the internal damage parameters and external loading conditions, which we further explore in the next section.

2.2. Rock fracture propagation

According to Griffith's fracture theory, rock damage initiates when the strain energy release rate exceeds the material's fracture toughness, leading to new crack formation (Griffith, 1921). The damage evolution progresses through distinct mechanical phases. Initially, when the stress exceeds dilation stress, the growth of radial strain begins to accelerate and the crack volume strain increases rapidly. As the cracks in the rock become interconnected and form fracture networks, there is a transition leading to the formation of a through-going rupture surface, and then the rock exhibits macroscopic failure (Yang et al., 2024c).

The extension of microscopic fractures in rocks and the accumulation of damage exhibit nonlinear behavior that is analogous to the logical growth patterns observed in natural biological communities (Li et al., 2023a). The fractures in the rock develop into interconnected fracture networks under the action of external loads (Zhao et al., 2022b), As the normal stress increases, the deformation of the fracture surface leads to non-uniform changes in the geometric configuration of the space geometry. The application of shear stress to the rock results in the opening of fractures, after the peak shear stress is reached, during the residual stage of the stress-strain curve, the flow tendency returns to an isotropic pattern (Rahimzadeh Kivi et al., 2018). Post-damage rock permeability is governed by pore connectivity and crack aperture (Zhang et al., 2025). Pore failure behavior is typically characterized by changes in the permeability of the rock, which increases sharply as microcracks coalesce and remains stable once peak strength is reached. However, permeability can decrease if internal pores are compressed or blocked by stress, the primary flow characteristic within the rock is fracture flow, with fracture pressures decreasing by almost an order of magnitude (Dilshan et al., 2024a).

The key distinction of UHS from other gases lies in its intense geochemical interactions within geological formations. Hydrogen as a proton is the driver of all acid-base reactions. UHS is the supply of a vast quantity of protons, which leads to a highly reactive and acidic aqueous solution that can dissolve most subsurface minerals. This shifts the analytical focus from traditional fluid-solid coupling to a detailed analysis of solute migration. In coupled stress-flow-transport simulations of non-reactive fracture networks, isotropic compressive stresses predominantly induce fracture deformation (Jiang et al., 2024), the solute migration path remains essentially unchanged, but the breakthrough time is delayed (Pan et al., 2023; Saeibehrouzi et al., 2024). Under anisotropic stress conditions, if the compressive stress difference is large, the dilatancy effect can alter the flow channels within the fracture network (Wang et al., 2024d), high dissolution reaction rates initially suppress fracture permeability during early seepage stages, followed by rapid permeability escalation as dissolution channels widen (Wang et al., 2024f).

Beyond mechanical effects, mineral dissolution and strength reduction driven by geochemical processes further govern crack propagation (Perera, 2023), These geochemical interactions can be either abiotic reactions or microbially mediated biotic reactions, with the latter inducing higher hydrogen loss and significant mineralogical alterations (Dilshan et al., 2024b). While abiotic reactions dominate under extreme reservoir conditions, pyrite reduction to pyrrhotite is a key abiotic reaction in UHS (Eq.1) (Alpermann and Ostertag-Henning, 2020; Bo et al., 2021; Zeng et al., 2023). It should be noted that abiotic and biotic reactions typically co-occur, with biotic reactions often leading to more severe consequences due to their capability for concurrent reaction processes (Table 1), subcritical cracking can be induced under the influence of oxidation-reduction conditions and geochemical interactions, and cracks are influenced by geochemical interactions and mechanical forces (Freiman, 1984). In fact, stress corrosion is the most common mechanism for subcritical crack propagation, with the crack rate primarily influenced by the long-term gas-rock-brine interaction, the effect of the biological reaction on crack growth is significant (Liao et al., 2020).

$$FeS_2 + (1-x)H_2 \rightarrow FeS_{1+x} + (1-x)H_2S (0 < x < 0.125) \quad (1)$$

The staged evolution of rock fracture propagation from accelerated radial strain under dilatancy stress to interconnected fracture networks and residual isotropic flow reveals a nonlinear coupling between fracture dynamics and permeability evolution. Geochemical interactions further modulate fracture geometry. These chemo-mechanical interactions amplify stress-dependent permeability anisotropy, bridging microscale fracture behavior to macroscale fluid transport. The chemically and physically altered fracture networks directly influence stress sensitivity of reservoirs. Building on quantified fracture-permeability relationships, the subsequent section investigates how stress sensitivity modulates reservoir permeability through fracture closure/open under effective stress variations.

Table 1
Typical growth conditions for biological reactions during UHS (Hematpur et al., 2023).

Biological type	Temperature (°C)		Salinity (g/L)		pH	
	Optimal	Critical	Optimal	Critical	Optimal	Critical
Methanogenesis	30–40	122	<60	200	6.0–7.5	4.5–9
Acetogenesis	30–40	72	<40	300	6.0–7.5	3.6–10.7
Sulfate reduction	20–30	113	<100	240	6.0–7.5	0.8–11.5
Iron (III) reduction	0–30	90	<40	200	6.0–7.5	1.6 > 9

Note: Optimum conditions represent peak growth, while critical conditions define the highest limits beyond which growth cannot occur.

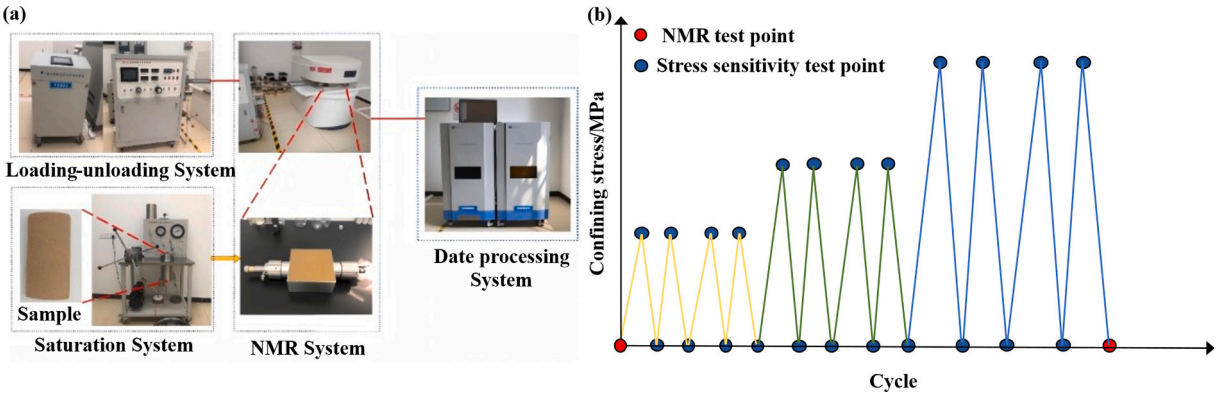

Fig. 4. Testing methods for reservoir stress sensitivity. Figure Modified from (Deng et al., 2023; Ho et al., 2024). (a) NMR experimental setup. (b) Experimental scheme for NMR and stress sensitivity testing under varying confining pressure.

2.3. Stress sensitivity of reservoir

During hydrogen storage, the injection fluid pressure causes the reservoir to expand, while rapid gas withdrawal causes the reservoir pressure to decrease rapidly, changing the effective stress (Amid et al., 2016). This in turn indirectly affects the pore structure of the reservoir rock and is referred to as reservoir stress sensitivity (Lorenz, 1999). The rocks in the formation are extensively fractured, forming dual-porosity rock sample structures with the matrix, which provide channels for hydrogen flow and storage, thereby affecting reservoir permeability. At this point, the commonly used linear effective stress theory of Terzaghi is difficult to apply to complex mineral components, pore structures, and dual-medium rocks (Sun et al., 2024a). Non-linear effective stress analysis can more effectively capture the variation in permeability with effective stress (Eq.2):

$$p_{\text{eff}} = p_c - \alpha p_f \tag{2}$$

where, p_{eff} is the effective stress, p_c represents the external stress, αrepresents the effective stress coefficient, which is dimensionless, p_f represents the pore pressure, when $\alpha \neq 1$ and varies with confining pressure and pore pressure, the effective stress coefficient has non-linear characteristics and the corresponding effective stress is called non-linear effective stress.

The stress path is a key factor influencing the pore structure and stress sensitivity of the rock (Farahani et al., 2022). To observe the evolution of the pore space at different scales and stress path, NMR tests can be performed at each loading and unloading node (Fig. 4), the evolution laws of micropores, medium pores and large pores under different confining pressures are determined. An increase in the cumulative amplitudes of micropores, medium pores, and total pores indicates the formation of microcracks. As the confining pressure changes, the pores are compacted and reopened, while water in the large pores is compressed and diffuses into micropores or medium pores, increasing the total pore volume (Chu et al., 2021).

Hydrogen storage in low-permeability reservoirs enhances safety due to limited hydrogen migration. Stress sensitivity is governed by rock properties (*e.g.,* particle arrangement and cementation) (Okere et al., 2024), fluid behavior (*e.g.,* seepage dynamics and initial pressure gradient), and geological stress fields (Wen et al., 2024b). Microscopically, the reservoir exhibit small pore diameters, large specific surface areas, and significant boundary layer effects. Densely packed particles with low compressibility reduce stress sensitivity (Penggao, 2019). However, increased effective stress can induce pore closure, surpass the critical flow threshold, and raise the initial pressure for fluid flow, and enhance permeability sensitivity (Cheng et al., 2023). Two mechanisms dominate stress sensitivity: fracture system deformation and variations in pore-throat size. Reservoirs contain multi-scale fractures (Du and Shi, 2024). High extraction rates or pressure gradients rapidly deplete fracture-stored hydrogen without sufficient replenishment from the matrix, thereby lowering fluid pressure, increasing effective stress, and inducing irreversible closure of microcracks during depressurization (Liu et al., 2024a). Additionally, pore-throat permeability depends on diameter and cementation (Dang et al., 2024). Clay-rich cements deform under stress, mobilizing particles that block throats and reduce permeability (Hu et al., 2024b).

The theoretical storage capacity of the reservoir is dynamically influenced by pore compressibility and stress sensitivity. Due to its smaller kinetic diameter (0.289 nm), H_2 has greater accessibility in rock pores during stress cycling. Consequently, changes in pore structure play a critical role in hydrogen storage capacity. To optimize injectivity, operational pressures should align with pore compressibility variations under cyclic stresses (Zhou et al., 2023). The storage capacity of the reservoir (C) can be estimated from Eq.3 (W. G. P, K. and P.G, R, 2023). Due to porosity changes caused by periodic gas injection and production, Eq.3 can be rewritten as Eq.4 (Zhou et al., 2023).

$$C = AH\varphi_R\rho_{H_2}S_{H_2} \tag{3}$$

where A is the lateral cross-sectional area, H is the formation thickness, φ_R is the porosity of the reservoir rock, ρ_{H_2} is the bulk density of hydrogen, and $S_{H_2}$is the H_2 saturation.

$$C = \mathrm{A} \times H \times E \times \rho_{(p,T)} \times \varphi_{i0}\left[1 + c_p(p_{cb} - p_0)\right] \tag{4}$$

where $\rho_{(p,T)}$represents the gas density at reservoir conditions, Erepresents the storage capacity coefficient, φ_{i0} is the initial porosity corresponding to the pore pressure of at the i-th cycle ($i = 1, 2, 3, \ldots\ldots n$), $c_p$represents the pore compressibility of rock, p_{cb} represents the overburden pressure, and p_0 represents the pore pressure.

Hydrogen storage operations reveal that cyclic injection/production induces nonlinear effective stress, driving pore-throat closure and fracture deformation. Hysteresis in pore evolution: microcracks form during unloading, while large-pore compression redistributes hydrogen into smaller pores, amplifying stress sensitivity. Dual-porosity systems exhibit distinct chemo-mechanical feedbacks, while H_2's small kinetic diameter enhances accessibility in compressed nanopores. To quantify these coupled processes, storage capacity models integrate pore compressibility and cyclic porosity decay, explicitly linking microscale pore-throat dynamics to macroscale hydrogen storage performance.

The stress-induced permeability anisotropy and pore pressure redistribution directly govern fault zone effective stress. Building on the quantified nonlinear stress-permeability relationship, the subsequent section incorporates friction laws with hydrogen-specific pore pressure diffusion to discuss fault stability. This framework evaluates how reservoir-scale stress sensitivity cascades into fault reactivation risks,

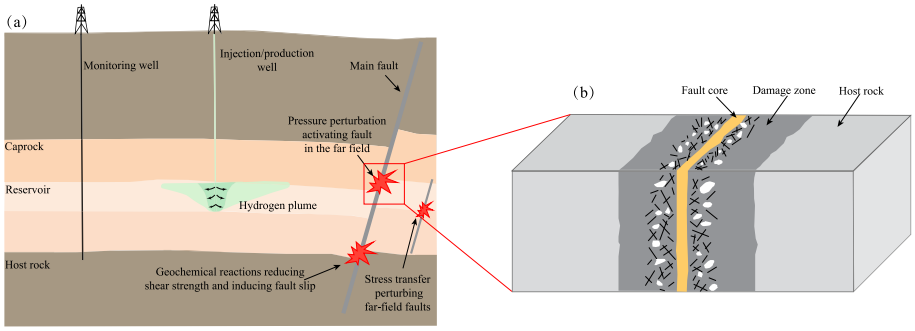

Fig. 5. Impact of fault core and damage zone on the stability and permeability of geological bodies. Figure modified from (Zhong et al., 2024).

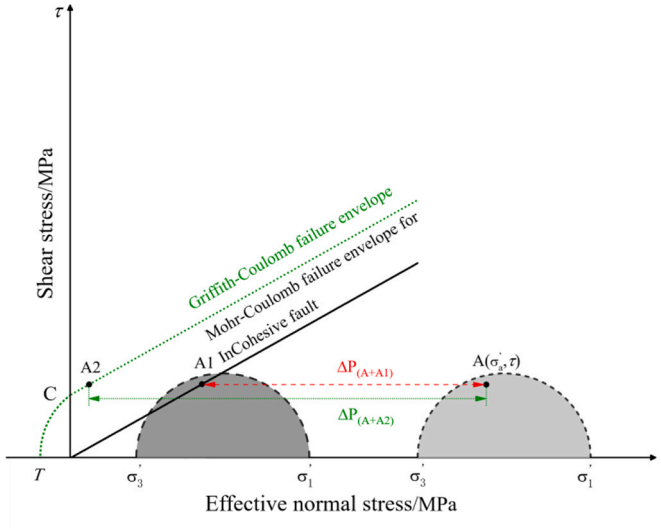

Fig. 6. Critical pore pressure of faults with different cohesion. ΔP_{A-A1} and ΔP_{A-A2} represent the maximum continuous fluid pressures for non-viscous and viscous faults respectively.

particularly in high-permeability formations. Field data from hydrogen storage sites will validate the coupled hydro-mechanical (HM) stability criteria, bridging microscale pore dynamics to macroscale geohazard mitigation.

2.4. Fault stability

Cyclic hydrogen injection induces pore pressure oscillations, triggering *in-situ* stress perturbations that may reactivate pre-existing faults (Preisig and Prévost, 2011). Such reactivation risks compromise caprock integrity through creating high-permeability conduits as shown in Fig. 5 (a), which are 4–5 orders of magnitude higher than leakage through caprocks (Goodman Hanson et al., 2022). The tripartite fault architecture, comprising a low-permeability fault core, fractured damage zone, and host rock, dictates stress redistribution patterns (Fig. 5(b)). Sibson first proposed the possibility of fault activation in 1990 (Sibson, 1990), the slip within the fault zone creates flow paths for hydrogen migration. Methods for determining fault activation include slip tendency, dilation tendency, and the Coulomb Failure Function (CFF) rupture criterion (Buchmann, 2008), with the Mohr-Coulomb criterion being the most commonly used. An increase (or decrease) in pore fluid pressure leads to a corresponding decrease (or increase) in effective normal stress at the fault plane, it is required that the Mohr circle does not contact the failure envelope (Mollon et al., 2024). For a fault plane with cohesion, the critical pore pressure is defined as the difference between the initial state and the critical state where the Mohr circle intersects the Coulomb failure envelope (Fig. 6).

Table 2
Redox reactions of sensitive minerals with H_2 (Malki et al., 2024).

Minerals	Reductive Dissolution
Carbonates	
Calcite	$CaCO_3 + 4H_2 = Ca^{2+} + CH_4 + 2OH^- + H_2O$
Dolomite	$CaMg(CO_3)_2 + 8H_2 = Ca^{2+} + Mg^{2+} + 2CH_4 + 4OH^- + 2H_2O$
Magnesite	$CO_3 + 4H_2 = Mg^{2+} + CH_4 + 2OH^- + H_2O$
Siderite	$FeCO_3 + 4H_2 = Fe^{2+} + CH_4 + 2OH^- + H_2O$
Sulfate	
Anhydrite	$CaSO_4 + 4H_2 = Ca^{2+} + H_2S + 2OH^- + 2H_2O$
Barite	$BaSO_4 + 4H_2 = Ba^{2+} + H_2S + 2OH^- + 2H_2O$
Celestite	$SrSO_4 + 4H_2 = Sr^{2+} + H_2S + 2OH^- + 2H_2O$
Sulfide	
Pyrite	$FeS_2 + H_2 = FeS + H_2S$
Fe^{3+} Oxides	
Hematite	$Fe_2O_3 + H_2 + H_2O = 2Fe(OH)_2$

Studies have demonstrated that during hydrogen storage, fault slip and dilation occur, which results in a two-order magnitude increase in aperture (Burtonshaw et al., 2024). *In-situ* stress, fault orientation, and pore pressure are the key factors influencing fault stability (Zhao et al., 2024). During injection/production cycles, pore pressure perturbs the stress field, potentially switching faulting mechanisms among normal, strike-slip, and reverse modes. Normal faults enhance effective stress *via* fracture opening, whereas reverse faults exhibit lower porosity due to fracture closure, promoting high-pressure fluid accumulation (Wang and Zhou, 2017). Fault dip angle critically influences stability: increasing dips improve stability near normal fault walls but reduce it at the lower wall of reverse faults. Conversely, caprock stability near the upper wall of a reverse fault increases with increasing dip angle (Gheibi et al., 2017). Fault activation risk depends on dip angle, permeability, and friction coefficient. High overburden permeability amplifies fault slip and seismic magnitudes, while faults with permeability lower than surroundings remain stable. In the overburden unit, as the friction coefficient increases, the fault slip and slip area decrease, while the stick area increases, reducing the propensity of the fault to slip. Thus, the frictional coefficient of the overburden fault plays a significant role in the slip behavior of the fault (Yang et al., 2024b). Larger Shear stress promotes slip, but higher friction coefficients decrease slip magnitude and potential seismicity. Under isotropic stress, fault slips are stress-magnitude-insensitive, and fault slips tend to initiate during early injection and operation regime transitions. Injection rates (5–40 m^3/s) approximately linearly correlate with average fault slip, despite no direct hydraulic connectivity between reservoir and fault-containing under burden. Aperture remains rate-insensitive, and withdrawal rates negligibly affect seismicity (Burtonshaw et al., 2024).

For low-risk hydrogen storage, target faults should exhibit high friction coefficients and low permeability. Further experiments must quantify fault-specific leakage thresholds, and this will determine which types of faults can effectively reduce the risk of hydrogen leakage.

3. Geochemical reactions and microbial activity

Hydrogen injection disrupts reservoir geochemical equilibrium, triggering hydrogen-water-rock interactions and microbial activity. These processes may induce mineral dissolution/precipitation (Table 2), potentially altering porosity, permeability, and rock strength (Flesch et al., 2018). For example, reductive dissolution of carbonates (*e.g.,* calcite), sulfide (*e.g.,* pyrite), and Fe (III)-bearing minerals (*e.g.,* hematite) can compromise formation integrity by increasing pore connectivity and reducing compressive strength (Kampman et al., 2016; Heinemann et al., 2021a; Hussain et al., 2022). This section reviews studies on hydrogen-water-rock geochemical interactions and microbial activity within the reservoir.

3.1. Hydrogen-water-rock geochemical reactions

Most studies currently focus on specific lithologies, such as sandstone, shale, and carbonate rocks, and discuss changes in porosity, permeability, and mineral composition before and after hydrogen treatment. In dry reservoir or caprock formations, hydrogen typically shows little or no reactivity with minerals and appears inert. In contrast, when hydrogen dissolves in formation fluids, its reactivity remains limited due to slow reaction rates, with most reservoir and caprock exhibiting low reactivity under hydrogen-rich conditions. (Yekta et al., 2018; Al-Yaseri et al., 2024b) For clay-bearing sandstones, after exposure to hydrogen at 1500 psi and 75 °C for 75 days, porosity shows minimal change, and dissolution or expansion of clay and quartz is also negligible (Al-Yaseri et al., 2024b), following hydrogen treatment at 75 °C and 1400 psi for 6 months, analyses using thin section optical microscopy and nuclear magnetic resonance indicate that the average increase in porosity does not exceed 5% and that no significant changes occur in the pore structure or geometric properties of the rock (Al-Yaseri et al., 2024a). Similarly, in clay-free sandstones, even under conditions of 100 °C to 200 °C and a maximum pressure of 10 MPa for periods of 1.5 to 6 months, the reaction between minerals in the sandstone and hydrogen is found to be very limited (Yekta et al., 2018). Even when CO_2 is used as a cushion gas for co-storage with H_2 in underground formations, H_2 losses remain within 2% over a 30-year period (Saeed et al., 2023). Therefore, some researchers believe that sandstones do not pose a risk of hydrogen loss or degradation of reservoir integrity due to abiotic geochemical reactions (Hassanpouryouzband et al., 2022).

Shale typically contains higher organic matter and clay content than sandstone (Gao et al., 2024c). H_2 and CH_4 adsorb preferentially to the hydrophilic surfaces of inorganic minerals, forming water and gas films that prevent direct contact between H_2 and minerals, thereby reducing the amount of hydrogen available for reactions with inorganic minerals. In clay-rich rocks such as Callovo-Oxfordian formations, H_2 adsorption reaches up to 0.1 wt% at pressures ≤90 bar. As water and H_2 compete for adsorption sites in clay minerals, the uptake of H_2 would be significantly lower in brine saturated reservoirs (Bardelli et al., 2014). Therefore, the degree of reaction of shale is generally lower than that of sandstone (Mu et al., 2024). Hydrogen has caused minimal dissolution of silicate minerals, approximately 0.001% by volume over an eight year period (Labus and Tarkowski, 2022).

In salt caverns, evaporite minerals (*e.g.,* anhydrite, gypsum, halite) exhibit high stability under hydrogen storage conditions (1450 psi, 75 °C). After 90 days of H_2 exposure, thermogravimetric analysis, nitrogen (N_2) adsorption/desorption isotherms, and SEM revealed negligible changes (<5%) in pore structure, specific surface area, and total pore volume (Fatah et al., 2024). For carbonate-rich rocks, X-ray computed micro-tomography (μCT) scans were conducted on limestone and dolomite cores both before and after exposure to hydrogen pressurization for 75 days at 700 psi and 75 °C. For the first time, a significant expansion of calcite was observed, resulting in a 47% reduction in effective porosity and, consequently, a decrease in storage capacity (Al-Yaseri et al., 2023b). The expansion of calcite grains during interactions with H_2 has been identified as a significant chemical phenomenon, leading to a reduction in effective reservoir porosity of up to 50%, However, calcite only dissolves at temperatures below 100 °C (Zhan et al., 2024). Limestone is a calcite rich type of carbonate rock, and limestone samples treated with H_2 (75 °C, 1400 psi) for 6 months showed minimal porosity increase (<5%) and no significant T2 distribution shifts in NMR analysis (Al-Yaseri et al., 2024a). This occurred while under the same temperature and pressure conditions, limestone saturated with 3 wt% NaCl brine (pH = 7) was pressurized with H_2 for 125 days. X-ray computed micro-tomography (μCT) and NMR analysis showed that the NMR porosity of Sample 1 increased from 18.55% to 20.96%, while the μCT porosity increased from 5% to 6.6%. In contrast, Sample 2 showed almost no change (Al-Yaseri et al., 2023a), these discrepancies may arise from variations in pore connectivity or mineral distribution. However, sandstones containing carbonates or anhydrite display complex behavior. Under H_2 exposure (10–20 MPa, 313–403 K, 6 weeks), porosity and permeability increased from 7% to 15% and 289 mD to 400 mD, respectively, due to mineral dissolution. Thus, oversaturation may trigger pore-blocking precipitation, leading to a reduction in both porosity and permeability (Flesch et al., 2018).

In a hydrogen storage environment, not only can the mineral composition within the rock change, but geochemical reactions may lead to the generation of gas components. Specifically, reactions between hydrogen and minerals in the rock (*e.g.,* sulfides or carbonates) may release gaseous byproducts such as CO_2, methane (CH_4), and H_2S. In underground H_2S is a highly toxic and corrosive gas that poses significant risks to reservoir stability as well as subsurface and surface environments, among these minerals, pyrite is the most reactive (Heinemann et al., 2021a). Hydrogen acts as a reducing agent, donating electrons to pyrite, which serves as an electron acceptor and undergoes reduction to produce H_2S (Morad, 1986). Pyrite typically constitutes no more than 1% to 2% of the rock volume, and that concentration of pyrite in the rock matrix does not appear to significantly affect H_2S generation. Instead, the amount of H_2S produced is primarily influenced by factors such as the volume of hydrogen injected and the content of sulfate minerals (Al Homoud et al., 2024).

Research on H_2-water-rock geochemical reactions shows significant discrepancies between experiments and simulations, leading to inconsistencies in the assessment of reactivity under UHS conditions. Systematic experiments under different conditions and an integrated database combining geochemistry, geomechanics, and micro-scale analysis are essential to better understand mineral-hydrogen reaction mechanisms and their impact on reservoirs. In addition, studying the coupling effects between microscopic chemical reactions and macroscopic rock mechanical properties is critical to understanding the long-

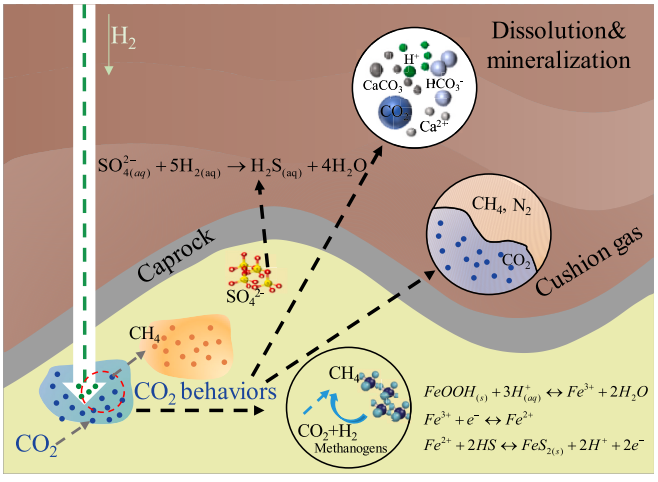

Fig. 7. Microbial reaction processes within geological formations. Figure modified from (Wu et al., 2024).

Table 3
The reaction of microorganisms with hydrogen.

H_2–consuming Process	Reaction Equation	Free Energy (kJ·(mol H_2)$^{-1}$)
Acetogenesis	$\frac{1}{2}HCO_3^- + H_2 + \frac{1}{4}H^+ \rightarrow \frac{1}{4}CH_3COO^- + H_2O$	−26.1
Sulfur Reduction	$H_2 + S \rightarrow H_2S$	−33.1
Hydrogenotrophic Methanogenesis	$\frac{1}{4}HCO_3^- + H_2 + \frac{1}{4}H^+ \rightarrow \frac{1}{4}CH_4 + \frac{3}{4}H_2O$	−33.9
Sulfate Reduction	$\frac{1}{4}SO_4^{2-} + H_2 + \frac{1}{4}H^+ \rightarrow \frac{1}{4}HS^- + H_2O$	−38.0
Nitrate Reduction	$4H_2 + 2H^+ + NO_3^- \rightarrow NH_4^+ + 3H_2O$	−150.0
Ferric Iron Reduction	$2FeOOH + H_2 + 4H^+ \rightarrow 2Fe^{2+} + 4H_2O$	−228.3
Denitrification	$\frac{2}{5}NO_3^- + H_2 + \frac{2}{5}H^+ \rightarrow \frac{1}{5}N_2 + \frac{6}{5}H_2O$	−240.1
Acetate Oxidation	$\frac{1}{4}CH_3COO^- + \frac{1}{4}H^+ + \frac{1}{2}H_2O \rightarrow H_2 + \frac{1}{2}CO_2$	23.7

term performance of geological formations.

3.2. Microbial activity

Microorganisms are critical agents in subsurface environments due to their adaptability to extreme conditions (*e.g.,* temperatures: −15 °C to 121 °C, pH: 3). For example, methanogens survive at 122 °C and 3.4 mol/L salinity, while sulfate-reducing bacteria (SRB) can function at temperatures up to 113 °C and in environments with 1.7 mol/L NaCl (Thaysen et al., 2021). During the process of UHS, microorganisms can influence the safety and efficiency of hydrogen storage through metabolic activities. As early as 1994, Buzek analyzed changes in the composition of hydrogen, methane (CH_4) and acid gases during the injection cycle and explained the decrease in reservoir pressure by the Sabatier reaction (Buzek et al., 1994). The study confirmed that H_2 molecules can be broken at high temperatures (several hundred degrees Celsius) or by the activity of methanogenic archaea. It can be seen that certain anaerobic microorganisms, such as methanogens and SRB, can use hydrogen as an energy source and convert it through biochemical reactions into gases such as CH_4 and H_2S (Tremosa et al., 2023), this reduces the hydrogen content in the reservoir and affects its diffusion below the caprock (Dopffel et al., 2021), On the other hand, these metabolic by-products can react chemically with the minerals in the reservoir, leading to pore plugging, reservoir acidification, changes in the physical properties and chemical environment of the reservoir, and even reservoir instability (Fig. 7).

Hydrogen acts as an electron donor for microbial respiration in subsurface environments, directly impacting storage efficiency through four key biotic processes: (1) methanogenesis, (2) acetogenesis, (3) sulphate reduction, and (4) iron (III) reduction (Dopffel et al., 2021), SRB and methanogenesis in the reservoir are the primary biological processes (Hemme and Van Berk, 2018). The fastest acetogens growth scenario caused ~2.4–5.2% loss per year, much lower than methanogens due to lower maximum specific growth rate (1.9–4.1 day^{-1} in methanogenesis) (Malki et al., 2024). Iron–III reducing bacteria metabolism relies on ferric oxide consuming H_2, provoking corrosion, and producing water (Thaysen et al., 2021). Notably, subsurface microbial diversity exceeds current understanding (Table 3). For example, denitrifying bacteria and acetogens may also be involved in complex biochemical reactions. Collectively, these activities reduce stored hydrogen purity and jeopardize long-term reservoir integrity.

Microbial activity can alter reservoir properties through pore clogging caused by biofilms and mineral precipitates, which reduce hydrogen injectivity and recovery efficiency by increasing flow resistance, consuming H_2, and producing water (Kryachko, 2018; Yang et al., 2021). For example, in the presence of dissolved iron in combination with either nitrate or low concentrations of oxygen, iron-oxidizing microbes will cause ferric iron minerals precipitation in form of ferrihydrite, goethite, magnetite, or other varieties. Several microbes, especially microaerophilic iron-oxidizers form significant amounts of biofilms and minerals, and they are often the cause of plugging in systems with oxygen ingress (Dopffel et al., 2021). Concurrently, SRB including Desulfovibrio, Desulfobacterium, and sulfate-reducing archaea, generate H_2S *via* sulfate reduction in the presence of dissolved sulfates or sulfidic minerals (*e.g.,* gypsum) (Pallud and Van Cappellen, 2006). Although SRB activity is observed up to 110 °C, optimal H_2S production occurs near 38 °C (Bernardez et al., 2013). For example, 45–60 vol% of H_2 in the urban natural gas in the aquifer can be converted to CH_4 and H_2S at 35 °C (Amigáň et al., 1990).

Microbial clogging severity depends on environmental factors. High salinity (100–150 g/L) in salt caverns inhibits SRB activity (Du et al., 2024), especially in pure rock salt with low sulfate content (Bordenave et al., 2013). In contrast, bedded salt formations with anhydrite layers are more prone to H_2S production (Laban, 2020). Additionally, the interaction of ferrous iron with the generated H_2S may precipitate pyrrhotite, clogging pores and reducing injectivity (Gregory et al., 2019). At temperatures above 40 °C, the reduction of other minerals, such as pyrite, is limited and is therefore considered to occur in a non-biological context (Hemme and Van Berk, 2018). Notably, pore clogging may enhance hydrogen distribution uniformity by enhancing this migration *via* capillary forces, despite its inherent risks (Eddaoui et al., 2021). In addition, microbially influenced corrosion (MIC) poses a critical threat to steel infrastructure, primarily through three microbial groups: acid-producing bacteria, methanogens, and SRB, such corrosion processes may degrade the integrity of subsurface infrastructure (Javaherdashti and Alasvand, 2019).

4. Multiphysics-coupling numerical simulation

The injection or withdrawal of hydrogen causes temperature changes in the formation, while variations in fluid pressure redistribute the subsurface stress field. Geochemical reactions consume hydrogen and produce by-products, which trigger geological deformation, fracture propagation, and thermo-elastic effects. These processes are further influenced by mineral dissolution/precipitation, multiphase transformations, and solute transport. Advances in mathematical models and numerical methods of multi-physics coupling are important for elucidating the mechanism of multi-field coupling. The representative theory mainly includes the effective stress principle, convective heat transfer in porous media, solute mass transfer, chemical reaction, mineral dissolution and its influence on physical parameters and damage of the solid medium. This description suggests that an ideal simulator for UHS models the coupled effects of THMC processes. However, current research focuses primarily on interactions between two fields, which is insufficient to fully capture the dynamic behavior of hydrogen storage systems. This section reviews the basic THMC concepts, modeling methods, and key findings that have promise for advancing UHS modeling and simulation studies. (Fig. 8).

4.1. Fundamental theory of Thermal-Hydraulic-Mechanical-Chemical (THMC)

Thermodynamic theory. Current thermodynamic studies of UHS focus on site-scale salt caverns (Tietze and Stolten, 2015; Böttcher et al., 2017; AbuAisha et al., 2021; Roa Pinto et al., 2021; Dias et al., 2023; Minougou et al., 2023; Ruiz Maraggi and Moscardelli, 2023; Zhang

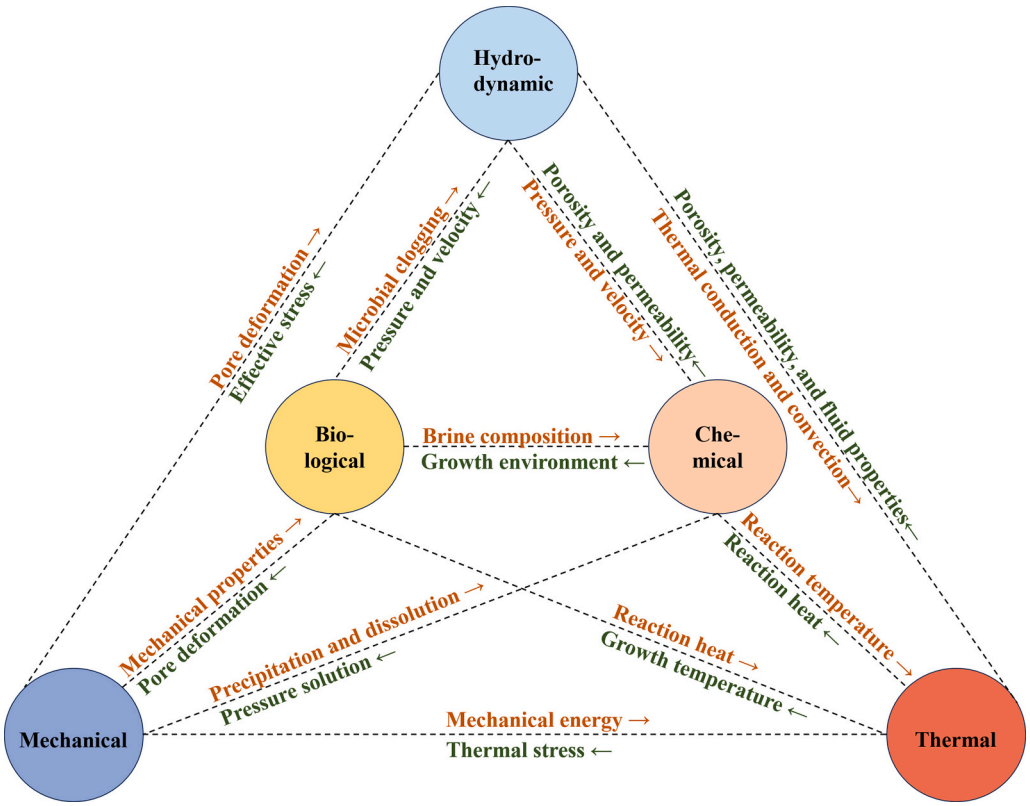

Fig. 8. THMC coupling processes at multiple scales in UHS (Wu et al., 2024).

et al., 2023b; Bachand et al., 2024; Tackie-Otoo and Haq, 2024; Wang et al., 2024g), where temperature variations caused by natural convection and geothermal gradients are generally neglected. Instead, the primary focus is on the Joule-Thomson effect induced by alternating pressure, frequent hydrogen cycles tend to limit temperature effects to a thin layer at the wall (Carter et al., 1993). The compressibility and creep behavior of salt caverns (governed by the Arrhenius law) lead to cyclic temperature-pressure variations, which reduce compressive stress and may induce crack propagation during operations (Ramesh Kumar et al., 2023). To model these effects, constitutive equations integrate the first and second laws of thermodynamics (Eq.5-Eq.6), Helmholtz free energy (Eq.7), and Gibbs free energy (Eq.8) (Hassanpouryouzband et al., 2020)

$$\rho u - \mathbf{D} : \sigma - \rho\gamma + \mathrm{div}(\vec{\mathbf{q}}) = 0 \tag{5}$$

where, ρ represents the material density of the medium, u represents the specific internal energy, $\boldsymbol{\sigma}$ represents the stress tensor, $\mathbf{D}$ represents the strain rate tensor, γ represents the power of external force fields acting on the system, and $\vec{\mathbf{q}}$ represents the divergence of the heat flux.

$$\dot{S}_{total} = \int_v \rho s \mathrm{d}v \geq \dot{S}_i + \dot{S}_e \tag{6}$$

where, $\dot{S}_{total}$ represents the total entropy of the system, s represents the specific entropy, $\dot{S}_i$ represents the entropy increase per unit time caused by internal changes within the system, and $\dot{S}_e$ represents the external entropy exchanged across the system boundaries. Additionally,

$$\varphi = \rho(u - Ts) \tag{7}$$

where, T represents the temperature. The other relationship is

$$G = H - TS \tag{8}$$

where, H represents the enthalpy, and S represents the entropy.

Hydraulic theory. In UHS systems, multiphase fluid-flow processes (*e.g.,* H_2-brine displacement) govern storage efficiency and caprock stability, it is significantly influenced by temperature gradients, pressure variations, and the characteristics of multiphase flow (Bai and Tahmasebi, 2022). As a result, the constitutive equations for seepage during the hydrogen storage process must typically be based on the laws of conservation of energy and conservation of mass, while incorporating various models (*e.g.,* PR equation, Fick's law, Henry's law, Langmuir adsorption, the Van-Genuchten model or Brooks-Corey model, and the Young-Laplace equation). These models account for the coupling effects of thermodynamics, fluid dynamics, and geomechanics to accurately describe the hydraulic behavior in complex subsurface environments (Eqs.9–12). It is important to note that in porous media, hydrogen typically coexists with other fluids, forming a complex multiphase system. The basic theory still follows the multiphase Darcy law (Darcy, 1856).

$$v_\alpha = -\frac{k k_{r\alpha}}{\mu_\alpha}(\nabla P_\alpha - \rho_\alpha g) \tag{9}$$

where, v_α represents the darcy velocity of the fluid, k represents the absolute permeability, $k_{r\alpha}$ represents the relative permeability of the α, μ_α represents the dynamic viscosity of the α, P_α represents the pressure of the α, and g represents the gravitational acceleration. The law of mass conservation is used to derive the continuity equation for hydrogen seepage in surrounding rocks:

$$\frac{\partial \phi \rho_s}{\partial t} + \nabla \cdot (\rho_g \mathbf{u}_g) = q_g \tag{10}$$

where, ρ_g is the gas density, and $\phi$are the porosity, $\mathbf{u}_g$ is the gas velocity, and $q_g$is a mass source term.

Due to the high diffusivity of hydrogen, the ideal storage medium is a low permeability porous medium, for porous media with low permeability, the slippage effect has a significant impact on gas permeability.

Considering the expansion deformation due to the pore pressure of hydrogen and the thermoelastic expansion of solid skeleton, the porosity is expressed as:

$$\phi = 1{\cdot}\frac{1{\cdot}\phi_0}{1+\varepsilon_v}\left[1{\cdot}\frac{\alpha_B}{K}(p{\cdot}p_0)+\alpha_T(T{\cdot}T_0)\right] \tag{11}$$

where, α_B is the Biot's coefficient, $\alpha_T$is the volumetric thermal expansion coefficient of the solid skeleton, and K is the bulk modulus of the rock.

The seepage control equation in the surrounding rock is:

$$\begin{aligned}&\left(p\frac{1-\phi_0}{1+\epsilon_0}\frac{\alpha_B}{K_A}+\phi\right)\frac{\partial p}{\partial t}-p\left(\frac{1-\phi_0}{1+\epsilon_0}\alpha_T+\frac{\phi}{T}\right)\frac{\partial T}{\partial t}\\&-T\left[\nabla{\cdot}\left(\frac{p}{T}\frac{k}{\mu}\nabla p\right)\right]=R_h T q_g\\&-p\frac{1{\cdot}\phi_0}{(1+\varepsilon_v)^2}\left[1-\frac{\alpha_B}{K}(p-p_0)+\alpha_T(T-T_0)\right]\frac{\partial\varepsilon_v}{\partial t}\end{aligned} \tag{12}$$

where, ε_v is the bulk strain, and the subscript 0 indicates the initial value.

Mechanical theory. Biot's theory links the changes in pore pressure caused by fluid seepage to the mechanical behavior of the porous medium (Biot, 1956), and it affects the transfer and distribution of thermodynamic energy (Eq.13) (Wang et al., 2024g), effectively characterizing the mechanical response of the solid skeleton to fluid pressure and, conversely, the effect of solid deformation on fluid flow (Eq.14). At the site-scale, the deformation of the surrounding rock is generally within a relatively small deformation range and is dominated by elastic responses (Li et al., 2023b). Therefore, the mechanical behavior can be described by a small-deformation elastic constitutive equation (Eq.15). This assumption simplifies model calculations while being sufficient to capture the stress redistribution in the surrounding rock caused by pressure and temperature changes during the hydrogen storage process (Kuang, 2014) within both rock and closed fractures. Even after damage, deformation can be considered as linear elastic materials that follow Hooke law (Ramesh Kumar et al., 2023). The stress changes are then compared to the strength of the rock, as described by the Mohr-Coulomb criterion or Drucker-Prager criterion, to evaluate the potential for reservoir failure (Bai and Tahmasebi, 2022).

$$(\rho C)_{eff}\frac{\partial T}{\partial t}-\rho_g C_g\frac{k}{\mu}\nabla p{\cdot}\nabla T-\nabla{\cdot}\left(\lambda_{eff}\nabla T\right)+TK\alpha_T\frac{\partial\varepsilon_v}{\partial t}=Q_t \tag{13}$$

where, $(\rho C)_{eff}$ is the total heat source, λ_{eff} is the total heat source, Q_t is the total heat source, T is the temperature of the surrounding rock, K is the bulk modulus of the rock, ρ_g is the gas density, C_g is the **heat capacity of the liquid phase**, α_T is the volumetric thermal expansion coefficient of the solid skeleton, ε_v is the bulk strain, and p is the pore gas pressure. Furthermore, stress is determined following

$$\sigma = \sigma_0 + D:(\varepsilon-\varepsilon_{th}-\varepsilon_{cr})-\alpha_B(p-p_0)\mathbf{I} \tag{14}$$

where, σ_0 is the initial stress tensor, ε_{th} andε_{cr} are the thermal strain tensor and the creep strain tensor, respectively, and $\mathbf{I}$ denotes the identity matrix. The resulting expression is

$$\frac{G}{1-2\nu}\nabla\varepsilon+G\nabla^2\boldsymbol{u}+\alpha\nabla p+F_i=0 \tag{15}$$

where, G is the shear modulus, ν is Poisson's ratio, $\boldsymbol{\varepsilon}$is the strain, $\boldsymbol{u}$ is the displacement vector, $p$is the pore pressure, α is the Biot's coefficient, and F_i represents the body loads in different directions.

In geological settings, rocks undergo significant inelastic deformations (*e.g.,* plasticity, viscoplasticity, creep) under cyclic loading, particularly under long-term stress, high temperature/pressure, or localized stress concentrations. Kumar et al. demonstrated that hydrogen injection-induced cyclic loading amplifies these deformations in reservoirs (Kumar et al., 2022). Subsequent studies revealed that rock viscoelasticity alone cannot fully describe such behavior (Ramesh Kumar et al., 2023), which instead required a combination various

Table 5
Geochemical reaction processes in UHS (Zivar et al., 2021).

Reactions	Equation	Annotation
Equilibrium reactions	aR + bS→cP	a, b and c are the stoichiometric coefficients of geochemical species; R, S and P represent the reactants and product, respectively
Ion exchange reactions	$\zeta_i = \frac{z_i c_i}{\sum_{i=1}^{N_{cx}} z_i c_i}$	c_i is the concentration of the exchange species, z_i is the valence number of the exchange species, and N_{cx} is the total number of exchange species
Mineral dissolution and precipitation reactions	$r_\beta = \widehat{A}_\beta k_\beta\left(1-\frac{Q_\beta}{K_{eq,\beta}}\right)$, $\beta = 1\ldots, n\_(r,m)n$	$\widehat{A}_\beta$ is the reactive surface area of reactant mineral β per unit bulk volume of porous medium, k_β is the rate constant of mineral reaction β. k_β is the chemical equilibrium constant of mineral reaction, Q_β is the activity product of reaction and $n\_(r,m)n$ is the number of mineral reactions.

Table 4
Constitutive models for inelastic deformation (Han, 2022).

Name	Represents Material Properties	Constitutive Equation
Kelvin Model	Viscoelastic	$\sigma = E\varepsilon+\eta\dot{\varepsilon}$
Maxwell Model	Elastoviscous	$\sigma+\frac{\eta}{E}\dot{\sigma}=\eta\dot{\varepsilon}$
Viscoplastic Model	Viscoplastic	$\sigma<\sigma_s, \varepsilon=0$ $\sigma\geq\sigma_s, \dot{\varepsilon}=\frac{\sigma-\sigma_s}{\eta}$
Saint-Venant Model	Elastoplastic	$\sigma<\sigma_s, \varepsilon=\frac{\sigma}{E}$ $\sigma\geq\sigma_s, \varepsilon\to\infty$
Bingham Model	Elasto-visco-plastic	$\sigma<\sigma_s, \varepsilon=\frac{\sigma}{E_1}$ $\sigma\geq\sigma_s, \dot{\varepsilon}=\frac{\dot{\sigma}}{E_1}+\frac{\sigma-\sigma_s}{\eta_1}$
Burgers Model	Elastoviscous	$\sigma+\left(\frac{\eta_2}{E_1}+\frac{\eta_1+\eta_2}{E_2}\right)\dot{\sigma}+\left(\frac{\eta_1\eta_2}{E_1E_2}\right)\ddot{\sigma}=\eta_2\dot{\varepsilon}+\frac{\eta_1\eta_2}{E_2}\ddot{\varepsilon}$
Nishihara Model	Elastoviscous	$\sigma<\sigma_s, \sigma+\frac{\eta_1}{E_1+E_2}\dot{\sigma}=\frac{E_1E_2}{E_1+E_2}\varepsilon+\frac{E_1\eta_1}{E_1+E_2}\dot{\varepsilon}$ $\sigma\geq\sigma_s, (\sigma-\sigma_s)+\left(\frac{\eta_2}{E_1}+\frac{\eta_1+\eta_2}{E_2}\right)\dot{\sigma}+\left(\frac{\eta_1\eta_2}{E_1E_2}\right)\ddot{\sigma}=\eta_2\dot{\varepsilon}+\frac{\eta_1\eta_2}{E_2}\ddot{\varepsilon}$

possibilities of inelastic deformation models (Table 4) is required once stresses exceed the rock yield strength.

The multiphase flow of hydrogen, water, and other fluids within the rock pores increases the capillary pressure in the rock, which may enlarge the fracture aperture and lead to shrinkage cracking (Dilshan et al., 2024b). The mechanical properties and fluid behavior of subterranean rocks are strongly influenced by fracture characteristics, a phenomenon particularly pronounced in carbonate or shale reservoirs. After hydrogen enters the porous medium, the pore pressure around the fractures increases at a faster rate as the injection time progresses, and the stress fields near the fractures interact (Wang et al., 2024c). Even after hydrogen injection stops, a relatively high concentration of hydrogen remains in the fracture channels. To more accurately describe the diffusion and flow behavior of hydrogen, a dual-porosity model is typically used (Zamehrian and Sedaee, 2022). When hydrogen invades the matrix, during the production cycle, the hydrogen cannot be fully produced due to the low permeability of the matrix. The larger the depletion volume in a single-porosity model, the more hydrogen will penetrate into the matrix during injection, which is unfavorable for hydrogen production. The mixing effect of hydrogen and natural gas is better in dual-permeability reservoirs (Song et al., 2024).

Chemical theory. At the microscale, geochemical reactions including mineral dissolution/precipitation and ion exchange-further alter rock mechanics (Table 5). For instance, hydrogen-induced mineral dissolution may enhance fracture apertures, while precipitation could clog pores, complicating reservoir management.

The microbial life cycle generally flows through four key phases: the lag phase, exponential phase, stationary phase, and decay phase (Muloiwa et al., 2020). There are seven growth kinetics equations for microbial metabolism, namely the Classical Monod, Moser Equation, Panfilov Model, Double Monod Model, Haldane Model, Teissier Model, and Contois Model. The majority of studies have employed a Double Monod Model to compute microbial specific growth rates (Eq.16) (Jahanbani Veshareh et al., 2022; Shojaee et al., 2024), because it accounts for two limiting substrates, such as hydrogen and sulfate, commonly used for environments involving multiple substrate limitations, which is computed following

$$\mu_{gr} = \mu_{max}\frac{C_A}{C_A + K_A}\frac{C_D}{C_D + K_D} \tag{16}$$

where, μ_{gr} represents the specific growth rate, μ_{max} denotes the maximum specific growth rate, and $C_A$andC_D are the concentrations of electron acceptor and donor, respectively, with K_A and K_D being their corresponding half-saturation constants. The maximum specific growth rate is not a constant value but varies with changes in environmental conditions by applying influencing coefficients. Influencing factors can include temperature, salinity, pH, microbial concentration, and more. Therefore, the maximum specific growth rate can be presented in the following general formulation

$$\mu_{max} = \mu_{opt}\prod\psi_i \tag{17}$$

where, μ_{opt} represents the specific growth rate of microbes under optimal conditions, s^{-1}; and ψ_i is the influencing coefficient of each factor. The Haldane model can be used when higher substrate concentrations in the porous medium inhibit microbial growth.

In addition to the classical Double Monod Model, microbial constitutive models can be considered from different perspectives to provide a more comprehensive description of microbial growth and metabolic activity. The Moser model or the Tessier model can also be included for this purpose, when microorganisms begin to decay, a constant specific decay rate can be used to represent the rate of biomass change. The first approach utilizes a constant specific decay rate (Wu et al., 2023). The second approach allows the decay rate to vary linearly with microbial population size (Hogeweg et al., 2022). The specific methods vary slightly across different studies , Regardless of the model chosen, it is essential to accurately capture the impact of microbial growth and metabolic behavior on the environment, including factors such as temperature (Shojaee et al., 2024), pH (Jahanbani Veshareh et al., 2022), salinity (Peleg, 2022), and thermodynamic conditions (Tremosa et al., 2023). Existing research has proposed a series of models that integrate microbial growth, decay, and diffusion processes into a mass conservation framework (Hagemann et al., 2016). By incorporating the variation patterns of the specific decay rate, it is possible to simulate the dynamic response of microbial decay and metabolic rates over different time scales (Eqs.18 to 21). Solute transport within water and gas is determined by

$$\phi\frac{\partial\left(\rho_g c_g^k S_g + \rho_w c_w^k S_w\right)}{\partial t} + \nabla\cdot\left(\rho_w c_w^k v_w + J_w^k + \rho_g c_g^k v_g + J_g^k\right) = q^k \tag{18}$$

where, ϕ represents porosity; $\rho$is molar density, c is mole fraction; S is saturation; v is convective flux, J is dispersion/diffusion flux, and q is the source or sink term related to microbial consumption. The subscripts g and w refer to the gas phase and the water phase, respectively, and the superscript k represents the chemical composition.

Microbes can attach to and detach from rocks, and they move through random motion (similar to diffusion) and chemotaxis, which makes the conservation equations for microbes highly complex. The non-structural mass conservation equation, which considers only microbial growth, decay, and diffusion, is as follows.

$$\frac{\partial n}{\partial t} = S_w\mu_{gr}n - \mu_{dec}n + \nabla\cdot(D\nabla n) \tag{19}$$

where, D is the cell diffusion coefficient, andμ_{dec} varies linearly with the microbial population size (Wu et al., 2024).

Permeability dynamically changes under the joint impacts of microbial clogging, mineral dissolution/precipitation and effective stress. Among these three factors, effective stress plays the dominant role, while microbial clogging only influences permeability in the initial few cycles of hydrogen injection and withdrawal (Gao et al., 2024b). Zhang et al. (1992) believed that microbial clogging effects might not notably alter porosity but could significantly impact permeability. The permeability taking into account microbial mobility and microbial adsorption can be expressed by the following equation

$$k_p = 1 + (R_r - 1)\frac{ad}{ad_{max}} \tag{20}$$

where, R_r represents the resistance factor; ad_{max}denotes maximum adsorption capacity of microbes, and adsignifies the number of adsorbed microbes. The porosity is described by

$$\phi = \frac{\phi_0}{1 + \left(\frac{n_a + n_d}{n_c}\right)^2} \tag{21}$$

where, n_c represents the quantity of microbes required to induce maximal bio-clogging effect, and ϕ_0 denotes the porosity of a clean reservoir devoid of microbes. In addition, a macro-micro scale HMCB model can be established based on the governing equations of effective stress, gas-water two-phase flow, multicomponent transport, and mineral dissolution and precipitation, as well as desorption/growth-decay processes, to analyze the impact of microorganisms in underground hydrogen storage (Gao et al., 2024b).

Beyond microbial interactions, thermo-hydro-mechanical (THM) coupling critically governs UHS stability. The THM framework builds on Terzaghi's effective stress principle and Biot's 3D consolidation theory (Terzaghi, 1943), which quantify stress field perturbations during hydrogen cycling (Dilshan et al., 2024b). By combining linear elasticity theory with fracture mechanics theory, the hydromechanical elastic solution for the UHS process can be obtained. The thermo-mechanical behavior can be simulated using the modified LUBBY2 creep law and

the heat conduction equation (Böttcher et al., 2017). For instance, Liu et al. (2024b) derived analytical solutions for the variation of gas pressure and temperature over time and they found that changes in gas temperature and pressure induce thermal stress in the surrounding rock. This thermal stress could potentially lead to stress concentration phenomena in interlayers within the surrounding rock or salt caverns resulting in tensile failure.

The injection-production behavior of hydrogen in geological formations exhibits distinct short-term and long-term effects on rock mechanics and transport processes. In the short term, elastoplastic deformation and instantaneous damage dominate due to rapid temperature and stress fluctuations, leading to rock volume expansion. In the long term, steady-state creep and delayed damage become significant, while hydrogen migration transitions to diffusion-dominated mechanisms. Even with substantial permeability changes, the hydrogen plume remains spatially limited (Coarita-Tintaya et al., 2023). A Thermal-Hydraulic-Chemical (THC) model study indicates dissolved hydrogen converts to CH_4, with peak CH_4 concentrations observed at the plume front (Pfeiffer et al., 2016b).

Further application of the two-phase flow Darcy's law and Fick's diffusion model to describe the migration behavior of hydrogen in rocks has shown that the Darcy flow shows minimal dependence on model parameters, while the Fick diffusion coefficient indirectly affects the Darcy flow. The amount of hydrogen loss is negligible compared to the total volume of hydrogen circulated (AbuAisha et al., 2021). In low-permeability reservoirs, nonlinear flow emerges under high pressure due to the Klinkenberg effect. Fracture complexity further induces relative permeability hysteresis (RPH), impacting multiphase flow (Liu et al., 2024c; Wang et al., 2024g). Wang et al. (2024e) developed a multiscale model integrating organic matter, shale matrix, natural/hydraulic fractures, and stimulated zones. This framework captures gas-liquid multiphase transport in shale reservoirs. Their results suggest selecting reservoirs with high adsorption capacity, diffusion coefficients, and inter-porosity flow rates enhances hydrogen storage potential.

4.2. THMC coupled numerical simulation methods

Numerical simulation has become an essential tool for the strategic development and safety assessment of UHS. Current simulation platforms exhibit distinct technical orientations in addressing the complex physicochemical interactions inherent in UHS. For instance: CMG is capable of characterizing compositional migration and complex phase behavior of hydrogen-bearing systems (Safari et al., 2023; Naderi et al., 2024); the TOUGH is distinguished by its capacity to model multiphase, multicomponent, and non-isothermal fluid flow, heat transfer, and solute transport, making it a robust choice for environmental remediation and resource development (Luboń and Tarkowski, 2021). Meanwhile, COMSOL provide versatile frameworks for multiphysics coupling and user-defined constitutive equations (Wang et al., 2024g).

However, technical challenges persist in capturing the intricate coupling processes of UHS. Resolving complex geochemical interactions in subsurface systems using COMSOL Multiphysics typically necessitates the integration of external thermodynamic data or the implementation of user-defined equations and secondary development subroutines to enhance its simulation capacity for specialized scenarios. Similarly, the performance of CMG in large-scale reservoirs may require specialized parameterization or external tool integration when addressing highly specific biogeochemical kinetics or micro-scale processes. Furthermore, the TOUGH series frequently relies on modular coupling with external geomechanical codes to achieve rigorous geomechanical representation in subsurface reservoirs. Given the inherent uncertainties arising from the general scarcity of specialized thermodynamic and kinetic datasets tailored for actual subsurface conditions, a synergistic numerical strategy incorporating cross-platform coupling, site-specific experimental calibration, and customized database supplementation is essential for enhancing the reliability of UHS predictions.

Thermodynamic modeling. Thermodynamic modeling at the site-scale quantifies hydrogen expansion/compression under varying temperatures and pressures (Table 6) (Tietze and Stolten, 2015). For example, central difference discretization of improved thermodynamic equations in MATLAB enables analysis of thermal conductivity gradients through adaptive meshing (Bachand et al., 2024). Alternatively, the H2ThermoBank software (C#-based) combines the GERG-2008 equation of state, Super TRAPP transport model, and Michelsen phase stability method to predict mixture properties (Hassanpouryouzband et al., 2020). Dias et al. (2023) developed a thermodynamic simulator based on non-adiabatic solutions to evaluate hydrogen properties using the REFPROP library, gas pressure and temperature were updated at each time step, and the estimated salt cavern pressure and temperature were integrated into the in-house developed GeMA framework for thermo-mechanical analysis. Coupling thermodynamic and mechanical processes requires specialized numerical strategies. OpenGeoSys implements unidirectional thermal-mechanical coupling (*i.e.,* with temperature variations unidirectionally affecting the mechanical behavior) *via* staggered methods for salt rock analysis (Böttcher et al., 2017). For large-deformation scenarios (*e.g.,* salt caverns), axisymmetric finite difference models improve computational efficiency (Passaris and Yfantis, 2019). The COMSOL framework allows users to customizedly couple partial differential equation and ordinary differential equation for THMC modeling (Wang et al., 2024g).

For UHS, comprehensive thermodynamic databases for hydrogen-bearing systems (both pure and blended gases) are essential for deciphering complex porous media reactions and form the bedrock of THMC coupled numerical simulations (Hassanpouryouzband et al., 2020). While the thermodynamic properties of pure hydrogen—including enthalpy, entropy, and viscosity—are well-documented in authoritative repositories such as the NIST Chemistry WebBook, providing core support for thermal and chemical modules, the properties of hydrogen-bearing mixtures remain insufficiently explored. Currently, available experimental data are sparse, limited to specific studies such as PVT measurements for H_2-CH_4 at high pressures (Machado et al., 1988) and the Nitrogen–Hydrogen Binary System from 240 to 350 K and Pressures up to 20 MPa (Hernández-Gómez et al., 2017). Due to the complexity and prohibitive costs of high-pressure sealing experiments, thermodynamic properties like density and phase equilibria for mixtures are predominantly derived *via* the GERG-2008 Equation of State, calibrated by limited experimental datasets (Zhao et al., 2024b). However, a discrepancy persists between these Equation of State-derived

Table 6
Reviews on thermodynamic modeling of UHS.

Modeling tool and Application software	Physio-chemical process	*Method*	*Programming Language*
/	T	Central difference discretization	Matlab (Tietze and Stolten, 2015)
OpenGeoSys	TM	FEM	C++ (Böttcher et al., 2017)
/	TM	FDM (Passaris and Yfantis, 2019)	/
H_2ThermoBank (Hassanpouryouzband et al., 2020)	T		C#
GeMA (Dias et al., 2023)	TM	/	LUA
$GeoH_2$ (Ruiz Maraggi and Moscardelli, 2023)	TM		Python
COMSOL (Wang et al., 2024g)	THM	FEM	Matlab

Note: Thermodynamic(T), Thermo-mechanical (TM), Finite Element Method (FEM), Finite Difference Method (FDM).

Table 7
Reviews on hydrodynamics modeling of UHS.

Modeling tool and Application software	Physio-chemical process	*Method*	*Programming Language*
GPSFLOW (Cai et al., 2022)	Hydro-Thermodynamic (HT)	FDM	/
PETRASIM-TOUGH$_2$ (Luboń and Tarkowski, 2021; Luboń and Tarkowski, 2023)		FDM、FVM(Finite Volume Method)	C++、Fortran
TOUGH$_2$-EWASG (Mahdi et al., 2021)		FVM	Fortran
ECLIPSE (Pfeiffer and Bauer, 2015; Pfeiffer et al., 2017; Enigbokan et al., 2021; Lysyy et al., 2021)		FDM	Fortran
CMG (Delshad et al., 2022a; Delshad et al., 2022b; Kanaani and Sedaee, 2022; Abdellatif et al., 2023; Alhotan et al., 2023; Chai et al., 2023; Jadhawar and Saeed, 2024)	HM	FDM	/
TOUGH (Huang et al., 2023a)		FVM	Fortran
COMSOL (Sainz-Garcia et al., 2017)		FEM	Matlab
DUMUX (Hagemann et al., 2015; Feldmann et al., 2016; Hagemann et al., 2016; Hashemi et al., 2021; Hogeweg et al., 2022)		FVM	C++
AusH$_2$((Aftab et al., 2023)		/	/
MRST (Liu et al., 2024c)		FVM	Matlab
Imperial College Geomechanics Toolkit (ICGT) (Burtonshaw et al., 2024)		FEM	C++
MD model (Ghasemi et al., 2022)	The microscopic diffusion of hydrogen gas	/	/

parameters and the high-precision NIST data for pure hydrogen. Furthermore, existing thermodynamic modeling frequently adopts simplified isothermal or isentropic processes (Hu et al., 2024a) , whereas rigorous THMC simulations necessitate the calibration of thermodynamic trajectories based on actual subsurface temperature and pressure characteristics. Crucially, thermodynamic data for water–rock–hydrogen mixture systems remain deficient. While databases utilized by GeMA (REFPROP), OpenGeoSys, and COMSOL can accommodate fundamental water-hydrogen simulations, they offer only rudimentary support for complex thermochemical reactions involving water-rock-mixed gas interfaces. Key interfacial parameters, such as mineral adsorption enthalpy and multiphase reaction rate constants, are notably absent even in specialized databases like TOUGH series EOS3/6. These inherent deficiencies underscore the imperative for experimental calibration and data augmentation. Specifically, hydrogen adsorption in subsurface systems can be modeled and subsequently validated using the NIST database (Lee et al., 2025). For practical UHS scenarios, core-scale hydrogen-rock experiments are indispensable to acquire multiphase reaction parameters and calibrate numerical models, thereby constructing a more robust thermodynamic framework to enhance the fidelity of THMC coupled simulations.

Hydraulic modeling. Hydrodynamic processes in UHS are governed by fluid properties, fluid-rock interactions, and injection-production strategies. Numerical tools such as DUMUX have been widely applied to investigate the dominance of gravitational *vs.* viscous forces under varying injection rates (Hagemann et al., 2015; Hagemann et al., 2016) (See Table 7). Key challenges in UHS optimization include controlling hydrogen injection/production behavior to stabilize flow regimes and enhance storage efficiency. Macro-scale simulators such as ECLIPSE, CMG-GEM enable analyses of operational parameters, cushion gas selection, and geological heterogeneity impacts on hydrogen purity and recovery (Luboń and Tarkowski, 2020; Enigbokan et al., 2021; Huang et al., 2023a; Jadhawar and Saeed, 2023). The modeling approach transitioning from site-scale to pore scale aims to refine the understanding of fluid flow and gas storage processes. Pore-scale modeling captures the effects of relative permeability and capillary pressure forces on the seepage process (Hashemi et al., 2021) Additionally, advanced imaging techniques (*e.g.,* x-ray microtomography) reconstruct 3D pore structures for dynamic flow simulations. Recent studies further leverage machine learning (ML) to augment traditional methods: Generative adversarial network (GAN) predict two-dimensional multiphase flow patterns (Alhotan et al., 2023), and hybrid pore-scale-ML frameworks improve accuracy in modeling hydrogen hydrogen-brine two-phase flow (Zhao et al., 2024a). These integrated methodologies provide critical insights into the coupled physicochemical processes controlling UHS performance.

Geomechanical modeling. Geomechanical modeling of underground hydrogen storage requires addressing stress field perturbations induced by injection/production cycles, which may trigger fractures, leakage, and induced seismicity. While laboratory tests cannot fully replicate long-term multi-physics coupling effects, numerical simulations provide critical insights through coupling approaches (Table 8). First, one-way coupling sequentially executes independent modules with unidirectional data transfer. This approach offers computational efficiency and robust convergence, albeit at the cost of omitting bidirectional feedback. For instance, Böttcher et al. (2017) implemented a staggered coupling scheme where thermal solutions were unidirectionally transferred to mechanical calculations. In solving the HM problem, a sequentially coupled method can be used to transfer fluid field results (*e.g.,* pressure, velocity) to the mechanical field to calculate maximum

Table 8
Reviews on geomechanical modeling of UHS.

Modeling tool and Application software	Physio-chemical process	*Method*	*Programming Language*
OpenGeoSys (Böttcher et al., 2017)	TM	FEM	C++
Developed an open source 2D finite element simulator (Ramesh Kumar et al., 2021)	Mechanical(M)	FEM	PYTHON
FLAC3D-TOUGH2MP (Fang et al., 2022)	THM	FEM、IFDM	C++、FORTRAN
3D coupled hydro-mechanical model (Bai and Tahmasebi, 2022)	HM	/	/
COMOSL (Coarita-Tintaya et al., 2023)	M	FEM	MATLAB
CMG (Safari et al., 2023; Laalam et al., 2024)	HM	FDM	/
PETREL (Wang et al., 2024c)	HM	FVM	PYTHON
/	Hydro-mechanical-chemical-biological (HCMB) (Gao et al., 2024b)	/	/
COMSOL (Wang et al., 2024g)	THM	FEM	MATLAB

Table 9
Reviews on geochemical modeling of UHS.

Geochemical process	*Objective*	Application software
Geochemical	Assessing H_2 depletion in a sandstone reservoir through geochemical modeling, the loss of H_2 due to solubility is not significantly affected by pressure and temperature (Bo et al., 2021). Explore the impacts of geochemistry on fluid-carbonate rock contains UHS, H_2 reduction of up to 6.6% in the first year due to fluid-rock reactions, whereas after 500 years of storage, the reduction is expected to be as high as 81.1%(Zeng et al., 2022b). Increasing the temperature and decreasing the salinity increase the disjoining pressure within the hydrogen-brine-calcite and increasing water wettability (Zeng et al., 2022a). Explored the function of oxidative-reduction reactions in UHS, carbonates can initiate more H_2 dissociation and redox reactions (Zhang et al., 2023a). Geochemical processes have little effect on H_2, however utilizing CO_2 as a cushion gas may dissolve calcite and feldspars, increasing permeability and rock porosity (Saeed et al., 2023).	PHREEQC
Bio-geochemical	Microbial activity converts hydrogen into methane and hydrogen sulfide, while gas-water-rock interactions result in a slight decrease in the porosity of reservoir rocks (Hemme and Van Berk, 2018). The growth rate of bacteria is correlated with the sulfate concentration in brine, while the iron ion concentration is the most critical factor influencing the production of H_2S through hydrogen (Laban, 2020). Assessment of bio-geochemical effects on UHS (Jahanbani Veshareh et al., 2022). Assessing H_2 reactivity in UHS; Evaluate the effects of geochemical reactions on cap rock integrity during UHS; Minimal shale minerals dissolution is expected during UHS and hence integrity of seal is preserved against H_2-brine-rock. Geochemical reactions (Tremosa et al., 2023). Analysis of the risks arising from the interactions between microbial activity and geochemical reactions (Wu et al., 2023). Assessing the impact of bio-geochemical on UHS (Elgendy et al., 2023; Rivolta et al., 2024).	CMG
Bio-hydrodynamic	Assessing H_2 loss due to bio-geochemical reactions in UHS (Minougou, 2022). The reservoir's hydrogen-to-methane conversion process is significantly impacted by the abundance of microorganisms (Hagemann et al., 2016).	DUMUX
	Analyzing the impacts of bio-methanation on UHS performance (Wang et al., 2024a). Evaluation of H_2 loss due to methanogenesis (Ali et al., 2022).	CMG
	Evaluating the impact of H_2S generation on UHS (Rosman et al., 2023). Salinity effects on H_2S generation in UHS (Hamdi et al., 2024).	ECLIPSE

and minimum effective stresses. The effect of hydrogen storage operations on the mechanical stability of the formation can then be assessed using the Mohr-Coulomb criterion (Safari et al., 2023; Laalam et al., 2024). While computationally efficient, this method neglects real-time mechanical feedback to the fluid flow, as updates occur only in a single direction. The fully coupled strategy synchronizes the solution of hydromechanical and flow equations within a unified framework. The non-Darcy flow equations are discretized using the finite volume method, while geomechanical deformation is addressed *via* the virtual element method. Key variables—phase pressures, saturations, displacement, and Biot pressure are iteratively updated in a single stiffness matrix at each time step. This approach ensures real-time interaction between fluid dynamics and mechanical responses, enhancing accuracy. While this method provides highly accurate results, it is time consuming and best suited to small scale and relatively simple geometric model (Liu et al., 2024c).

Geochemical and Reactive Transport modeling. Slow geochemical reactions, governed by the subsurface fluid environment (*e.g.,* pressure, temperature, fluid composition, and redox conditions), gradually alter the structure of porous media, affecting hydrogen diffusion, dissolution and purity, while weakening the sealing capacity and long-term stability of geological formations. The core role of Reactive Transport Modeling (RTM) in UHS extends beyond predicting static chemical equilibrium, it serves as a critical bridge coupling fluid hydrodynamics with chemical kinetics to capture the spatiotemporal evolution of the storage system. Current studies focus mainly on solute migration and microbial activities induced by geochemical reactions, where solute migration refers mainly to the damage caused to porous media by mineral dissolution and precipitation (Table 9). However, a fundamental challenge in RTM is capturing the dynamic “feedback loop” where mineral dissolution and precipitation continuously modify the reservoir's pore structure, which in turn redistributes the flow field. PHREEQC geochemical software is widely used for geochemical reaction modeling, and Geochemist's Workbench (GWB) and DUMUX are used for microbial and geochemical reaction modeling. GWB's and PHREEQC thermodynamic database is constantly updated (Hassannayebi et al., 2019). Despite its importance, RTM in UHS currently faces several critical limitations. First, the “upscaling” discrepancy remains significant, as reaction rates measured in laboratory-scale batch experiments often fail to represent field-scale heterogeneity due to preferential flow paths (Cao et al., 2024). Second, while the porosity-permeability relationship is often simplified *via* empirical equations, these models frequently struggle to capture the non-linear permeability evolution caused by localized mineral dissolution or precipitation at pore throats. Furthermore, the scarcity of high-pressure, high-salinity kinetic data remains a primary challenge for accurate long-term predictions.

The practical application of RTM is exemplified in studies integrating thermodynamic and kinetic modeling with experimental data to investigate the dynamic interaction between injected H_2 and porous media. For instance, Gholami (2023) utilized PHREEQC to simulate the geochemical interactions induced by hydrogen injection, revealing that the time-dependent dissolution of carbonates, anhydrite, and halite leads to calcite precipitation, H_2S formation, and long-term pore structure closure due to scale formation. Furthermore, the reduction of pyrite to pyrrhotite is likely to occur at temperatures exceeding 90 °C, which potentially facilitates abiotic H_2S generation. During the injection process, phenomena such as salt diffusion, dry zone formation, and salt precipitation are highly dependent on the salinity and temperature of the formation water, which collectively influence the hydraulic evolution of the reservoir.

The complexity of these coupled phenomena in which fluid transport, phase behavior, and chemical reactions interact underscores the necessity of advancing beyond macro-scale approximations. To accurately capture these localized alterations, researchers are increasingly integrating multi-scale modeling approaches. Laboratory-scale to laboratory-scale numerical simulations can quantify the H_2-water-rock reactions within the reservoir, overcoming the limitations of experimental studies. This is particularly important for predicting hydrogen storage behavior over long time scales and under complex geological conditions. Currently, simulation tools based on thermodynamic and kinetic models (*e.g.,* PHREEQC) allow in-depth investigation of acid-base and redox reactions between hydrogen and minerals (*e.g.,* carbonates, silicates, and sulfates) and their impact on the reservoir

Table 10
Reviews on ML modeling of UHS performance.

Prediction Tasks	Prediction Targets	ML Algorithm	Optimal ML Algorithm
Wettability	Predicting the wettability rocks-minerals-brine-hydrogen system	XGBoost, RF, LGRB, AdaBoost_DT (Vo Thanh et al., 2023)	XGBoost
Trapping Rate	A relationship model between rock structure and hydrogen trapping rates was established using LSF and SVM	LSF, SVM (Zhao et al., 2024a)	SVM
Solubility	Predict the solubility of hydrogen in water; Temperature has a non-linear effect on hydrogen solubility in water.	ANN, RFR, XGBoost, AdaBoost, SVR, LARS, BRR, LR (Zhang et al., 2023a)	ANN、XGBoost
	Predicting hydrogen solubility in water, pressure is the most impactful parameter on the hydrogen's solubility in brine followed by temperature and NaCl salinity	RBF, LSSVM, BBO, CA, ICA, TLBO (Ansari et al., 2022)	RBF + CA
		WNN (Zhu et al., 2022)	/
		XGBoost、SVR、DT (Kalam et al., 2024)	XGBoost
IFT	Predicting the H_2-brine IFT	MLP_LMA, MLP_Adam, GBR, GP (Ng et al., 2022)	MLP_LMA
		BTA, GPR, ENN, Logistic regression (Gbadamosi et al., 2024)	GPR_M2
Adsorption	adsorption in porous bio-derived carbon	SVM, MLP, RBFNN (Rahimi et al., 2021)	SVM
	Hydrogen uptake ability of a wide range of zeolites	ANN (Seyed Alizadeh et al., 2022)	/
	Prediction of hydrogen adsorption in various kerogen types	XGBoost、NGBM、LGBM、RF (Vo Thanh et al., 2024a)	NGBM

Note: Logistic regression boosting (LGRB), AdaBoost with decision trees (AdaBoost_DT), Least squares fitting (LSF), Random forest regression (RFR), Adaptive boosting (AdaBoost), Support vector regression (SVR), Least angle regression (LARS), Bayesian ridge regression (BRR), Linear regression (LR), Radial basis function (RBF), Least square support vector machine (LSSVM)、Biogeography-based optimization (BBO), Cultural algorithm (CA), Imperialist competitive algorithm (ICA), Teaching-learning-based optimization (TLBO), Wavelet neural network (WNN), Decision tree (DT), Multi-layer perceptron using levenberg-marquardt algorithm (MLP_LMA), Multi-layer perceptron using adam optimizer (MLP_Adam), Gaussian process (GP), Bat algorithm (BTA), Elman neural network (ENN), Radial basis function neural network (RBFNN).

environment. These dynamic RTM frameworks are essential as they capture kinetically slow processes, such as halite dissolution, which may only induce significant pore-scale alterations over extended operational timescales.

However, significant discrepancies persist between simulations and experimental observations. Hassannayebi et al. (2019) developed a geochemical model to study H_2 geochemical reactions in UHS, highlighting the equilibrium interactions commonly present in sandstone reservoirs under conditions of 7.5 bar and 40 °C, particularly within the optimal storage period. Bo et al. (2021) developed another geochemical model to assess H_2 loss in sandstone reservoirs. They concluded that sandstone reservoirs are more suitable for H_2 storage than carbonate reservoirs due to their lower reactivity. In carbonate reservoirs, calcite dissolution results in approximately 9.3% H_2 loss. Zeng et al. (2022b) used PHREEQC to evaluate the degree of H_2 loss during H_2-water-rock interactions and showed an increase in H_2 loss from 6.5% to 81.1% over a 500-year storage period, accompanied by calcite dissolution. Both Bo et al. and Zeng et al. incorporated methanogenesis reactions into their computational frameworks. However, Gelencsér et al. (2023) performed static batch experiments on the calcite-H_2 brine system at 100 °C and 105 bar, and found that calcite showed no reactivity.

In contrast, PHREEQC simulations using a general thermodynamic database for the same experiments suggested extensive dissolution of both hydrogen and calcite. By refining the database and excluding methanogenesis reactions, simulation results can be brought within the same order of magnitude as the experimental observations. Consequently, it is recommended to adjust key thermodynamic parameters including equilibrium constants, enthalpies of reaction, and activity coefficients within the model database to better reflect specific geological environments. Complementarily, Saeed et al. (2023) demonstrated the effects of geochemical reactions on H_2, reservoir rock porosity, and permeability alteration during UHS in aquifers. Their PHREEQC simulations over 30 years showed minimal effects of geochemical reactions on H_2, indicating that mineral-fluid stability plays a critical role in hydrogen storage environments. Some researchers have used simulations to study the redox reactions of H_2 in porous formations (Bai et al., 2014). The effects on H_2 solubility and pH are relatively small. However, under high-pressure conditions, the presence of siderite and calcite can lead to H_2 loss through redox reactions acid-base reactions, producing CH_4 from reactions between H_2 and carbonate minerals (Bai et al., 2014; Vo Thanh et al., 2023). Extensive modeling further quantifies these impacts across varying salinities, pressures, and water-rock ratios. Cumulative H_2 loss over a century has been estimated at 8.38%, with 2.31% attributed to reservoir rock reactivity and 6.07% resulting from aqueous diffusion into and reaction within the caprock. In these scenarios, carbonate dissolution emerged as a dominant process leading to substantial H_2 loss, particularly when influenced by methanogenic bacteria. Notably, while reservoir porosity showed a minimal decrease of 0.41%, the porosity of carbonate caprocks increased by 56%, potentially enhancing hydrogen leakage risks (Dodangoda, and P. G, R, 2024).

Despite these findings, discrepancies remain between static simulations (assuming no flow conditions) and dynamic simulations (incorporating fluid flow conditions). This discrepancy highlights another limitation: the reliance on standard thermodynamic databases that may not fully account for the high-salinity and high-pressure conditions specific to H_2 storage, emphasizing the need for site-specific thermodynamic corrections to constrain modeling results with experimental observations.

4.3. *Applications of machine learning methods*

Traditional numerical simulations for UHS face critical limitations in processing large datasets, resolving nonlinear interactions, and optimizing multiphase systems. These bottlenecks drive the adoption of ML as a transformative alternative. ML has demonstrated breakthroughs in subsurface characterization through intelligent identification of heterogeneous structures and multi-physics coupling analysis (Zhan et al., 2022b; Cao et al., 2025). Successful precedents include carbon dioxide geological storage (CGS) optimization (Dai et al., 2020), monitor of mine water inflow (Chen et al., 2021), and scale effects of solute transport parameters (Cao et al., 2024), laying a foundation for ML-driven UHS optimization.

The choice of ML algorithms in UHS modeling is governed by four core principles: data characteristics, physical constraints, computational efficiency, and task-specific requirements (Table 10). For high-dimensional structured data (*e.g.,* hydrogen storage characteristics), ensemble methods like extreme gradient boosting (XGBoost) and **Categorical Boosting** (CatBoost) are prioritized for their efficiency and

Table 11
Reviews on ML modeling of UHS Management.

Prediction Tasks	Prediction Targets	ML Algorithm	Optimal ML Algorithm
Site Selection	Assessment of salt caverns for UHS	KNN、SVM、LightGBM、XGBoost、MLP、CatBoost、GBR、MLR (Derakhshani et al., 2024b)	CatBoost
Hydrogen Production	Hydrogen production technologies from water industries	SVM, GBM, RF, KNN (Kabir et al., 2023)	KNN、RF
MOO	The design of hydrogen saline aquifer storage processes using a machine-learning assisted multi objective optimization protocol	MOPSO (Sun et al., 2024b)	/
UHS and CCS	Using ML for the synergistic optimization of UHS and carbon capture and storage (CCS) to enhance economic benefits and minimize carbon emissions.	MLNN、NSGA-II (Kanaani et al., 2023)	/

Note: Multi-objective particle swarm optimization (MOPSO), Multilayer neural network (MLNN).

precision in handling feature interactions and missing values (Derakhshani et al., 2024b). Small-sample or non-physical datasets, such as rock trapping rate estimation, benefit from support vector machine (SVM) kernel-driven generalization despite limited training data (Zhao et al., 2024a). Complex nonlinear problems (*e.g.,* temperature-pressure-salinity coupling) are best addressed by Artificial neural network (ANN) when sufficient data are available, leveraging their deep architectures to capture intricate relationships (Zhang et al., 2023a). MOO tasks, including economic-environmental trade-offs in storage design, require evolutionary algorithms like Non-dominated sorting genetic algorithm II (NSGA-II) to navigate competing constraints (Table 11) (Kanaani et al., 2023). For uncertainty-aware predictions, Gaussian process regression (GPR) and natural gradient boosting (NGBM) provide probabilistic outputs critical to managing geological heterogeneity in H_2-brine IFT or salt cavern systems (Vo Thanh et al., 2024a).

Building upon these selection principles, the strategic implementation of ML in UHS is elucidated across the following functional domains:

Site Screening and Characterization. Initial site selection strategies typically rely on Multi-Criteria Decision-Making techniques, such as the Analytic Hierarchy Process, which combine expert judgment with quantitative reservoir modeling to evaluate criteria importance. However, to efficiently explore the complex interactions between geological heterogeneity, operational parameters, and biogeochemical reactions, ML has emerged as a vital supportive tool. ML-driven frameworks enable exhaustive sensitivity analyses that are often computationally prohibitive for traditional methods. Consequently, this transition from expert-based qualitative assessment to ML-assisted quantitative evaluation provides a more efficient and accurate approach for UHS site selection. Specifically, the integration of spatial data analysis with deep learning architectures, CNN, has demonstrated superior performance in assessing the hydrogen storage potential of complex structures like bedded salt formations by generating highly accurate suitability maps (Derakhshani et al., 2024a). To balance storage capacity with operational efficiency, generalized workflows now employ high-fidelity simulation datasets to train reduced-order models (ROMs), for instance, this approach successfully identified 3 high-potential saline aquifers from 12 candidates across the Intermountain West region in the United States (Chen et al., 2024). Furthermore, researchers have employed decision trees alongside weighted decision matrices as dual Multi-Criteria Decision-Making methods to evaluate the technical suitability of depleted reservoirs and deep saline aquifers, focusing on critical parameters such as storage capacity, reservoir depth, injectivity, and containment integrity (Higgs et al., 2024). Building on these technical assessments, ML-driven frameworks further extend to predicting dynamic economic indicators including withdrawal efficiency, the production gas-water ratio, and injectivity to enable a comprehensive performance-based ranking. For example, such methodologies were utilized to evaluate 73 saline aquifer candidates, successfully identifying optimal storage locations by balancing long-term operational costs with technical viability (Zhao et al., 2025). In conclusion, the synergy between initial site-specific data collection and subsequent THMC numerical simulations provides the necessary high-fidelity datasets to train ML models. By leveraging these simulation-derived results for intelligent site ranking, this integrated workflow ensures a more reliable screening process that honors both the fundamental physics of hydrogen transport and the advanced predictive capabilities of machine learning.

Safety Assessment and Risk Prediction. The evaluation of caprock integrity, fault stability, and leakage risks is paramount for ensuring the long-term safety of UHS operations. In the absence of extensive field-scale studies, ML models are strategically applied to quantify fundamental parameters such as relative permeability, where GPR has demonstrated superior accuracy based on 130 data points covering variables like gas saturation, porosity, salinity, and pressure differential (Amjadi and Kord, 2025). Data-driven frameworks successfully capture the complex nonlinear relationships between mineralogy, salinity, and interfacial parameters (IFT and contact angles), surpassing traditional linear assumptions that often overlook salinity effects. By integrating these refined parameters into maximum hydrogen column height models, researchers can accurately assess capillary entry pressures (Sekar and Okoroafor, 2025). Furthermore, ROMs trained on 3000 simulation scenarios facilitate long-term leakage assessments across 11 critical parameters, these models reveal that 27% of depleted reservoir scenarios exhibit gas migration within five years—with volumes up to 10^6 ft^3—underscoring the importance of deep formations and low-permeability boreholes for millennium-scale containment (Malki et al., 2025).

System Optimization and Management. Advanced system optimization and management frameworks for UHS prioritize the integration of high-fidelity physical parameters with robust predictive algorithms to maximize storage efficiency. To achieve precise management, researchers have leveraged ML to quantify interfacial properties that govern storage capacity and pore-scale distribution. Regarding hydrogen-brine IFT prediction, Hosseini and Leonenko (2024) demonstrated the superiority of the random forest (RF) model over decision trees (DT), SVM, and multi-layer perceptron (MLP) in processing pressure, temperature, and molality. To further enhance physical consistency. To further enhance physical consistency, Ahmadi (2025) utilized a Physics-Informed Neural Network embedded with thermodynamic constraints, achieving high-precision predictions with errors below 1% across extensive datasets, SHapley Additive exPlanations analysis further identified temperature as the dominant factor influencing IFT. Additionally, Ibrahim (2025) developed ML frameworks using RF and ANN to predict H_2-brine IFT across diverse thermodynamic conditions, including various gas compositions (H_2, CO_2, CH_4) and salt types (NaCl, $CaCl_2$, KCl). By implementing physically meaningful input generalizations, such as NaCl-equivalent salinity and bulk gas properties, the study demonstrated that the RF model could significantly enhance the correlation between input features and IFT, ensuring robust performance across complex chemical environments. To address experimental challenges under extreme conditions, Alshehab and Kamrava (2026) integrated MD simulations (10–50 MPa, 50–250 °C and concentrations of 1–6 mol/kg) with ML algorithms. Among 24 tested algorithms, gradient boosting regression (GBR), multi-layer perceptron (MLP), and XGBoost were identified as the optimal frameworks for predicting H_2- $CaCl_2$ IFT.

In the assessment of wettability and hydrogen adsorption, ML has demonstrated a robust capacity for capturing non-linear behaviors. Nait

Table 12
Comparison of ML Algorithms for UHS.

Algorithm	Computational Efficiency	Robustness	Key Advantages	Limitations
XGBoost	High	High	Handles missing data, automatic feature interaction	Limited support for image/time-series data; sensitive to hyperparameters
CatBoost	High	High	Robust to categorical features, minimal preprocessing	
ANN	Low	Moderate	Model complex nonlinearities, multi-modal data fusion	Requires large datasets; computationally intensive
SVM	Moderate	Low	Small-sample performance, kernel flexibility	Performance degrades with high-dimensional data; high computational cost
RBF	Moderate	Moderate	Localized feature learning; fast training	Struggles with global patterns; requires kernel parameter optimization
CA	Moderate	High	Hybrid optimization with cultural evolution strategies	Limited standalone use; primarily auxiliary for other algorithms
KNN	High	Moderate	Real-time inference; intuitive distance-based learning	Memory-intensive for large datasets; sensitive to irrelevant features
MLP_LMA	Low	High	High-precision convergence; robust to local minima	Computationally expensive; requires expert tuning of LM parameters
GPR	Low	High	Uncertainty quantification, physics-compatible kernels	Computational complexity; unsuitable for large datasets
NSGA-II	Moderate	–	Multi-objective Pareto optimization	No precision metrics; computationally expensive

Amar et al. (2025) utilized a massive dataset of nearly 800 samples to develop an intelligent framework for predicting pure hydrogen contact angles under diverse conditions, including temperatures of 293–353 K, pressures of 0.1–25 MPa, and salinities of 0–3.9381 mol/kg. By comparing extreme learning machine, cascaded forward neural network, and Super Learner models, the study confirmed the superiority of the SL model in capturing intricate feature relationships. Similarly, Nassabeh et al. (2025) compiled 5200 data points from various sources, identifying that the feedforward neural network algorithm outperforms SVM, k-nearest neighbors (KNN), and recurrent neural network in simulating water-hydrogen-rock contact angles due to its superior scalability and robustness to noisy inputs. To align predictions with fundamental surface science concepts. Vo Thanh (2025) proposed an interpretable knowledge-guided ML framework (knowledge-guided CatBoost model) optimized *via* Bayesian optimization and trained on 623 experimental observations. Unlike typical data-driven methods, this approach integrates capillary pressure, wetting rate indices, and interfacial tension into the algorithm. SHAP-based feature importance analysis revealed that substrate type is the most critical factor regulating wettability, followed by pressure and salinity. Furthermore, using the Optimal Index for geological suitability, the study highlighted mica- and quartz-rich reservoirs as the most suitable candidates for UHS. For coal-based storage, Wang et al. (2025b). validated the reliability of general regression neural network and XGBoost in forecasting hydrogen adsorption.

At the level of operational performance evaluation, Vo Thanh (2026) developed a physics-informed extreme gradient boosting model to forecast hydrogen solubility in aqueous solutions, ensuring theoretical consistency by integrating key physical factors such as Henry's Law, the Setchenow effect, and gas compressibility. Shifting from fundamental fluid behavior to reservoir-scale management, Du et al. (2025) utilized advanced ML algorithms to develop surrogate models that significantly enhance computational efficiency for UHS optimization. By employing MOO alongside long short-term memory (LSTM)-based surrogates, the study established a Pareto front that categorizes operational regimes into low-loss/high-storage, balanced, and high-production modes, offering tailored injection-withdrawal strategies for diverse energy demands. To contextualize these findings across the broader landscape of machine learning applications in UHS. Table 12 presents a detailed comparison of various machine learning algorithms and their applications in UHS modeling. It outlines the computational efficiency, robustness, key advantages, typical applications, and limitations of each algorithm, offering insights into their suitability for different tasks and data types. It is important to note that the effectiveness of these algorithms is often constrained by the complex multiscale heterogeneities in hydrodynamic and geochemical behaviors found in UHS systems. Mineral composition, fracture networks, and porosity variations further amplify prediction uncertainties, particularly in systems with spatially varying lithology or reactive transport mechanisms. To mitigate above issues, ML must be trained with sufficient data and physics-based constraints (*e.g.,* mass conservation laws) (Viswanathan et al., 2022). Integrating ML into multi-fidelity simulation frameworks can significantly reduce computational costs while optimizing hydrogen storage efficiency and long-term stability (Wang et al., 2025a). As a complementary approach to enhance the robustness in ML-driven multiscale modeling, MD simulations can be used to analyses hydrogen diffusion in various types of clay minerals (*e.g.,* pyrophyllite, montmorillonite, and beidellite) under varying surface charge behaviors (Ghasemi et al., 2022). It is also possible to evaluate the solubility of hydrogen in brine at different salinities, pressures and temperatures (Zhang et al., 2023a). Concurrently, pore-network models characterize pore connectivity and assess uncertainties in fluid-rock interactions at reservoir scales (Wang et al., 2023b). Together, ML, MD, and pore-scale modeling form a cross-scale method to enhance UHS predictions in complex geological systems.

The evolution of ML in UHS modeling is poised to advance along three key trajectories: multiscale spatiotemporal integration, physics-informed hybrid architectures, and data-efficient learning paradigms. First, gradient-boosted spatiotemporal neural networks are emerging to resolve multiphase flow of UHS in both homogeneous and heterogeneous formations, as demonstrated in aquifer storage simulations (Wang et al., 2025a). Second, deep-learning frameworks, such as CNN, will increasingly leverage multimodal inputs (*e.g.,* reservoir CT images) to directly predict hydrogen trapping efficiency and phase behavior, bypassing computationally expensive pore-network simulations (Zhao et al., 2024a). Third, hybrid models integrating ML with multiscale simulations will address data scarcity by generating synthetic datasets constrained by physicochemical laws, while physics-informed regularization and active learning strategies optimize experimental design and economic-safety trade-offs for uncertainty-critical parameters. Current ROMs based on deep neural networks already exemplify this trend, being over 22,000 times faster than physics-based simulations, with high accuracy in predicting UHS performance in depleted natural gas reservoirs (Mao et al., 2024). Future efforts must prioritize domain-embedded architectures and cross-scale validation, ensuring reliability under complex geological formations heterogeneities. These advancements will enable ML to transition from a purely data-driven tool to a multiscale digital twin framework for optimizing UHS sustainability and operational safety.

Table 13
Comparative table for several available simulators.

Capabilities	PHREEQC	DUMUX	TOUGH	Schelumberger	CMG	COMSOL	OGS
Dimensions	1D	1,2,3D		3D	1,2,3D		
Multiphase–multi-component flow	×	√					×
Thermo-dynamic laws	–	C E, GERG-2008	C E			–	
Non-isothermal flow	×	√					
Molecular diffusion	√						
Mechanical dispersion	×	√					×
Surface Complexa-tion	DDL, Non-edl	–	DDL, CC	–	–	DDL, Non-edl, CC	DD, Non-edl
Ion exchange/ Kinetic mineral precipitation dissolution	√	×	√	×		√	
Bio-chemical reactions	√		REACT	√			
Monod kinetics	√	×	√	×		√	
Time discretiza-tion	–	Back Eueler	I / E	I		Adaptive	I
Fractures	×	√	×	√			
Wells	×	√					N

Note: No (×), Yes (√),Diffuse Double Layer (DDL), Non-Electrostatic mode (Non-edl), Constant Capacitance (CC), Cubic EOS (C E), Implicit (I), Explicit (E), OpenGeoSys (OGS) and.

In summary, the integration of ML algorithms enables a comprehensive multi-scale framework that spans from initial geological site screening and safety risk characterization to dynamic physics-aware operational optimization, thereby ensuring both the technical feasibility and long-term reliability of UHS. While this section focuses on the modeling and evaluation aspects, the essential monitoring technologies required for real-time data integration are discussed in Section 5.

Numerical simulation of UHS is an important tool for studying hydrogen behavior and safety in geological formations. By exploiting the technical strengths of methods such as finite element method, finite difference method and multiphase flow modeling (Table 13), together with the geological engineering integration approach from oil and gas field development, the THMC model can effectively predict hydrogen flow and interactions. In the future, multi-software collaborative simulation or the integration of ML technology is expected to improve simulation efficiency and accuracy while overcoming the limitations of single software tools.

5. Monitoring in UHS

The operational success of future UHS projects will likely be governed by a rigorous Measurement, Reporting, and Verification (MRV) framework, a structured methodology designed to ensure containment integrity and regulatory compliance. Given that large-scale UHS is still in the early deployment phase with limited long-term operational history, establishing a robust MRV framework is essential to bridge the gap between experimental pilots and commercial-scale implementation. This approach allows operators to translate raw monitoring data into actionable safety protocols, drawing conceptual parallels from established subsurface energy systems.

Measurement serves as the primary technical layer, requiring multi-physics data acquisition to resolve complex hydrogen-reservoir interactions. Numerical simulations using the Mohr-Coulomb criterion (zero cohesion assumption) indicate that caprock retains stability under maximum pore pressure after three hydrogen injection cycles, despite inducing 1.6 cm of surface deformation (Bai and Tahmasebi, 2022). However, frequent injection-withdrawal cycles and reservoir heterogeneity (*e.g.,* spatial heterogeneity of porosity/permeability) trigger dynamic redistribution of hydrogen, residual oil, and formation water, thereby compromising pressure stability and hydrogen recovery efficiency (Gao et al., 2024a; Pirrone et al., 2024). Consequently, real-time monitoring of reservoir pressure, temperature, and fluid composition (*e.g.,* H_2/CH_4 ratio) is required to optimize injection rates and cycling schedules, balancing operational efficiency with system safety (Yang et al., 2024a).

To establish an experimental baseline for seismic monitoring, K C et al. (2025) measured the sensitivity of P-wave signatures in Berea sandstone, revealing that P-wave velocity decreased by 3.5% and attenuation increased by 66% as H_2 saturation reached 36%. These results confirm that current four-dimensional seismic techniques are sufficiently sensitive to monitor gas plume migration and detect leakage. Furthermore, in depleted gas reservoirs. Song et al. (2026) proposed a dynamic monitoring method using triple-detector pulsed neutron–neutron logging. By utilizing a differential ratio response corrected for temperature, lithology, and shale content, this method provides accurate H_2 saturation measurements with typical errors of ±5%, offering a reliable technical foundation for UHS safety assessment. Beyond point-scale measurements, the dynamic behavior of hydrogen in heterogeneous reservoirs necessitates multi-physics monitoring to resolve limitations of single geophysical methods. Gravimetric methods infer spatial hydrogen distribution through mass variation, while Electrical Resistivity Tomography (ERT) tracks migration pathways and saturation evolution based on electrical property contrasts. Full Waveform Inversion (FWI) further enhances resolution by imaging reservoir structures and pressure perturbations through elastic wave velocity fields (Pfeiffer et al., 2016a; Masaya, 2024). The combined application of Continuous Active Source Seismic Monitoring (CASSM) and Time-Lapse Full Waveform Inversion (TLFWI) quantifies velocity field differences induced by hydrogen-water coexistence in fractured reservoirs. TLFWI coupled with White's model additionally resolves spatiotemporal distributions of free-phase hydrogen and its saturation-velocity coupling mechanisms (Yang et al., 2024a). Complementary to geophysical tools, quantifying microbial hydrogen depletion (*e.g.*, methanogenesis, sulfate reduction) requires multi-parameter geochemical analysis. Methanogenesis monitoring prioritizes temporal variations in CH_4 content over H_2/CO_2 concentrations to avoid cross-interference from acetogenesis. Although H_2S and acetate levels serve as markers for sulfate reduction, their gaseous concentrations may be systematically underestimated due to dissolution-precipitation processes. To overcome the limitations of single-parameter indicators, stable isotope analysis of H_2, CO_2 and CH_4 gases must be monitored to provide a reliable verification of gas inventory and biogeochemical stability (Lord, 2009; Truche et al., 2010). In addition to geochemical shifts, the geomechanical response of the reservoir serves as a critical indicator of containment integrity. Surface monitoring through Interferometric Synthetic Aperture Radar (InSAR) captures micron-scale deformation, such as the 2 cm uplift and microseismic events linked to pore pressure increases (Verdon et al., 2013; Ramesh Kumar et al., 2023). While these surface signals provide an indirect proxy for reservoir geomechanical changes, their interpretability is complicated by the mechanical damping effects of the overburden. Nevertheless, since only ~25% of reservoir deformation typically propagates to the surface (with magnitudes often ≤1 mm) due to the large scaling ratio between reservoir depth and lateral dimensions, conventional surface-only monitoring may lack the necessary

sensitivity to resolve deep-seated pressure perturbations (Tenthorey et al., 2024) To address this attenuation effect, measurement strategies must integrate subsurface diagnostic tools, such as pressure hysteresis analysis for closed reservoirs, to provide direct evidence of gas leakage through periodic lag curves (Feldmann et al., 2016).

The Reporting phase involves synthesizing multi-source datasets spanning the entire UHS value chain, including cyclic injection-withdrawal volumes, cushion gas dynamics, methane co-production, compression energy intensity, hydrogen losses, reservoir attributes, facility/wellbore metadata, and transport intensity, into transparent records of reservoir behavior and full-cycle operational performance. This synthesis is performed with explicit alignment to international standards such as the open footprint environmental model and open subsurface data universe subsurface schema, enabling cross-platform interoperability, seamless integration with open footprint environmental reporting frameworks, and support for downstream end-use modeling (*e.g.*, industrial, power, and mobility applications) (Muktevi et al., 2025). Within this standardized framework, ML serves as a pivotal bridge for extracting implicit relationships, enabling high-fidelity earthquake detection and reservoir leakage characterization (Gao et al., 2024a). However, the efficacy of purely data-driven ML models is often limited by the spatial variability and scale effects inherent in complex geological formations, which preclude direct parameter measurement. To resolve these uncertainties, Data Assimilation (DA)-based inverse modeling is widely employed (Persova et al., 2021). By utilizing algorithms such as ensemble kalman filters or markov chain monte carlo (Zhang et al., 2016), DA facilitates the reporting of dynamic reservoir states by continuously updating forward simulations with actual measurements (Luo et al., 2015; Zhao et al., 2022a; Luo et al., 2024). For example, recent quantitative reporting has combined pulsed neutron logging responses with probabilistic inversion to solve for component volume fractions while quantifying uncertainty *via* monte carlo simulations (Pirrone et al., 2024). As operational experience grows, these surrogates bypass the computational intensity of traditional physics-based simulations, allowing for real-time performance evaluation and inventory tracking within the MRV framework (Zhan et al., 2022a; Cao et al., 2025).

The reliability of a UHS project depends on Verification, which ensures that the monitoring data used for safety reporting is both accurate and representative. However, the quality of this verification is governed by the spatial and temporal resolution of the monitoring network (Rajabi et al., 2018). To capture a complete geomechanical and geochemical profile, a strategic multi-layer deployment is necessary: sensors placed above the reservoir detect caprock integrity and leakage signals, while internal strain gauges and micro-seismic arrays track localized deformation and induced seismicity (Nicol et al., 2022; Okoroafor, 2024). Because sensor deployment is both costly and technically challenging, the design of these networks must be mathematically optimized to maximize their information value (Chen et al., 2022). In the highly non-linear and uncertain subsurface environment of UHS, entropy-based criteria may offer an effective strategy for identifying optimal sensor layouts. For instance, relative entropy could be utilized to measure the potential reduction in uncertainty by evaluating the divergence between prior and posterior model states (Huan and Marzouk, 2013). Alternatively, conducting entropy analysis on monte carlo simulation results within a MOO framework presents a promising approach to distinguish between effective and redundant information, thereby prioritizing the most critical data points (Li et al., 2012).

In summary, the transition from experimental pilots to commercial-scale UHS requires a standardized MRV framework to ensure safety and transparency. Future efforts should focus on synthesizing multi-source monitoring observations into standardized, open-access datasets to bridge the current data gap. By establishing a rigorous verification process that adapts established CCS protocols, such as ISO 27914 to the specific requirements of hydrogen storage, the industry can ensure containment integrity and regulatory compliance (Standardization, I.O.f, 2017). This integrated approach, moving from precise Measurement to verified Reporting, provides the essential technical foundation for the long-term operational reliability of UHS.

6. Multi-objective optimization for safety and economic trade-offs in UHS

Research on UHS focuses on ensuring safety and economic viability. This is achieved by addressing stress evolution, fault reactivation, caprock integrity, and gas-water interactions, while also optimizing storage capacity, injection rates, and cycles. Lessons from UGS and CCS are being integrated to balance safety and economics, avoiding the risks of excessive cost cutting.

6.1. Safety of UHS

6.1.1. Hydrogen migration and stress path evolution

The main difference between hydrogen storage and other energy storage methods lies in hydrogen's low density and high mobility. Hydrogen gas properties govern its migration behavior in subsurface reservoirs and critically influence stress path evolution during injection/withdrawal cycles (Heinemann et al., 2021a; Burtonshaw et al., 2024). Hydrogen migration is governed by its low density, viscosity, and high mobility, which promote vertical buoyancy-driven accumulation at the reservoir top and horizontal spreading (Bai and Tahmasebi, 2022). Analogous to hydrocarbon reservoirs, structural traps (*e.g.,* anticlines, faults) and stratigraphic traps (*e.g.,* salt domes, unconformities) or abrupt lithological transitions may impede vertical migration, causing discontinuous hydrogen distribution. Additionally, injection pressures can induce localized hydrogen accumulation near wellbores, while high mobility increases risks of horizontal spread and gas loss (Ansari et al., 2022).

The change in pore pressure reshapes the stress field and the mechanical response of the rock is primarily influenced by the stress path effect. Based on the principle of effective stress, effective stress decreases during injection and increases during withdrawal, causing the stress path to approach the rock failure envelope. For reservoirs with a wide lateral distribution, where the transverse scale is much larger than the thickness, lateral strain is typically neglected. In addition, because gas reservoirs are deeply buried, the total vertical stress changes very little under the pressure of the overlying rock, and the change in total vertical stress due to pore pressure variation is considered negligible. Mechanically, this behavior arises because the top of the model represents free ground, allowing the rock mass to expand freely in the vertical direction. However, lateral displacement constraints on both sides of the model restrict the horizontal expansion of the rock mass. Therefore, the theoretical relationship between total lateral stress and pore pressure is shown in Eq.22 (Jia et al., 2023).

$$\Delta\sigma_{\mathrm{H/h}} = \alpha\frac{1-2\nu}{1-\nu}\Delta p = \beta\Delta p \tag{22}$$

Where, $\Delta\sigma_{\mathrm{H/h}}$ represents the change in total stress, ν represents Poisson's ratio, Δp represents the change in pore pressure, and β represents the stress path coefficient, which is further defined as $\beta = \alpha\frac{1-2\nu}{1-\nu}$.

Stress changes significantly affect pore pressure, which directly affects pore volume and facilitates hydrogen migration and diffusion. While temperature has a greater effect on the stress field than on pore pressure in CCS, similar cooling effects from hydrogen injections reduce compressive stress, although the overall temperature effect on pore pressure remains uncertain. Long-term geochemical effects, over hundreds of years, increase fracture widths, weaken rock properties, and expand stress disturbance zones (Gao et al., 2024b).

6.1.2. Caprock integrity

The caprock serves as the primary barrier for UHS, preventing vertical leakage through three interdependent mechanisms: capillary

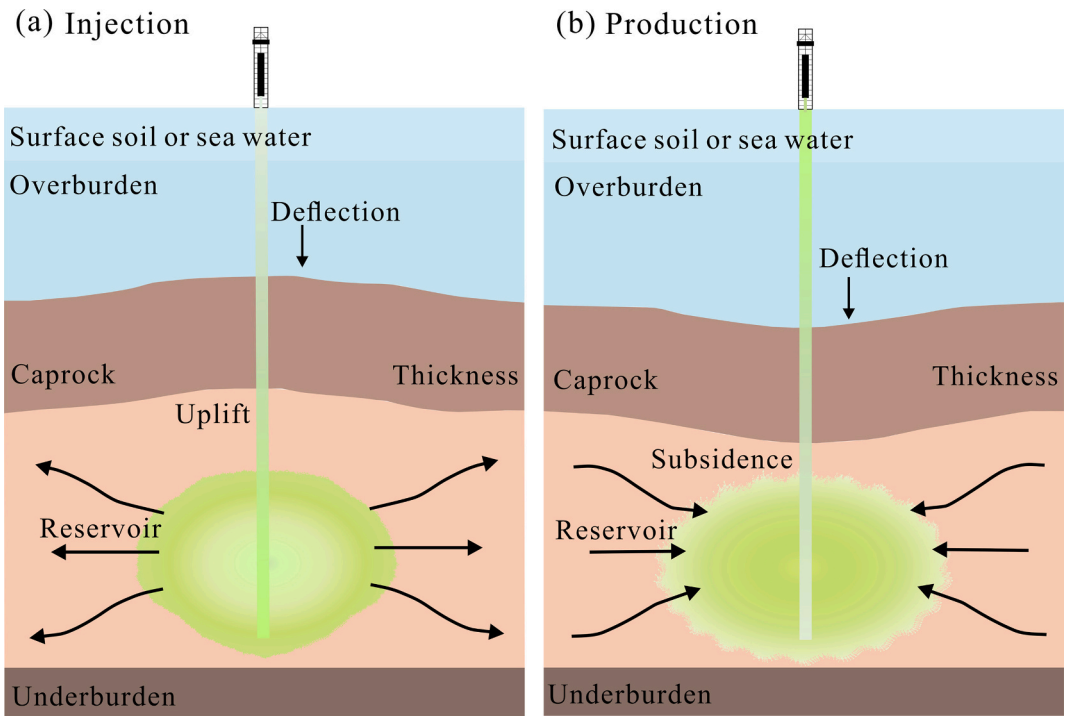

Fig. 9. Caprock bending deformation induced by (a) production, and (b) injection (bending beam effect) (Wen et al., 2024a).

sealing (short-term), chemical sealing (long-term reactivity), and mechanical sealing (injection/production stresses). Below we define each mechanism, contrast their spatiotemporal roles.

The capillary sealing mechanism relies on capillary pressure, which is influenced by cap layer thickness and pressure, as well as factors such as wettability, interfacial tension, organic acid concentration, and total organic content (TOC). Higher pressure and lower temperature enhance sealing efficiency, while elevated TOC reduces hydrogen column height (Hosseini et al., 2022). Shale caprocks trap hydrogen more effectively than CO_2 due to higher hydrogen-water interfacial tension (Cui et al., 2024). For caprocks thicker than 50 m, hydrogen leakage rates drop below 3 kg/m^2/year. Pore network models predict lower leakage rates than capillary bundle models by accounting for small-channel shielding effects (Wang et al., 2024b).

Chemical sealing involves mineral-fluid interactions altering caprock properties. Short-term experiments (96–960 h, 40–50 °C, 100–150 bar, hydrogen concentrations of 50% and 100%) detected no mineral changes using X-ray diffraction, Raman spectroscopy, field emission scanning electron microscopy and energy dispersive X-ray spectroscopy (Chiodoni et al., 2024). However, long-term hydrogen exposure (>1000 days) modifies pore structures. Claystone porosity decreases by 17.3% in the Zaosie anticline but increases by 64.9% in the Chabowo anticline, while mudstone porosity rises by 7.56–11% (Labus and Tarkowski, 2022). These clay minerals introduce uncertainty in sealing capacity through the adsorption of hydrogen (Gut, 2017). Based on the interlayer charge distribution and interlayer cation study, when the pore size exceeds 2 nm, the hydrogen diffusion coefficient of clay minerals does not show significant changes (Ghasemi et al., 2022). In contrast to traditional brine environments, shale samples exposed to a salt-free environment at 6.9 MPa hydrogen pressure showed minimal changes in porosity and permeability at 10 and 45 days. However, by 90 days, porosity and permeability increased by approximately 80% and 120%, respectively. Micro-fractures induced by hydrogen exposure may accelerate hydrogen loss (Ajibona and Pandey, 2024). From a geochemical perspective, the amount of hydrogen penetrating the caprock is typically less than 1% of the stored volume and only affects the caprock a few meters above the reservoir. The dissolution of all

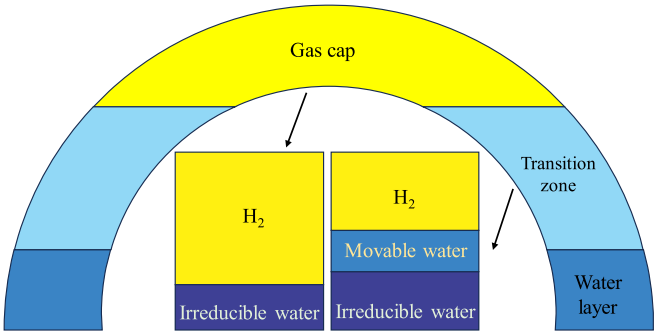

Fig. 10. Evolution of the reservoir gas-water interface (Wang et al., 2023a).

tested shale minerals is also below 1% over 30 years. Therefore, geochemical interactions between hydrogen, brine, and shale are unlikely to affect the integrity of the caprock (Zeng et al., 2023).

Mechanical sealing prevents failure during hydrogen injection/production. Overpressure generates bending stresses in the caprock (Fig. 9), governed by maximum deflection of the caprock (Eq.23) and the maximum bending stress on the top surface of the bending beam (Eq.24) (Young et al., 2002).

$$\Delta H/H = C_m \Delta p \tag{23}$$

Where, Hrepresents the initial thickness of the reservoir, $C_m$represents the uniaxial compression coefficient of the reservoir, $C_m = \frac{(1+\nu)(1-2\nu)}{E(1-\nu)}$.

$$\sigma_{\max} = 6M_{\max}/\mathrm{h}^2 \tag{24}$$

Where, $M_{\max}$ is the maximum bending stress on the top surface of the beam, h is the thickness of the caprock bending beam.

Hydrogen exposure for 1 to 5 days under high pressure and saline conditions reduces dynamic Young's modulus and Poisson's ratio, increasing deformation susceptibility (Aluah et al., 2024). Under deep high-temperature conditions, the effect of hydrogen on the mechanical

properties of rocks (*e.g.*, Young's, Poisson's ratio, and fracture toughness) is limited, with changes of less than 10%. The overall impact on inelastic axial strain is less than 1% after 10 cycles. In intermediate-depth reservoirs, the influence is minimal or negligible. Crack initiation and propagation are key processes in rock deformation (Nath et al., 2024). However, creep accelerates crack closure and is a critical factor in the permanent deformation of the caprock under long-term loading (Zhang et al., 2024a). When pore pressure exceeds fracture toughness, high-pressure hydrogen injection can cause critical fractures in the caprock. The injected hydrogen accumulates beneath and diffuses into the caprock, which increases capillary pressure and forms shrinkage cracks. In biological environments, subcritical fractures can form even at low injection pressures (Dilshan et al., 2024b). The fluid pressure acting on the caprock or fault must remain below the fracture pressure.

6.1.3. Evolution of the reservoir gas-water interface

The dynamic evolution of the gas-water interface and water intrusion can reduce gas permeability and lead to the "water blocking gas" effect (Naseer, 2023). Considering the RPH effect, the gas-water transition zone expanded by 30%, and the peak volume of gas-containing pores in the water zone increased by 1.48 times. Ignoring the RPH effect led to a 19.73% overestimation of the utilization rate of the gas-containing pore space (Liu et al., 2024c). The evolution of the gas-water interface has a significant impact on hydrogen productivity (Fig. 10) (Shi et al., 2023), frequent hydrogen injection-production cycles increase interface migration and redistribution, resulting in reduced recovery rates. Gravity assisted hydrogen injection can enhance recovery by creating a gas-rich zone to displace water and enrich hydrogen, reducing migration and water intrusion while improving recovery efficiency (Sun et al., 2023).

6.2. Economic analysis of UHS

6.2.1. Upper and lower pressure limits of the geological formations

Increasing the upper pressure limit enhances storage capacity and peak shaving capability, while reducing the lower pressure limit expands the working pressure range, improving overall utilization efficiency (Kanaani and Sedaee, 2022). Pressure control and optimization are crucial for maintaining the mechanical stability of geological formations. Based on UGS experience, porous reservoirs have a maximum pressure coefficient of 1.4 to 1.8, while salt caverns should not exceed 80% of the failure pressure, a minimum operating pressure of 30 to 40% of the vertical roof stress is recommended to prevent tensile failure (Liu et al., 2024b).

The upper pressure limit of geological bodies is determined by the load-bearing capacity of the overburden and faults, assessed using indicators such as fracture pressure and shear safety index. Optimizing the lower pressure limit requires balancing hydrogen productivity and preventing water intrusion, focusing on factors such as injection production volume and storage capacity. Determining the optimal upper and lower pressure limits for hydrogen storage is a complex, multifactorial process (Luboń and Tarkowski, 2023), MOO and Monte Carlo analysis can help achieve a balance between UHS stability and efficiency, ensuring long-term reliability (Alessa et al., 2022).

6.2.2. Cushion gas

Cushion gas is essential for optimizing UHS by maintaining formation pressure, suppressing water intrusion, cushion gas enhances the efficiency of utilizing existing capacity (Huang et al., 2023b), and mitigating hydrogen losses (up to 15.5% without cushion gas) (Sainz-Garcia et al., 2017; Heinemann et al., 2021b; Kanaani et al., 2022). A sufficient volume of cushion gas limits the impact of capillary pressure on gas flow behavior (Wang et al., 2022b; Wang et al., 2022a), reducing the potential for viscous fingering and lateral spreading between hydrogen and fluids (Kanaani et al., 2022; Abdellatif et al., 2023). Reservoir volume depends on reservoir type: aquifers require more cushion gas than depleted hydrocarbon reservoirs (Delshad et al., 2022a; Delshad et al., 2022b). Key selection criteria include gas density, adsorption capacity, and compatibility with reservoir type (Zamehrian and Sedaee, 2022).

N_2 is the most effective cushion gas due to its low density contrast with hydrogen, minimizing gravity segregation and achieving 91% hydrogen recovery (73% without cushion gas) (Huang et al., 2023a). **In fractured media,** CH_4 accelerates pore space pressurization, reducing the gas volume required by 30.3% at 1000 psi, it improves brine displacement by 28.3%, and this enables more efficient sweeping of water in the porous media (Mirchi et al., 2023)(Mirchi et al., 2023). CH_4's adsorption on clay minerals further reduces hydrogen retention, but its intermixing with hydrogen may lower purity (Luo et al., 2019; Raza et al., 2022). Thus, CH_4 is more efficient as a cushion gas compared to N_2 and CO_2 (Saeed and Jadhawar, 2023; Saeed and Jadhawar, 2024b).

CO_2 presents trade-offs, CO_2 presents some trade-offs. While its high solubility in brine risks environmental leakage (86–87% co-produced during extraction) (He et al., 2024), it reduces hydrogen adsorption on mineral surfaces. In condensate reservoirs, CO_2 boosts condensate yield but shows limited impact on hydrogen recovery compared to N_2 (Zamehrian and Sedaee, 2022).

Reservoir type critically influences performance. Seasonal UHS in depleted oil and gas reservoirs achieves a hydrogen recovery rate of 87% in the gas zone compared to 77% in the oil zone and 49% in the water zone. Therefore, the gas zone is the preferred option for UHS (Lysyy et al., 2021), hydrogen storage in deeper geological structures with higher permeabilities requires less cushion gas (Heinemann et al., 2021b).

N_2 and CH_4 are the most effective cushion gases for minimizing mixing and improving storage efficiency, with N_2 being the most efficient due to its lower density contrast with hydrogen (Kanaani et al., 2022; Abdellatif et al., 2023). Hydrogen recovery decreases as the molecular weight of the cushion gas increases, and further research is needed to determine the suitability of CO_2 as a cushion gas (Zhang et al., 2024b).

6.2.3. Injection and production gas rate and cycle

The efficiency and safety of UHS systems depend critically on balancing injection/production rates, cycle duration, and frequency. High injection rates increase pressure fluctuations, raising risks of tensile failure and seismic activity during production (Liu et al., 2024b). Although higher rates enhance hydrogen saturation in fractures, they promote gas fingering near wellheads, leading to hydrogen loss (Sainz-Garcia et al., 2017; Luboń and Tarkowski, 2020; Zamehrian and Sedaee, 2022; Malki et al., 2024). Conversely, moderate rates minimize both capillary and viscous fingering, which tends to reduce leakage risks (Bagheri et al., 2023).

Seasonal storage in aquifers shows 24-month cycles achieve higher recovery efficiency (25.4%) than 36-month cycles (17.8%) (Wang et al., 2024c). Increasing the injection rate during short stages can help to limit the effects of gravity segregation (Kanaani et al., 2022). Rapid cycling improves hydrogen recovery through reduced time for matrix penetration and microbial degradation (Zamehrian and Sedaee, 2022; Gao et al., 2024b), though excessively frequent cycles compromise system stability compared to seasonal operations (Coarita-Tintaya et al., 2023). A key trade-off exists: prolonged injection phases increase diffusion losses, while extended production phases (3× injection duration) improve storage efficiency (>85%) (Luboń and Tarkowski, 2023).

In the early part of the production cycle, rapid molecular diffusion leads to higher gas mixing (Mahdi et al., 2021). Initial cycles exhibit high hydrogen purity during early withdrawal, but purity declines progressively. Cumulative efficiency improves with repeated cycles due to saturation buildup near wellbores (Saeed and Jadhawar, 2023; Saeed and Jadhawar, 2024b). Microbial activity primarily affects early cycles, diminishing as geochemical equilibrium becomes established (Gao et al.,

2024b).

Increased injection/withdrawal frequency (FHIW) induces pronounced “seepage step” and “seepage peak” phenomena during cycling operations, with amplification of these effects at higher frequencies, this frequency dependence extends to temperature/pressure extremes – maximum values increase while minimum values decrease with rising FHIW (Wang et al., 2024g). Hydrogen loss ratios exhibit positive correlation with FHIW, while excessive cycling elevates tensile failure risks through repeated pressure cycling (Liu et al., 2024b).

Rapid injection/production cycles with optimized durations exhibit two opposing effects on UHS performance: enhanced near-wellbore hydrogen saturation *versus* accelerated gas migration risks (Zamehrian and Sedaee, 2022; Jadhawar and Saeed, 2024). Shorter cycle intervals and increased storage frequency mitigate hydrogen diffusion losses by progressively increasing saturation around the wellbore. To balance these effects, a hybrid strategy combining medium flow rates and staged rapid injection maximizes recovery efficiency. Extended initial filling phases further improve long-term storage capacity by establishing stable saturation profiles prior to cyclic operations (Luboń and Tarkowski, 2023).

6.3. Multi-Objective Optimization in UHS

The development of conventional oil/gas reservoirs prioritizes static resource recovery metrics (*e.g.,* maximizing oil production). In contrast, UHS requires dynamic MOO integrating storage capacity, injection-withdrawal efficiency, gas purity, and leakage risks, while coupling economic indicators (*e.g.,* net present value (NPV)) with safety constraints (*e.g.*, hydrogen diffusion control). Furthermore, hydrogen's significantly stronger gravity segregation effects in aquifers compared to hydrocarbons necessitate a more rigorous characterization of fluid dynamics. This paradigm shift from single-resource exploitation to coupled “storage-economy-safety” objectives highlights the urgent need for advanced multi-physics modeling.

Traditional reservoir simulations face computational bottlenecks in addressing UHS cyclic operations. To address this, researchers have drawn inspiration from the temporal modeling capabilities of LSTM surrogate models in the oil and gas sector (Zhuang et al., 2024). However, hydrogen's high diffusivity and distinct rock-fluid interactions necessitate the integration of spatial-temporal gradient operators from flow-diffusion equations as physical constraints. By integrating CNN-LSTM architectures with physics-informed spatiotemporal gradient regularization, the gradient-boosted spatiotemporal neural network framework and its variant enables high-precision, multivariate field predictions (pressure, saturation, and concentration) in heterogeneous aquifers, significantly improving the computational efficiency and generalization of UHS numerical simulations (Wang et al., 2025a).

Though hydrocarbon optimization has achieved a paradigm shift from full-physics models (weeks of computation) to surrogate models (95% efficiency improvement) (Zhuang et al., 2024). In optimizing the UHS and CCS processes, the reservoir model is first established to simulate the operational process, the MLNN-NSGA-II algorithm has been employed to perform MOO of hydrogen recovery, CO_2 storage, and NPV. Under this framework, when prioritizing hydrogen recovery as the maximum objective function, the CO_2 storage volume, hydrogen recovery rate, and NPV reach 28,380 t, 95.78%, and − 43.17 MS, respectively (Kanaani et al., 2023).

In emphasizing the operational costs of UHS, GA is used to optimize operational parameters such as the type of cushion gas, H_2 injection rate, gas production rate, and injection-production cycle intervals to maximize NPV. After optimization over 50 generations with 50 individuals, the results indicate that selecting hydrogen as the primary cushion gas, with a small amount of carbon dioxide used, allows for hydrogen recovery purity ranging from 50% to 99.9%. Hydrogen is injected at the maximum safe rate, achieving a recovery rate between 81% and 96%. Over a 30-year period, a net profit of 15 billion USD is expected (Amiri et al., 2024). However, achieving such substantial economic performance in real-world applications requires moving beyond simplified reservoir assumptions toward a more comprehensive understanding of complex subsurface dynamics. Future research priorities should include incorporating high-fidelity 3D heterogeneous geo-models, including stochastic fracture networks and fault-seal integrity, to optimize MOO techniques, as well as advancing adaptive optimization algorithms capable of resolving the multi-objective conflict between renewable energy intermittency and geomechanical stability to generate robust Pareto-optimal operational strategies.

7. Summary and outlook

This article reviews advancements in geomechanics and multiphysics-coupling for UHS, highlighting key challenges and future research priorities in THMC processes. It discusses how these advancements contribute to safer and more efficient UHS strategies by maximizing storage efficiency, minimizing risks, and supporting the transition to low-carbon energy systems.

Prior studies indicate that cyclic injection-extraction processes significantly alter reservoir permeability and mechanical stability by reducing the critical stress of rocks and promoting microcrack propagation. Low-permeability reservoirs exhibit stress sensitivity linked to fracture networks, while faults with low permeability may reduce seismic risks. Geochemical analyses suggest that while reservoir rocks such as shale and mudstone show minimal reactivity with hydrogen, microbial activity can threaten reservoir integrity and environmental safety through biofilm clogging, H_2S generation, and mineral dissolution. In multiphysics-coupling analysis, weak coupling methods and continuous-discontinuous models effectively simulate fracture-matrix co-evolution, with long-term stress evolution identified as critical for storage stability. ML improves predictive accuracy by correlating porosity-permeability relationships with other geomechanical parameters, while multi-objective optimization such as adjusting injection-extraction parameters, optimizing cushion gas composition (*e.g.,* methane and N_2 mixtures), and deploying monitoring wells enhances both safety and efficiency.

Despite these advancements, several limitations remain:

(1) THMC models often rely on idealized boundary conditions, failing to fully capture the random effects of fractures in heterogeneous geological formations, limiting model adaptability and accuracy.
(2) Hydrogen-water-rock interaction databases are primarily based on laboratory-scale studies, that lack *in-situ* and long-term monitoring data, which reduces their reliability for practical applications.
(3) Machine learning models remain limited in interpretability, and further research is needed to incorporate physical constraints, improving their credibility and predictive capabilities.

To address these challenges, we propose the following key research directions:

(1) Multiscale experimental investigation in heterogeneous geological formations.

Cyclic hydrogen injection/extraction induces fatigue damage, crack propagation, and stress redistribution in rock formations. Microbial-geochemical interactions alter both permeability and mechanical strength, where increased permeability due to fractures may enhance storage capacity but also weaken shear/tensile strength, increasing leakage risk. Multiscale models that integrate continuous/discontinuous media are essential for predicting pore-fracture evolution and its impact on geomechanics. Future work should focus on experimental validation of rock fatigue behavior, fracture-fluid interactions, and fault stability under cyclic loading to develop high-precision geomechanical models.

(2) Establishing a geochemical reaction mechanism database.

Redox reactions and microbial metabolism (*e.g.,* H_2 conversion to CH_4/H_2S) alter rock porosity, permeability, and mechanical strength, increasing risks of hydrogen leakage and contamination. Additionally, biofilm formation and mineral precipitation may clog pores, which could storage efficiency. To quantify these interactions under subsurface conditions, future research should integrate experimental studies, numerical simulations, and field-scale monitoring to assess long-term impacts on reservoir stability and hydrogen purity.

(3) Multiscale modeling and simulations.

Advanced simulations must bridge micro-scale mineral reactions to reservoir-scale stress evolution. This may include developing upscaling relationships, whereas hybrid multiscale method alternatives may also be considered (Scheibe et al., 2015). Developing efficient coupled models, enhanced by physics-guided machine learning, will improve predictions of hydrogen migration and storage stability.

(4) Multi-objective optimization strategies for UHS.

MOO for UHS must balance safety, cost efficiency, and real-time monitoring. Safety necessitates mitigating risks (*e.g.,* fracture propagation and caprock failure), while cost efficiency requires minimizing operational expenses and maximizing storage capacity. High-precision monitoring technologies provide critical data to support dynamic regulation. Integrating coupled process models with physics-constrained ML will enable adaptive optimization of safety and cost efficiency within controlled risk thresholds.

(5) Optimizing UHS monitoring networks with inversion and ML.

Future UHS monitoring research should prioritize multi-parameter sensors, real-time geophysical imaging, and inversion techniques to optimize data use. Integrating physics-guided ML (*e.g.,* probabilistic inversion, ensemble smoothing) will improve hydrogen migration tracking, reservoir stability analysis, and leakage detection. This approach establishes an efficient data-driven framework for long-term safety and operational optimization.

Nomenclature

UHS	Underground Hydrogen Storage
THMC	Thermal-Hydraulic-Mechanical-Chemical
ML	Machine Learning
MOO	Multi-Objective Optimization
H_2	Hydrogen
CO_2	Carbon Dioxide
CH_4	Methane
CAE	Computer-Aided Engineering
H_2S	Hydrogen Sulfide
MD	Molecular Dynamics
RF	Random Forest
AI	Artificial Intelligence
UGS	Underground Gas Storage
CAES	Compressed Air Energy Storage
AE	Acoustic Emission
SEM	Scanning Electron Microscopy
X-CT	X Ray Computed Tomography
NMR	Nuclear Magnetic Resonance
DIC	Digital Image Correlation
CFF	Coulomb Failure Function
N_2	Nitrogen
μCT	X-Ray Computed Micro-Tomography
THC	Thermal-Hydraulic-Chemical
RTM	Reactive Transport Modeling
OGS	OpenGeoSys
GAN	Generative Adversarial Network
HT	Hydro-Thermodynamic
FVM	Finite Volume Method
FEM	Finite Element Method
FDM	Finite Difference Method
HM	Hydro-Mechanical
ICGT	Imperial College Geomechanics Toolkit
HCMB	Hydro-Mechanical-Chemical-Biological
GWB	Geochemist's Workbench
XGBoost	Extreme Gradient Boosting
LGRB	Logistic Regression Boosting
AdaBoost_DT	AdaBoost With Decision Trees
LSF	Least Squares Fitting
SVM	Support Vector Machine
CGS	Carbon Dioxide Geological Storage
ANN	Artificial Neural Network
RFR	Random Forest Regression
RF	Random Forest
KNN	K-Nearest Neighbors
AdaBoost	Adaptive Boosting
SVR	Support Vector Regression
LARS	Least Angle Regression
BRR	Bayesian Ridge Regression
LR	Linear Regression
RBFNN	Radial Basis Function Neural Network
DT	Decision Tree
GBR	Gradient Boosting Regression
MLP	Multi-Layer Perceptron
MLP_LMA	Multi-Layer Perceptron Using Levenberg-Marquardt Algorithm
MLP_Adam	Multi-Layer Perceptron Using Adam Optimizer
GP	Gaussian Process
RBF	Radial Basis Function
LSSVM	Least Square Support Vector Machine
BBO	Biogeography-Based Optimization
CA	Cultural Algorithm
ICA	Imperialist Competitive Algorithm
TLBO	Teaching-Learning-Based Optimization
BC	Boundary Conditions
WNN	Wavelet Neural Network
LSTM	Long Short-Term Memory
MRV	Measurement, Reporting, and Verification
GBM	Gradient Boosting Machine
MLNN	Multilayer Neural Network
GPR	Gaussian Process Regression
NSGA-II	Non-Dominated Sorting Genetic Algorithm II
BTA	Bat Algorithm
ENN	Elman Neural Network
LR	Logistic Regression
MOPSO	Multi-Objective Particle Swarm Optimization
BP	Back Propagation
CNN	Convolutional Neural Network
TOC	Total Organic Content
RPH	Relative Permeability Hysteresis
CMG	Computer Modeling Group
FHIW	Increased Injection/Withdrawal Frequency
NPV	Net Present Value
ERT	Electrical Resistivity Tomography
FWI	Full Waveform Inversion
CASSM	Continuous Active Source Seismic Monitoring
TLFWI	Time-Lapse Full Waveform Inversion
SRB	Sulfate-Reducing Bacteria
MIC	Microbially Influenced Corrosion
MICP	Microbial Induced Carbonate Precipitation
ST	Stress Tensor
DDL	Diffuse Double Layer
Non-edl	Non-Electrostatic model
CC	Constant Capacitance

Declaration of competing interest

The authors declare that they have no known competing financial interests or personal relationships that could have appeared to influence the work reported in this paper.

Acknowledgments

This work was funded by the National Key Research and Development Program of China (No.2024YFC3713800), the National Natural Science Foundation of China (No.U2267217, No.42141011), the Shandong Key Water Conservancy Science, and Technology Project (No.2024370203001957). The work of coauthor Hung Vo Thanh was partially supported by JSPS KAKENHI Grant Number 25K17986.

Data availability

Data will be made available on request.

References

Abdellatif, M., Hashemi, M., Azizmohammadi, S., 2023. Large-scale underground hydrogen storage: Integrated modeling of reservoir-wellbore system. Int. J. Hydrog. Energy 48 (50), 19160–19171. https://doi.org/10.1016/j.ijhydene.2023.01.227.

AbuAisha, M., Rouabhi, A., Billiotte, J., Hadj-Hassen, F., 2021. Non–isothermal two–phase hydrogen transport in rock salt during cycling in underground caverns. Int. J. Hydrog. Energy 46 (9), 6632–6647. https://doi.org/10.1016/j.ijhydene.2020.11.152.

Aftab, A., Hassanpouryouzband, A., Xie, Q., Machuca, L.L., Sarmadivaleh, M., 2022. Toward a Fundamental Understanding of Geological Hydrogen Storage. Ind. Eng. Chem. Res. 61 (9), 3233–3253. https://doi.org/10.1021/acs.iecr.1c04380.

Aftab, A., Hassanpouryouzband, A., Naderi, H., Xie, Q., Sarmadivaleh, M., 2023. Quantifying onshore salt deposits and their potential for hydrogen energy storage in Australia. J. Energy Storage 65, 107252. https://doi.org/10.1016/j.est.2023.107252.

Ahmadi, M., 2025. Physics-informed neural modeling of interfacial tension in hydrogen-rich systems using attention-based learning. Int. J. Hydrog. Energy 163, 150829. https://doi.org/10.1016/j.ijhydene.2025.150829.

Ajibona, A.I., Pandey, R., 2024. Evaluating Caprock Integrity During Underground Hydrogen Storage (UHS) in Subsurface Rocks. In: 58th U.S. Rock Mechanics/Geomechanics Symposium pp. D031S033R003.

Al Homoud, R., Machado, M.V.B., Daigle, H., 2024. Assessing hydrogen sulfide generation from pyrite reduction: Implications for underground hydrogen storage. In: Unconventional Resources Technology Conference, 17?19 June 2024. SEG Global meeting Abstracts. Unconventional Resources Technology Conference (URTeC), pp. 1518–1532.

Alessa, S., Sakhaee-Pour, A., Alipour, M., 2022. Safe pressure for hydrogen storage in subsurface. Energy Rep. 8, 15702–15711. https://doi.org/10.1016/j.egyr.2022.11.141.

Alhotan, M., Delshad, M., Sepehrnoori, K., 2023. Effect of Grid Resolution on Underground Hydrogen Storage Compositional Reservoir simulation, Middle East Oil. Gas and Geosci. Show pp. D031S097R002. doi: 10.2118/213276-MS.

Ali, H., Hamdi, Z., Talabi, O., Pickup, G., Nizam, S., 2022. Comprehensive Approach for Modeling Underground Hydrogen Storage in Depleted Gas Reservoirs. SPE Asia Pacific Oil & Gas Conference and Exhibition. https://doi.org/10.2118/210638-MS pp. D031S011R001.

Alpermann, T., Ostertag-Henning, C., 2020. Kinetics of the Abiotic Oxidation of Hydrogen (H_2) by Hematite at Subsurface Storage Conditions. In: Thirtieth Annual Goldschmidt Conference, p. 40.

Alshehab, N., Kamrava, S., 2026. Integrating molecular dynamics and machine learning to predict hydrogen–brine interfacial tension for subsurface storage. Int. J. Hydrog. Energy 204, 153347. https://doi.org/10.1016/j.ijhydene.2025.153347.

Aluah, R., Fadairo, A., Opeyemi, O., Ni, R., Foerster, I., 2024. An Experimental Study on the Caprock Integrity of Reservoirs to Assess the Repurposing Depleted Bakken Formation Oil and Gas Fields for Underground Hydrogen Storage. SPE Energy Transit. Sympos. https://doi.org/10.2118/221398-MS pp. D012S002R002.

Al-Yaseri, A., Al-Mukainah, H., Yekeen, N., 2023a. Experimental insights into limestone-hydrogen interactions and the resultant effects on underground hydrogen storage. Fuel 344, 128000. https://doi.org/10.1016/j.fuel.2023.128000.

Al-Yaseri, A., Al-Mukainah, H., Yekeen, N., Al-Qasim, A.S., 2023b. Experimental investigation of hydrogen-carbonate reactions via computerized tomography: Implications for underground hydrogen storage. Int. J. Hydrog. Energy 48 (9), 3583–3592. https://doi.org/10.1016/j.ijhydene.2022.10.148.

Al-Yaseri, A., Fatah, A., Adebayo, A.R., Al-Qasim, A.S., Patil, P.D., 2024a. Pore structure analysis of storage rocks during geological hydrogen storage: Investigation of geochemical interactions. Fuel 361, 130683. https://doi.org/10.1016/j.fuel.2023.130683.

Al-Yaseri, A., Yekeen, N., Al-Mukainah, H., Hassanpouryouzband, A., 2024b. Geochemical interactions in geological hydrogen Storage: the role of sandstone clay content. Fuel 361, 130728. https://doi.org/10.1016/j.fuel.2023.130728.

Amid, A., Mignard, D., Wilkinson, M., 2016. Seasonal storage of hydrogen in a depleted natural gas reservoir. Int. J. Hydrog. Energy 41 (12), 5549–5558. https://doi.org/10.1016/j.ijhydene.2016.02.036.

Amigáň, P., Greksák, M., Kozánková, J., Buzek, F., Onderka, V., Wolf, I., 1990. Methanogenic bacteria as a key factor involved in changes of town gas stored in an underground reservoir. FEMS Microbiol. Ecol. 6 (3), 221–224. https://doi.org/10.1111/j.1574-6968.1990.tb03944.x.

Amiri, B., Ghaedi, M., Andersen, P.Ø., Luo, X., 2024. Techno-Economic Optimization of Underground Hydrogen Storage in Aquifers. SPE Eur. Energy Conference and Exhibi. https://doi.org/10.2118/220044-MS pp. D031S021R005.

Amjadi, A., Kord, S., 2025. Analysis and prediction of hydrogen relative permeability in underground storage systems using machine learning. Sci. Rep. 15 (1), 37719. https://doi.org/10.1038/s41598-025-21507-3.

Ansari, S., Safaei-Farouji, M., Atashrouz, S., Abedi, A., Hemmati-Sarapardeh, A., Mohaddespour, A., 2022. Prediction of hydrogen solubility in aqueous solutions: Comparison of equations of state and advanced machine learning-metaheuristic approaches. Int. J. Hydrog. Energy 47 (89), 37724–37741. https://doi.org/10.1016/j.ijhydene.2022.08.288.

Bachand, A., Doyon, B., Raymond, J., 2024. Thermo-physical numerical model for hydrogen storage in underground tanks and caverns. Int. J. Hydrog. Energy 66, 66–80. https://doi.org/10.1016/j.ijhydene.2024.03.246.

Bagheri, M., Mahani, H., Ayatollahi, S., Zivar, D., 2023. Direct pore-scale simulation of the effect of capillary number and gas compressibility on cyclic underground hydrogen storage & production in heterogeneous aquifers. Adv. Water Resour. 181, 104547. https://doi.org/10.1016/j.advwatres.2023.104547.

Bai, T., Tahmasebi, P., 2022. Coupled hydro-mechanical analysis of seasonal underground hydrogen storage in a saline aquifer. J. Energy Storage 50, 104308. https://doi.org/10.1016/j.est.2022.104308.

Bai, M., Song, K., Sun, Y., He, M., Li, Y., Sun, J., 2014. An overview of hydrogen underground storage technology and prospects in China. J. Pet. Sci. Eng. 124, 132–136. https://doi.org/10.1016/j.petrol.2014.09.037.

Bardelli, F., Mondelli, C., Didier, M., Vitillo, J.G., Cavicchia, D.R., Robinet, J.-C., Leone, L., Charlet, L., 2014. Hydrogen uptake and diffusion in Callovo-Oxfordian clay rock for nuclear waste disposal technology. Appl. Geochem. 49, 168–177. https://doi.org/10.1016/j.apgeochem.2014.06.019.

Bernardez, L.A., de Andrade Lima, L.R.P., de Jesus, E.B., Ramos, C.L.S., Almeida, P.F., 2013. A kinetic study on bacterial sulfate reduction. Bioprocess Biosyst. Eng. 36 (12), 1861–1869. https://doi.org/10.1007/s00449-013-0960-0.

Biot, M.A., 1956. General Solutions of the Equations of Elasticity and consolidation for a Porous Material. J. Appl. Mech. 23 (1), 91–96. https://doi.org/10.1115/1.4011213.

Bo, Z., Zeng, L., Chen, Y., Xie, Q., 2021. Geochemical reactions-induced hydrogen loss during underground hydrogen storage in sandstone reservoirs. Int. J. Hydrog. Energy 46 (38), 19998–20009. https://doi.org/10.1016/j.ijhydene.2021.03.116.

Bordenave, S., Chatterjee, I., Voordouw, G., 2013. Microbial community structure and microbial activities related to CO2 storage capacities of a salt cavern. Int. Biodeterior. Biodegradation 81, 82–87. https://doi.org/10.1016/j.ibiod.2012.08.001.

Böttcher, N., Görke, U.-J., Kolditz, O., Nagel, T., 2017. Thermo-mechanical investigation of salt caverns for short-term hydrogen storage. Environ. Earth Sci. 76 (3), 98. https://doi.org/10.1007/s12665-017-6414-2.

Braid, H., Taylor, K., Hough, E., Rochelle, C., Niasar, V., Ma, L., 2024. Hydrogen-induced mineral alteration: A review in the context of underground hydrogen storage (UHS) in saline aquifers. Earth Sci. Rev. 259, 104975. https://doi.org/10.1016/j.earscirev.2024.104975.

Buchmann, T.J., 2008. 3D Multi-Scale Finite Element Analysis of the Present-Day Crustal State of Stress and the Recent Kinematic Behaviour of the Northern and Central Upper Rhine Graben. Logos Verlag Berlin GmbH.

Burtonshaw, J.E.J., Paluszny, A., Mohammadpour, A., Zimmerman, R.W., 2024. Effects of Underburden Fault Properties, Operational Properties, and Stresses on Induced Basement Fault Seismicity During Hydrogen Storage in Depleted Gas Fields. In: 58th U.S. Rock Mechanics/Geomechanics Symposium pp. D031S033R005.

Buzek, F., Onderka, V., Vančura, P., Wolf, I., 1994. Carbon isotope study of methane production in a town gas storage reservoir. Fuel 73 (5), 747–752. https://doi.org/10.1016/0016-2361(94)90019-1.

Cai, Z., Zhang, K., Guo, C., 2022. Development of a novel simulator for modelling underground hydrogen and gas mixture storage. Int. J. Hydrog. Energy 47 (14), 8929–8942. https://doi.org/10.1016/j.ijhydene.2021.12.224.

Cao, M., Dai, Z., Jia, S., Samper, J., Ling, H., Du, Z., Zhan, C., Yang, Z., Thanh, H.V., Soltanian, M.R., 2024. Identification of solute transport parameters in fractured granites with heterogeneous apertures. J. Hydrol. 633, 130938. https://doi.org/10.1016/j.jhydrol.2024.130938.

Cao, M., Dai, Z., Chen, J., Yin, H., Zhang, X., Wu, J., Thanh, H.V., Soltanian, M.R., 2025. An integrated framework of deep learning and entropy theory for enhanced high-dimensional permeability field identification in heterogeneous aquifers. Water Res. 268, 122706. https://doi.org/10.1016/j.watres.2024.122706.

Carter, N.L., Horseman, S.T., Russell, J.E., Handin, J., 1993. Rheology of rocksalt. J. Struct. Geol. 15 (9), 1257–1271. https://doi.org/10.1016/0191-8141(93)90168-A.

Cerfontaine, B., Collin, F., 2018. Cyclic and Fatigue Behaviour of Rock Materials: Review, Interpretation and Research Perspectives. Rock Mech. Rock. Eng. 51 (2), 391–414. https://doi.org/10.1007/s00603-017-1337-5.

Chai, M., Chen, Z., Nourozieh, H., Yang, M., 2023. Numerical simulation of large-scale seasonal hydrogen storage in an anticline aquifer: A case study capturing hydrogen interactions and cushion gas injection. Appl. Energy 334, 120655. https://doi.org/10.1016/j.apenergy.2023.120655.

Chen, J., Dai, Z., Yang, Z., Pan, Y., Zhang, X., Wu, J., Reza Soltanian, M., 2021. An improved Tandem Neural Network Architecture for Inverse Modeling of Multicomponent Reactive Transport in Porous Media. Water Resour. Res. 57 (12), e2021WR030595. https://doi.org/10.1029/2021WR030595.

Chen, J., Dai, Z., Dong, S., Zhang, X., Sun, G., Wu, J., Ershadnia, R., Yin, S., Soltanian, M. R., 2022. Integration of Deep Learning and Information Theory for Designing monitoring Networks in Heterogeneous Aquifer Systems. Water Resour. Res. 58 (10), e2022WR032429. https://doi.org/10.1029/2022WR032429.

Chen, F., Chen, B., Mao, S., Malki, M., Mehana, M., 2024. Integrating Capacity and Efficiency for Optimal Hydrogen Storage Site selection in Saline Aquifers. Energy Fuel 38 (5), 4733–4742. https://doi.org/10.1021/acs.energyfuels.3c04852.

Cheng, H., Wang, F., Guan, X., Yang, G., Yuan, Y., Feng, G., 2023. A mathematical model for pre-Darcy flow in low permeability porous media with stress sensitivity and the boundary-layer effect. Eng. Geol. 324, 107257. https://doi.org/10.1016/j.enggeo.2023.107257.

Chiodoni, A., Fontana, M., Bejtka, K., Gho, C.I., Marzano, F., Pozzovivo, V., Scapolo, M., Mantegazzi, A., Coti, C., Verga, F., Pirri, C.F., 2024. Reservoir and Caprock Compositional Assessment Strategy for Hydrogen Storage. SPE Eur. Energy Conferen. Exhibi. https://doi.org/10.2118/220077-MS pp. D031S017R005.

Chu, Z., Wu, Z., Liu, Q., Weng, L., Wang, Z., Zhou, Y., 2021. Evaluating the Microstructure Evolution Behaviors of Saturated Sandstone using NMR Testing under Uniaxial Short-Term and Creep Compression. Rock Mech. Rock. Eng. 54 (9), 4905–4927. https://doi.org/10.1007/s00603-021-02538-4.

Coarita-Tintaya, E.-D., Golfier, F., Grgic, D., Souley, M., Cheng, L., 2023. Hydromechanical modelling of salt caverns subjected to cyclic hydrogen injection and withdrawal. Comput. Geotech. 162, 105690. https://doi.org/10.1016/j.compgeo.2023.105690.

Cui, G., Hu, Z., Wang, Y., Jiang, S., Wang, R., 2024. Migration characteristics and local capillary trapping mechanism after the CO2 leakage out of saline aquifers. Fuel 356, 129347. https://doi.org/10.1016/j.fuel.2023.129347.

Dabbaghi, E., Ng, K., Brown, T.C., Yu, Y., 2024. Experimental study on the effect of hydrogen on the mechanical properties of Hulett sandstone. Int. J. Hydrog. Energy 60, 468–478. https://doi.org/10.1016/j.ijhydene.2024.02.210.

Dai, Z., Xu, L., Xiao, T., McPherson, B., Zhang, X., Zheng, L., Dong, S., Yang, Z., Soltanian, M.R., Yang, C., Ampomah, W., Jia, W., Yin, S., Xu, T., Bacon, D., Viswanathan, H., 2020. Reactive chemical transport simulations of geologic carbon sequestration: Methods and applications. Earth Sci. Rev. 208, 103265. https://doi.org/10.1016/j.earscirev.2020.103265.

Dang, F., Li, S., Dong, H., Wang, Z., Zhu, J., 2024. Experimental study on the oil recovery characteristics of CO2 energetic fracturing in ultralow-permeability sandstone reservoirs utilizing nuclear magnetic resonance. Fuel 366, 131370. https://doi.org/10.1016/j.fuel.2024.131370.

Darcy, H., 1856. Les fontaines publiques de la ville de Dijon: Exposition et application des principes à suivre et des formules à employer dans les questions de distribution d'eau : Ouvrage terminé par un appendice relatif aux fournitures d'eau de plusieurs villes, au filtrage des eaux et à la fabrication des tuyaux de fonte, de plomb, de tôle et de bitume. Victor Dalmont, éditeur.

Delshad, M., Alhotan, M., Batista Fernandes, B.R., Umurzakov, Y., Sepehrnoori, K., 2022a. Pros and Cons of Saline Aquifers against Depleted Hydrocarbon Reservoirs for Hydrogen Energy Storage. In: SPE Annual Technical Conference and Exhibition, pp. D012S071R002.

Delshad, M., Umurzakov, Y., Sepehrnoori, K., Eichhubl, P., Batista Fernandes, B.R., 2022b. Hydrogen Storage Assessment in Depleted Oil Reservoir and Saline Aquifer (Energies).

Deng, G., Zhou, J., Tian, S., Xian, X., Zhou, L., Zhang, C., Li, S., Tan, Y., 2023. Pore structure changes and its stress-sensitive behavior in sandstone under cyclic stress: Implication for underground gas storage. Gas Sci. Eng. 119, 205130. https://doi.org/10.1016/j.jgsce.2023.205130.

Derakhshani, R., Lankof, L., GhasemiNejad, A., Zarasvandi, A., Amani Zarin, M.M., Zaresefat, M., 2024a. A Novel Sustainable Approach for Site selection of Underground Hydrogen Storage in Poland using Deep learning. Energies 17 (15), 3677. https://doi.org/10.3390/en17153677.

Derakhshani, R., Lankof, L., GhasemiNejad, A., Zaresefat, M., 2024b. Artificial intelligence-driven assessment of salt caverns for underground hydrogen storage in Poland. Sci. Rep. 14 (1), 14246. https://doi.org/10.1038/s41598-024-64020-9.

Dias, W., Roehl, D., Mejia, C., Sotomayor, P., 2023. Cavern integrity for underground hydrogen storage in the Brazilian pre-salt fields. Int. J. Hydrog. Energy 48 (69), 26853–26869. https://doi.org/10.1016/j.ijhydene.2023.03.292.

Dilshan, R., Perera, M., Matthai, S.K., 2024a. Effect of mechanical weakening and crack formation on caprock integrity during underground hydrogen storage in depleted gas reservoirs–A comprehensive review. Fuel 371, 131893.

Dilshan, R.A.D.P., Perera, M.S.A., Matthai, S.K., 2024b. Effect of mechanical weakening and crack formation on caprock integrity during underground hydrogen storage in depleted gas reservoirs – A comprehensive review. Fuel 371, 131893. https://doi.org/10.1016/j.fuel.2024.131893.

Ding, Z.W., Li, X.F., Huang, X., Wang, M.B., Tang, Q.B., Jia, J.D., 2022. Feature extraction, recognition, and classification of acoustic emission waveform signal of coal rock sample under uniaxial compression. Int. J. Rock Mech. Min. Sci. 160, 105262. https://doi.org/10.1016/j.ijrmms.2022.105262.

Doan, Q.T., Keshavarz, A., Miranda, C.R., Behrenbruch, P., Iglauer, S., 2024. A prediction of interfacial tension by using molecular dynamics simulation: A study on effects of cushion gas (CO2, N2 and CH4) for Underground Hydrogen Storage. Int. J. Hydrog. Energy 50, 1607–1615. https://doi.org/10.1016/j.ijhydene.2023.10.156.

Dodangoda, C., P. G, R, 2024. Quantification of hydrogen depletion and mineral reactivity in underground hydrogen storage reservoirs. Gas Sci. Eng. 126, 205318. https://doi.org/10.1016/j.jgsce.2024.205318.

Dopffel, N., Jansen, S., Gerritse, J., 2021. Microbial side effects of underground hydrogen storage – Knowledge gaps, risks and opportunities for successful implementation. Int. J. Hydrog. Energy 46 (12), 8594–8606. https://doi.org/10.1016/j.ijhydene.2020.12.058.

Du, S.-H., Shi, Y.-M., 2024. Concise extraction and characterization of the pore-throat network in unconventional hydrocarbon reservoirs: A new perspective. Pet. Sci. 21 (3), 1474–1487. https://doi.org/10.1016/j.petsci.2023.12.009.

Du, Z., Dai, Z., Yang, Z., Zhan, C., Chen, W., Cao, M., Thanh, H.V., Soltanian, M.R., 2024. Exploring hydrogen geologic storage in China for future energy: Opportunities and challenges. Renew. Sust. Energ. Rev. 196, 114366. https://doi.org/10.1016/j.rser.2024.114366.

Du, Z., Dai, Z., Yin, S., Dong, S., Zhang, X., Yin, H., Soltanian, M.R., 2025. Combining machine learning and multi-objective optimization algorithms to optimize key parameters for underground hydrogen storage. Gas Sci. Eng. 142, 205713. https://doi.org/10.1016/j.jgsce.2025.205713.

Eddaoui, N., Panfilov, M., Ganzer, L., Hagemann, B., 2021. Impact of Pore Clogging by Bacteria on Underground Hydrogen Storage. Transp. Porous Media 139 (1), 89–108. https://doi.org/10.1007/s11242-021-01647-6.

Elgendy, A.M.S., Pizzolato, A., Maniglio, M., Geloni, C., Panfili, P., Topini, C., 2023. Reactive Transport Modelling of H2 Storage in Depleted Gas Fields: An Approach to Implement Biogeochemical Reactions in a Compositional Reservoir Simulator. In: SPE EuropEC - Europe Energy Conference featured at the 84th EAGE Annual Conference & Exhibition pp. D011S009R002.

Enigbokan, T., Heinemann, N., Li, J., 2021. Application of CO2 geologic storage experience to underground hydrogen storage reservoirs. In: Proceedings of the 15th Greenhouse Gas Control Technologies Conference, pp. 15–18.

Fang, Y., Hou, Z., Yue, Y., Chen, Q., Liu, J., 2022. Numerical study of hydrogen storage cavern in thin-bedded rock salt, Anning of China, the mechanical behavior of salt X. CRC Press, pp. 652–661.

Farahani, M., Aghaei, H., Masoumi, H., 2022. Effect of pore type on porosity, permeability and pore volume compressibility of geological formations due to in-situ stress change. J. Pet. Sci. Eng. 218, 110986. https://doi.org/10.1016/j.petrol.2022.110986.

Fatah, A., Al-Yaseri, A., Theravalappil, R., Radwan, O.A., Amao, A., Al-Qasim, A.S., 2024. Geochemical reactions and pore structure analysis of anhydrite/gypsum/halite bearing reservoirs relevant to subsurface hydrogen storage in salt caverns. Fuel 371, 131857. https://doi.org/10.1016/j.fuel.2024.131857.

Feldmann, F., Hagemann, B., Ganzer, L., Panfilov, M., 2016. Numerical simulation of hydrodynamic and gas mixing processes in underground hydrogen storages. Environ. Earth Sci. 75 (16), 1165. https://doi.org/10.1007/s12665-016-5948-z.

Flesch, S., Pudlo, D., Albrecht, D., Jacob, A., Enzmann, F., 2018. Hydrogen underground storage—Petrographic and petrophysical variations in reservoir sandstones from laboratory experiments under simulated reservoir conditions. Int. J. Hydrog. Energy 43 (45), 20822–20835. https://doi.org/10.1016/j.ijhydene.2018.09.112.

Freiman, S.W., 1984. Effects of chemical environments on slow crack growth in glasses and ceramics. J. Geophys. Res. Solid Earth 89 (B6), 4072–4076. https://doi.org/10.1029/JB089iB06p04072.

Gao, K., Creasy, N.M., Huang, L., Gross, M.R., 2024a. Underground hydrogen storage leakage detection and characterization based on machine learning of sparse seismic data. Int. J. Hydrog. Energy 61, 137–161. https://doi.org/10.1016/j.ijhydene.2024.02.296.

Gao, Q., Liu, J., Elsworth, D., 2024b. Phenomenal study of microbial impact on hydrogen storage in aquifers: A coupled multiphysics modelling. Int. J. Hydrog. Energy 79, 883–900. https://doi.org/10.1016/j.ijhydene.2024.07.004.

Gao, Z., Bai, L., Hu, Q., Yang, Z., Jiang, Z., Wang, Z., Xin, H., Zhang, L., Yang, A., Jia, L., Liu, Z., Ma, G., 2024c. Shale oil migration across multiple scales: A review of characterization methods and different patterns. Earth Sci. Rev. 254, 104819. https://doi.org/10.1016/j.earscirev.2024.104819.

Gbadamosi, A., Adamu, H., Usman, J., Usman, A.G., Jibril, M.M., Salami, B.A., Gbadamosi, S.L., Oyedele, L.O., Abba, S.I., 2024. New-generation machine learning models as prediction tools for modeling interfacial tension of hydrogen-brine system. Int. J. Hydrog. Energy 50, 1326–1337. https://doi.org/10.1016/j.ijhydene.2023.09.170.

Gelencsér, O., Árvai, C., Mika, L.T., Breitner, D., LeClair, D., Szabó, C., Falus, G., Szabó-Krausz, Z., 2023. Effect of hydrogen on calcite reactivity in sandstone reservoirs: Experimental results compared to geochemical modeling predictions. J. Energy Storage 61, 106737. https://doi.org/10.1016/j.est.2023.106737.

Ghasemi, M., Omrani, S., Mahmoodpour, S., Zhou, T., 2022. Molecular dynamics simulation of hydrogen diffusion in water-saturated clay minerals; implications for Underground Hydrogen Storage (UHS). Int. J. Hydrog. Energy 47 (59), 24871–24885. https://doi.org/10.1016/j.ijhydene.2022.05.246.

Gheibi, S., Holt, R.M., Vilarrasa, V., 2017. Effect of faults on stress path evolution during reservoir pressurization. Int. J. Greenh. Gas Con. 63, 412–430. https://doi.org/10.1016/j.ijggc.2017.06.008.

Gholami, R., 2023. Hydrogen storage in geological porous media: Solubility, mineral trapping, H2S generation and salt precipitation. J. Energy Storage 59, 106576. https://doi.org/10.1016/j.est.2022.106576.

Goodman Hanson, A., Kutchko, B., Lackey, G., Gulliver, D., Strazisar, B.R., Tinker, K.A., Wright, R., Haeri, F., Huerta, N., Baek, S., 2022. Subsurface Hydrogen and Natural Gas Storage (State of Knowledge and Research Recommendations Report).

Gregory, S.P., Barnett, M.J., Field, L.P., Milodowski, A.E., 2019. Subsurface Microbial Hydrogen Cycling: Natural Occurrence and Implications for Industry (Microorganisms).

Griffith, A.A., 1921. VI. The phenomena of rupture and flow in solids. Philosophical transactions of the royal society of london. Series A, containing papers of a mathematical or physical character, 221 (582–593), 163–198.

Gut, D., 2017. The Effects of Hydrogen Injection in Natural Gas Networks for the Dutch Underground Storages. The Hague.
Hagemann, B., Rasoulzadeh, M., Panfilov, M., Ganzer, L., Reitenbach, V., 2015. Mathematical modeling of unstable transport in underground hydrogen storage. Environ. Earth Sci. 73 (11), 6891–6898. https://doi.org/10.1007/s12665-015-4414-7.
Hagemann, B., Rasoulzadeh, M., Panfilov, M., Ganzer, L., Reitenbach, V., 2016. Hydrogenization of underground storage of natural gas: Impact of hydrogen on the hydrodynamic and bio-chemical behavior. Comput. Geosci. 20 (3), 595–606. https://doi.org/10.1007/s10596-015-9515-6.
Hamdi, Z., Rosman, A., Partoon, B., Bataee, M., Hassan, A.M., 2024. Salinity Effects on H2S Generation in Subsurface Hydrogen Storage, GOTECH pp. D032S001R005.
Han, C., 2022. Study on Hysteretic Characteristics and Energy Dissipation Mechanism of Rock under Cyclic Loading. PhD Thesis,. China University of Mining & Technology, Beijing.
Han, G., Kwon, Y., Kim, J.B., Lee, S., Bae, J., Cho, E., Lee, B.J., Cho, S., Park, J., 2020. Development of a high-energy-density portable/mobile hydrogen energy storage system incorporating an electrolyzer, a metal hydride and a fuel cell. Appl. Energy 259, 114175. https://doi.org/10.1016/j.apenergy.2019.114175.
Hand, E., 2023. Hidden hydrogen. Science 379 (6633), 7.
Hashemi, L., Blunt, M., Hajibeygi, H., 2021. Pore-scale modelling and sensitivity analyses of hydrogen-brine multiphase flow in geological porous media. Sci. Rep. 11 (1), 8348. https://doi.org/10.1038/s41598-021-87490-7.
Hassannayebi, N., Azizmohammadi, S., De Lucia, M., Ott, H., 2019. Underground hydrogen storage: application of geochemical modelling in a case study in the Molasse Basin, Upper Austria. Environ. Earth Sci. 78 (5), 177. https://doi.org/10.1007/s12665-019-8184-5.
Hassanpouryouzband, A., Joonaki, E., Edlmann, K., Heinemann, N., Yang, J., 2020. Thermodynamic and transport properties of hydrogen containing streams. Sci. Data 7 (1), 222. https://doi.org/10.1038/s41597-020-0568-6.
Hassanpouryouzband, A., Adie, K., Cowen, T., Thaysen, E.M., Heinemann, N., Butler, I. B., Wilkinson, M., Edlmann, K., 2022. Geological Hydrogen Storage: Geochemical Reactivity of Hydrogen with Sandstone Reservoirs. ACS Energy Lett. 7 (7), 2203–2210. https://doi.org/10.1021/acsenergylett.2c01024.
He, Y., Xie, Y., Qiao, Y., Qin, J., Tang, Y., 2024. Estimation of underground hydrogen storage capacity in depleted gas reservoirs using CO2 as cushion gas. Appl. Energy 375, 124093. https://doi.org/10.1016/j.apenergy.2024.124093.
Heinemann, N., Booth, M.G., Haszeldine, R.S., Wilkinson, M., Scafidi, J., Edlmann, K., 2018. Hydrogen storage in porous geological formations – onshore play opportunities in the midland valley (Scotland, UK). Int. J. Hydrog. Energy 43 (45), 20861–20874. https://doi.org/10.1016/j.ijhydene.2018.09.149.
Heinemann, N., Alcalde, J., Miocic, J.M., Hangx, S.J., Kallmeyer, J., Ostertag-Henning, C., Hassanpouryouzband, A., Thaysen, E.M., Strobel, G.J., Schmidt-Hattenberger, C., 2021a. Enabling large-scale hydrogen storage in porous media–the scientific challenges. Energy Environ. Sci. 14 (2), 853–864. https://doi.org/10.1039/d0ee03536j.
Heinemann, N., Scafidi, J., Pickup, G., Thaysen, E.M., Hassanpouryouzband, A., Wilkinson, M., Satterley, A.K., Booth, M.G., Edlmann, K., Haszeldine, R.S., 2021b. Hydrogen storage in saline aquifers: the role of cushion gas for injection and production. Int. J. Hydrog. Energy 46 (79), 39284–39296. https://doi.org/10.1016/j.ijhydene.2021.09.174.
Hematpur, H., Abdollahi, R., Rostami, S., Haghighi, M., Blunt, M.J., 2023. Review of underground hydrogen storage: Concepts and challenges. Adv. Geo-Energy Res. 7 (2), 111–131.
Hemme, C., Van Berk, W., 2018. Hydrogeochemical Modeling to Identify Potential Risks of Underground Hydrogen Storage in Depleted Gas Fields. Appl. Sci. 8 (11), 2282. https://doi.org/10.3390/app8112282.
Hernández-Gómez, R., Tuma, D., Gómez-Hernández, A., Chamorro, C.R., 2017. Accurate Experimental (p, ρ, T) Data for the Introduction of Hydrogen into the Natural Gas Grid: Thermodynamic Characterization of the Nitrogen–Hydrogen Binary System from 240 to 350 K and Pressures up to 20 MPa. J. Chem. Eng. Data 62 (12), 4310–4326. https://doi.org/10.1021/acs.jced.7b00694.
Higgs, K.E., Strogen, D.P., Nicol, A., Dempsey, D., Leith, K., Bassett, K., Reid, C., Yates, E., Parker, M., Bischoff, A., Adam, L., Rowe, M., 2024. Prospectivity analysis for underground hydrogen storage, Taranaki basin, Aotearoa New Zealand: A multi-criteria decision-making approach. Int. J. Hydrog. Energy 71, 1468–1485. https://doi.org/10.1016/j.ijhydene.2024.05.098.
Ho, T.A., Dang, S.T., Dasgupta, N., Choudhary, A., Rai, C.S., Wang, Y., 2024. Nuclear magnetic resonance and molecular simulation study of H2 and CH4 adsorption onto shale and sandstone for hydrogen geological storage. Int. J. Hydrog. Energy 51, 158–166. https://doi.org/10.1016/j.ijhydene.2023.11.011.
Hogeweg, S., Strobel, G., Hagemann, B., 2022. Benchmark study for the simulation of Underground Hydrogen Storage operations. Comput. Geosci. 26 (6), 1367–1378. https://doi.org/10.1007/s10596-022-10163-5.
Hosseini, M., Leonenko, Y., 2024. Prediction of hydrogen−brine interfacial tension at subsurface conditions: Implications for hydrogen geo-storage. Int. J. Hydrog. Energy 58, 485–494. https://doi.org/10.1016/j.ijhydene.2024.01.227.
Hosseini, M., Fahimpour, J., Ali, M., Keshavarz, A., Iglauer, S., 2022. Capillary Sealing Efficiency Analysis of Caprocks: Implication for Hydrogen Geological Storage. Energy Fuel 36 (7), 4065–4075. https://doi.org/10.1021/acs.energyfuels.2c00281.
Hu, J.-H., Yang, D.-J., 2020. Meso-damage evolution and mechanical characteristics of low-porosity sedimentary rocks under uniaxial compression. Trans. Nonferrous Metals Soc. China 30 (4), 1071–1077. https://doi.org/10.1016/S1003-6326(20)65278-5.
Hu, B., Yu, L., Mi, X., Xu, F., Li, S., Li, W., Wei, C., Zhang, T., 2024a. Comparative analysis of thermodynamic and mechanical responses between underground hydrogen storage and compressed air energy storage in lined rock caverns. Int. J. Min. Sci. Technol. 34 (4), 531–543. https://doi.org/10.1016/j.ijmst.2024.04.005.
Hu, J., Yang, S., Yang, K., Deng, H., Wang, M., Li, J., Gao, X., 2024b. Enhanced Gas Recovery coupled with CO2 Sequestration in Tight Sandstone Reservoirs with Different Pore-Throat Structures. Energy Fuel 38 (13), 12005–12023. https://doi.org/10.1021/acs.energyfuels.4c01971.
Huan, X., Marzouk, Y.M., 2013. Simulation-based optimal Bayesian experimental design for nonlinear systems. J. Comput. Phys. 232 (1), 288–317. https://doi.org/10.1016/j.jcp.2012.08.013.
Huang, T., Moridis, G.J., Blasingame, T.A., Abdulkader, A.M., Yan, B., 2023a. Compositional reservoir simulation of underground hydrogen storage in depleted gas reservoirs. Int. J. Hydrog. Energy 48 (92), 36035–36050. https://doi.org/10.1016/j.ijhydene.2023.05.355.
Huang, T., Moridis, G.J., Blasingame, T.A., Afifi, A.M., Yan, B., 2023b. Feasibility Analysis of Hydrogen Storage in Depleted Natural Reservoirs through a Multi-phase Reservoir Simulator. In: SPE Reservoir Characterisation and simulation Conference and Exhibition, pp. D031S017R001.
Hussain, A., Al-Hadrami, H., Emadi, H., Altawati, F., Thiyagarajan, S.R., Watson, M., 2022. Experimental Investigation of Wellbore Integrity of Depleted Oil and Gas Reservoirs for Underground Hydrogen Storage, Offshore Technology Conference, pp. D021S028R005.
Ibrahim, A.F., 2025. A Comprehensive AI-Model for H_2-Brine Interfacial Tension Prediction: Implications for Underground Hydrogen Storage. Middle East Oil, Gas and Geosciences Show (MEOS GEO).
İlkiliç, C., Türkbay, İ., 2010. Determination and utilization of wind energy potential for Turkey. Renew. Sust. Energ. Rev. 14 (8), 2202–2207. https://doi.org/10.1016/j.rser.2010.03.033.
Jadhawar, P., Saeed, M., 2023. Optimizing the operational efficiency of the underground hydrogen storage scheme in a deep North Sea aquifer through compositional simulations. J. Energy Storage 73, 108832. https://doi.org/10.1016/j.est.2023.108832.
Jadhawar, P., Saeed, M., 2024. Mechanistic evaluation of the reservoir engineering performance for the underground hydrogen storage in a deep North Sea aquifer. Int. J. Hydrog. Energy 50, 558–574. https://doi.org/10.1016/j.ijhydene.2023.07.272.
Jahanbakhsh, A., Louis Potapov-Crighton, A., Mosallanezhad, A., Tohidi Kaloorazi, N., Maroto-Valer, M.M., 2024. Underground hydrogen storage: A UK perspective. Renew. Sust. Energ. Rev. 189, 114001. https://doi.org/10.1016/j.rser.2023.114001.
Jahanbani Veshareh, M., Thaysen, E.M., Nick, H.M., 2022. Feasibility of hydrogen storage in depleted hydrocarbon chalk reservoirs: Assessment of biochemical and chemical effects. Appl. Energy 323, 119575. https://doi.org/10.1016/j.apenergy.2022.119575.
Javaherdashti, R., Alasvand, K., 2019. Biological Treatment of Microbial Corrosion: Opportunities and Challenges. Elsevier.
Jia, H., Xiang, W., Shen, Y., Yang, G., 2017. Discussion of the key issues within calculation of the fatigue damage of rocks subjected to freeze-thaw cycles. Chin. J. Rock Mech. Eng. 36 (2), 335–346.
Jia, C., Xu, W., Wang, R., Wang, W., Zhang, J., Yu, J., 2018. Characterization of the deformation behavior of fine-grained sandstone by triaxial cyclic loading. Constr. Build. Mater. 162, 113–123. https://doi.org/10.1016/j.conbuildmat.2017.12.001.
Jia, H., Wang, E., Song, D., Wang, X., Ali, M., 2019. Precursory changes in wave velocity for coal and rock samples under cyclic loading. Results Phys. 12, 432–434. https://doi.org/10.1016/j.rinp.2018.11.096.
Jia, S., Wen, C., Fu, X., Song, W., Zhang, Y., Zhong, G., Shi, J., 2023. The evolution law of caprock stress field of gas reservoir-type gas storage. Acta Pet. Sin. 44 (6), 983. https://doi.org/10.7623/syxb202306008.
Jiang, C., Duan, M., Yin, G., Wang, J.G., Lu, T., Xu, J., Zhang, D., Huang, G., 2017. Experimental study on seepage properties, AE characteristics and energy dissipation of coal under tiered cyclic loading. Eng. Geol. 221, 114–123. https://doi.org/10.1016/j.enggeo.2017.03.005.
Jiang, C., Roubinet, D., Lei, Q., Wang, Y., Wang, X., 2024. Anomalous transport and upscaling in critically-connected fracture networks under stress conditions. J. Hydrol. 630, 130661. https://doi.org/10.1016/j.jhydrol.2024.130661.
K C, Li, D., Creasy, N.M., Frash, L.P., Li, W., Neil, C.W., Iyare, U.C., Meng, M., Gross, M. R., 2025. Ultrasonic Waves as a Monitoring Tool in Underground Hydrogen Storage Reservoirs, 59th U.S. Rock Mechanics/Geomechanics Symposium.
Kabir, M.M., Roy, S.K., Alam, F., Nam, S.Y., Im, K.S., Tijing, L., Shon, H.K., 2023. Machine learning-based prediction and optimization of green hydrogen production technologies from water industries for a circular economy. Desalination 567, 116992. https://doi.org/10.1016/j.desal.2023.116992.
Kabuth, A., Dahmke, A., Beyer, C., Bilke, L., Dethlefsen, F., Dietrich, P., Duttmann, R., Ebert, M., Feeser, V., Görke, U.-J., Köber, R., Rabbel, W., Schanz, T., Schäfer, D., Würdemann, H., Bauer, S., 2016. Energy storage in the geological subsurface: dimensioning, risk analysis and spatial planning: the ANGUS+ project. Environ. Earth Sci. 76 (1), 23. https://doi.org/10.1007/s12665-016-6319-5.
Kalam, S., Khan, M.R., Arif, M., 2024. Smart Computational Algorithms for the Prediction of Interfacial Tension between Water and Hydrogen – Insights into Underground Hydrogen Storage, International Petroleum Technology Conference, pp. D031S113R003.
Kalati, S.S., Pour Khiabani, N., Ayatollahi, S., Mahani, H., Zivar, D., Esmaeilbeig, M.A., 2024. Molecular dynamics simulation of hydrogen diffusion into brine: Implications for underground hydrogen storage. Int. J. Hydrog. Energy 53, 17–28. https://doi.org/10.1016/j.ijhydene.2023.11.318.
Kampman, N., Busch, A., Bertier, P., Snippe, J., Hangx, S., Pipich, V., Di, Z., Rother, G., Harrington, J.F., Evans, J.P., Maskell, A., Chapman, H.J., Bickle, M.J., 2016. Observational evidence confirms modelling of the long-term integrity of CO2-

reservoir caprocks. Nat. Commun. 7 (1), 12268. https://doi.org/10.1038/ncomms12268.
Kanaani, M., Sedaee, B., 2022. Impact of Dilation and Irreversible Compaction on Underground Hydrogen Storage in Depleted Hydrocarbon Reservoirs. Energy Fuel 36 (22), 13506–13517. https://doi.org/10.1021/acs.energyfuels.2c02150.
Kanaani, M., Sedaee, B., Asadian-Pakfar, M., 2022. Role of Cushion Gas on Underground Hydrogen Storage in Depleted Oil Reservoirs. J. Energy Storage 45, 103783. https://doi.org/10.1016/j.est.2021.103783.
Kanaani, M., Sedaee, B., Asadian-Pakfar, M., Gilavand, M., Almahmoudi, Z., 2023. Development of multi-objective co-optimization framework for underground hydrogen storage and carbon dioxide storage using machine learning algorithms. J. Clean. Prod. 386, 135785. https://doi.org/10.1016/j.jclepro.2022.135785.
Kennedy, J., Trewin, B., Betts, R., Thorne, P., Foster, P., Siegmund, P., Ziese, M., Mishra, S., Uhlenbrook, S., Alvar-Beltran, J., 2024. State of the Climate 2024. Update for COP29.
Kryachko, Y., 2018. Novel approaches to microbial enhancement of oil recovery. J. Biotechnol. 266, 118–123. https://doi.org/10.1016/j.jbiotec.2017.12.019.
Kuang, Z.-B., 2014. Theory of Electroelasticity. Springer, Berlin, Heidelberg, IX, p. 431.
Kumar, K.R., Honorio, H.T., Hajibeygi, H., 2022. Simulation of the inelastic deformation of porous reservoirs under cyclic loading relevant for underground hydrogen storage. Sci. Rep. 12 (1), 21404. https://doi.org/10.1038/s41598-022-25715-z.
Laalam, A., Chellal, H.A.K., Khalifa, H., Benarbia, A., Tomomewo, O.S., Benabid, M.K., 2024. Exploring the Potential and Geomechanical Implications of Underground Hydrogen Storage in the Broom Creek Saline Aquifer, 58th U.S. Rock Mechanics/Geomechanics Symposium pp. D032S038R013.
Laban, M., 2020. Hydrogen Storage in Salt Caverns: Chemical Modelling and Analysis of Large-Scale Hydrogen Storage in Underground Salt Caverns.
Labus, K., Tarkowski, R., 2022. Modeling hydrogen–rock–brine interactions for the Jurassic reservoir and cap rocks from Polish Lowlands. Int. J. Hydrog. Energy 47 (20), 10947–10962. https://doi.org/10.1016/j.ijhydene.2022.01.134.
Lee, H., Calvin, K., Dasgupta, D., Krinmer, G., Mukherji, A., Thorne, P., Trisos, C., Romero, J., Aldunce, P., Barret, K., 2023. Synthesis Report of the IPCC Sixth Assessment Report (AR6). Longer report, IPCC.
Lee, H., Germann, T.C., Gross, M.R., Mehana, M., 2025. Molecular simulation of hydrogen adsorption in subsurface systems with implications for underground storage. Int. J. Hydrog. Energy 114, 71–80. https://doi.org/10.1016/j.ijhydene.2025.02.451.
Li, C., Singh, V.P., Mishra, A.K., 2012. Entropy theory-based criterion for hydrometric network evaluation and design: Maximum information minimum redundancy. Water Resour. Res. 48 (5). https://doi.org/10.1029/2011WR011251.
Li, T., Pei, X., Wang, D., Huang, R., Tang, H., 2019. Nonlinear behavior and damage model for fractured rock under cyclic loading based on energy dissipation principle. Eng. Fract. Mech. 206, 330–341. https://doi.org/10.1016/j.engfracmech.2018.12.010.
Li, S., Xiao, J., Li, Y., Liu, X., Liang, Q., Chang, J., Liu, J., 2023a. A new damage constitutive model of rock considering microscopic crack growth. Chin. J. Rock Mech. Eng. 42 (3), 640–648.
Li, W., Miao, X., Wang, J., Li, X., 2023b. Study on thermodynamic behaviour of natural gas and thermo-mechanical response of salt caverns for underground gas storage. Energy 262, 125601. https://doi.org/10.1016/j.energy.2022.125601.
Li, K.-S., Yang, S.-Q., Liu, C.-X., Song, Y., 2024. Mechanical response and energy evolution of interbedded shales subjected to multilevel constant/increasing-amplitude cyclic loading. Can. Geotech. J. 61 (11), 2485–2504. https://doi.org/10.1139/cgj-2023-0486.
Liao, Z., Wu, M., Chen, X., Zou, H., 2020. Fracture mechanical properties of carbonate and evaporite caprocks in Sichuan Basin, China with implications for reservoir seal integrity. Mar. Pet. Geol. 119, 104468. https://doi.org/10.1016/j.marpetgeo.2020.104468.
Limaluka, A.K.L., Yogarajah, E., Hiroyoshi, N., Abu-AlSaud, M., Cha, D.K., Ayirala, S.C., 2024. Influence of Reservoir Salinity, Mineralogy, Temperature, and pressure on Geochemical Hydrogen loss in Depleted Carbonates. SPE J. 29 (10), 5690–5701. https://doi.org/10.2118/223081-PA.
Liu, E., He, S., 2012. Effects of cyclic dynamic loading on the mechanical properties of intact rock samples under confining pressure conditions. Eng. Geol. 125, 81–91. https://doi.org/10.1016/j.enggeo.2011.11.007.
Liu, J., Xie, H., Hou, Z., Yang, C., Chen, L., 2014. Damage evolution of rock salt under cyclic loading in unixial tests. Acta Geotech. 9 (1), 153–160. https://doi.org/10.1007/s11440-013-0236-5.
Liu, Y., Dai, F., Fan, P., Xu, N., Dong, L., 2017. Experimental Investigation of the Influence of Joint Geometric Configurations on the Mechanical Properties of Intermittent Jointed Rock Models under Cyclic Uniaxial Compression. Rock Mech. Rock. Eng. 50 (6), 1453–1471. https://doi.org/10.1007/s00603-017-1190-6.
Liu, Z.-H., Yu, J., Ren, C.-H., Zhu, D.-F., Chen, X.-Q., 2023. Mesomechanical characteristics of rock failure under variable amplitude cyclic loading by DEM. Bull. Eng. Geol. Environ. 82 (8), 311. https://doi.org/10.1007/s10064-023-03335-9.
Liu, J., Xu, X., Zhang, Y., Wang, Z., Arif, M., Wang, Q., 2024a. Understanding the Irreversible Evolution of Coal Permeability under Cyclic Axial Deviatoric stress. Nat. Resour. Res. 33 (2), 887–905. https://doi.org/10.1007/s11053-024-10318-4.
Liu, W., Dong, Y., Jiang, L., Wei, Y., Wan, J., 2024b. Studying injection-extraction induced thermal stress on hydrogen storage cavern in bedded salt rocks. Int. J. Hydrog. Energy 94, 626–638. https://doi.org/10.1016/j.ijhydene.2024.11.071.
Liu, X., Geng, S., Sun, J., Li, Y., Guo, Q., Zhan, Q., 2024c. Novel coupled hydromechanical model considering multiple flow mechanisms for simulating underground hydrogen storage in depleted low-permeability gas reservoir. Int. J. Hydrog. Energy 85, 526–538. https://doi.org/10.1016/j.ijhydene.2024.08.366.
Lord, A.S., 2009. Overview of Geologic Storage of Natural Gas with an Emphasis on Assessing the Feasibility of Storing Hydrogen, Sandia National Laboratories (SNL), Albuquerque, NM, and Livermore, CA.
Lorenz, J.C., 1999. Stress-Sensitive Reservoirs. J. Pet. Technol. 51 (01), 61–63. https://doi.org/10.2118/50977-JPT.
Luboń, K., Tarkowski, R., 2020. Numerical simulation of hydrogen injection and withdrawal to and from a deep aquifer in NW Poland. Int. J. Hydrog. Energy 45 (3), 2068–2083. https://doi.org/10.1016/j.ijhydene.2019.11.055.
Luboń, K., Tarkowski, R., 2021. Influence of capillary threshold pressure and injection well location on the dynamic CO2 and H2 storage capacity for the deep geological structure. Int. J. Hydrog. Energy 46 (58), 30048–30060. https://doi.org/10.1016/j.ijhydene.2021.06.119.
Luboń, K., Tarkowski, R., 2023. The influence of the first filling period length and reservoir level depth on the operation of underground hydrogen storage in a deep aquifer. Int. J. Hydrog. Energy 48 (3), 1024–1042. https://doi.org/10.1016/j.ijhydene.2022.09.284.
Luo, X., Stordal, A.S., Lorentzen, R.J., Nævdal, G., 2015. Iterative Ensemble Smoother as an Approximate solution to a Regularized Minimum-Average-cost Problem: Theory and applications. SPE J. 20 (05), 962–982. https://doi.org/10.2118/176023-PA.
Luo, P., Zhong, N., Khan, I., Wang, X., Wang, H., Luo, Q., Guo, Z., 2019. Effects of pore structure and wettability on methane adsorption capacity of mud rock: Insights from mixture of organic matter and clay minerals. Fuel 251, 551–561. https://doi.org/10.1016/j.fuel.2019.04.072.
Luo, X., Tveit, S., Gholami, R., Andersen, P.Ø., 2024. Underground hydrogen storage (UHS) in natural storage sites: A perspective of subsurface characterization and monitoring. Fuel 364, 131038. https://doi.org/10.1016/j.fuel.2024.131038.
Lysyy, M., Fernø, M., Ersland, G., 2021. Seasonal hydrogen storage in a depleted oil and gas field. Int. J. Hydrog. Energy 46 (49), 25160–25174. https://doi.org/10.1016/j.ijhydene.2021.05.030.
Ma, L.-J., Liu, X.-Y., Wang, M.-Y., Xu, H.-F., Hua, R.-P., Fan, P.-X., Jiang, S.-R., Wang, G.-A., Yi, Q.-K., 2013. Experimental investigation of the mechanical properties of rock salt under triaxial cyclic loading. Int. J. Rock Mech. Min. Sci. 62, 34–41. https://doi.org/10.1016/j.ijrmms.2013.04.003.
Machado, J.R.S., Streett, W.B., Dieters, U., 1988. PVT measurements of hydrogen/methane mixtures at high pressures. J. Chem. Eng. Data 33 (2), 148–152. https://doi.org/10.1021/je00052a027.
Mahdi, D.S., Al-Khdheeawi, E.A., Yuan, Y., Zhang, Y., Iglauer, S., 2021. Hydrogen underground storage efficiency in a heterogeneous sandstone reservoir. Adv. Geo-Energy Res. 5 (4), 437–443. https://doi.org/10.46690/ager.2021.04.08.
Malki, M.L., Chellal, H., Mao, S., Rasouli, V., Mehana, M., 2024. A critical review of underground hydrogen storage: from fundamentals to applications, unveiling future frontiers in energy storage. Int. J. Hydrog. Energy 79, 1365–1394. https://doi.org/10.1016/j.ijhydene.2024.07.076.
Malki, M.L., Chellal, H., Bijay, K.C., Indro, A., Rasouli, V., Mehana, M., 2025. Risk assessment of wellbore leakage during underground hydrogen storage. Gas Sci. Eng. 140, 205661. https://doi.org/10.1016/j.jgsce.2025.205661.
Mao, S., Chen, B., Malki, M., Chen, F., Morales, M., Ma, Z., Mehana, M., 2024. Efficient prediction of hydrogen storage performance in depleted gas reservoirs using machine learning. Appl. Energy 361, 122914. https://doi.org/10.1016/j.apenergy.2024.122914.
Masaya, S., 2024. Numerical experiments on hydrogen storage characterization in porous media using elastic full-waveform inversion. Lead. Edge 43 (12), 852–859. https://doi.org/10.1190/tle43120852.1.
Meng, Q., Zhang, M., Han, L., Pu, H., Chen, Y., 2018. Acoustic Emission Characteristics of Red Sandstone Specimens under Uniaxial Cyclic Loading and unloading Compression. Rock Mech. Rock. Eng. 51 (4), 969–988. https://doi.org/10.1007/s00603-017-1389-6.
Minougou, W., 2022. Numerical Study of Geological Hydrogen Conversion. Montanuniversitaet Leoben, Technical University of Leoben.
Minougou, J.D., Gholami, R., Andersen, P., 2023. Underground hydrogen storage in caverns: challenges of impure salt structures. Earth Sci. Rev. 247, 104599. https://doi.org/10.1016/j.earscirev.2023.104599.
Miocic, J.M., Alcalde, J., Heinemann, N., Marzan, I., Hangx, S., 2022. Toward Energy-Independence and Net-Zero: the Inevitability of Subsurface Storage in Europe. ACS Energy Lett. 7 (8), 2486–2489. https://doi.org/10.1021/acsenergylett.2c01303.
Mirchi, V., Dejam, M., Alvarado, V., Akbarabadi, M., 2023. Effect of Cushion Gas on Hydrogen/Brine Flow Behavior in Oil-Wet Rocks with Application to Hydrogen Storage in Depleted Oil and Gas Reservoirs. Energy Fuel 37 (19), 15231–15243. https://doi.org/10.1021/acs.energyfuels.3c02884.
Mollon, G., Aubry, J., Schubnel, A., 2024. Laboratory Earthquakes Simulations—Emergence, Structure, and Evolution of Fault Heterogeneity. J. Geophys. Res. Solid Earth 129 (6), e2023JB028626. https://doi.org/10.1029/2023JB028626.
Morad, S., 1986. Pyrite-chlorite and pyrite-biotite relations in sandstones. Sediment. Geol. 49 (3), 177–192. https://doi.org/10.1016/0037-0738(86)90037-0.
Mu, Y., Zou, C., Hu, Z., Pan, S., Duan, X., Gao, Y., Tang, Y., 2024. Hydrogen-water-rock interaction from the perspective of underground hydrogen storage: Micromechanical properties and mineral content of rock. Int. J. Hydrog. Energy 70, 79–90. https://doi.org/10.1016/j.ijhydene.2024.05.133.
Muktevi, S., Nagpal, Y., Leela, R., Muktevi, J., 2025. Synthetic UHS-MRV Dataset for OFP-OSDU Integration in Underground Hydrogen Storage Reporting (SUHS-MRV). Authorea Preprints. https://doi.org/10.36227/techrxiv.176110411.13527663/v1.
Muloiwa, M., Nyende-Byakika, S., Dinka, M., 2020. Comparison of unstructured kinetic bacterial growth models. South African J. Chem. Eng. 33, 141–150. https://doi.org/10.1016/j.sajce.2020.07.006.

Naderi, H., Hekmatnejad, A., Aftab, A., Sarmadivaleh, M., Pena, A., 2024. Integrating 1D and 3D geomechanical modeling to ensure safe hydrogen storage in bedded salt caverns: A comprehensive case study in canning salt, Western Australia. Int. J. Hydrog. Energy 81, 1073–1090. https://doi.org/10.1016/j.ijhydene.2024.07.341.
Nait Amar, M., Youcefi, M.R., Alqahtani, F.M., Djema, H., Ghasemi, M., 2025. An efficient super learner model for predicting wettability of the hydrogen/mineral/brine system: Implication for hydrogen geo-storage. Int. J. Hydrog. Energy 124, 47–58. https://doi.org/10.1016/j.ijhydene.2025.03.450.
Naseer, M.T., 2023. Appraisal of tectonically-influenced lowstand prograding clinoform sedimentary fairways of Early-cretaceous Sember deltaic sequences, Pakistan using dynamical reservoir simulations: Implications for natural gas exploration. Mar. Pet. Geol. 151, 106166. https://doi.org/10.1016/j.marpetgeo.2023.106166.
Nassabeh, M., You, Z., Keshavarz, A., Iglauer, S., 2025. Data-driven strategy for contact angle prediction in underground hydrogen storage using machine learning. J. Energy Storage 114, 115908. https://doi.org/10.1016/j.est.2025.115908.
Nath, F., Cabezudo, E., Romero, N.G., 2024. Quantitative Laboratory Assessment of Caprock Integrity for Geological Carbon and Hydrogen Storage, SPE Annual Technical Conference and Exhibition pp. D031S045R001.
Navaid, H.B., Emadi, H., Watson, M., 2023. A comprehensive literature review on the challenges associated with underground hydrogen storage. Int. J. Hydrog. Energy 48 (28), 10603–10635. https://doi.org/10.1016/j.ijhydene.2022.11.225.
Nejati, H.R., Ghazvinian, A., 2014. Brittleness effect on Rock Fatigue damage Evolution. Rock Mech. Rock. Eng. 47 (5), 1839–1848. https://doi.org/10.1007/s00603-013-0486-4.
Ng, C.S.W., Djema, H., Nait Amar, M., Jahanbani Ghahfarokhi, A., 2022. Modeling interfacial tension of the hydrogen-brine system using robust machine learning techniques: Implication for underground hydrogen storage. Int. J. Hydrog. Energy 47 (93), 39595–39605. https://doi.org/10.1016/j.ijhydene.2022.09.120.
Nicol, A., Dempsey, D., Yates, E., Higgs, K., Beggs, M., Adam, L., 2022. Underground Hydrogen Storage in the Taranaki Region (New Zealand).
Okere, C.J., Sheng, J.J., Ejike, C., 2024. Evaluating reservoir suitability for large-scale hydrogen storage: A preliminary assessment considering reservoir properties. Energy Geosci. 5 (4), 100318. https://doi.org/10.1016/j.engeos.2024.100318.
Okoroafor, E.R., 2024. Insights from Thermohydromechanical Simulations for Real-Time monitoring of UHS in Saline Aquifers. In: 58th U.S. Rock Mechanics/Geomechanics Symposium pp. D031S033R006.
Pallud, C., Van Cappellen, P., 2006. Kinetics of microbial sulfate reduction in estuarine sediments. Geochim. Cosmochim. Acta 70 (5), 1148–1162. https://doi.org/10.1016/j.gca.2005.11.002.
Pan, Y., Liu, X., Li, M., Gan, Q., Liu, S., Hao, Z., Qian, L., Luo, X., 2023. Non-Fickian solute transport in three-dimensional crossed shear rock fractures at different contact ratios. Comput. Geotech. 164, 105816. https://doi.org/10.1016/j.compgeo.2023.105816.
Panfilov, M., 2016. 4 - Underground and pipeline hydrogen storage. In: Gupta, R.B., Basile, A., Veziroğlu, T.N. (Eds.), Compendium of Hydrogen Energy. Woodhead Publishing, pp. 91–115.
Passaris, E., Yfantis, G., 2019. Geomechanical Analysis of Salt Caverns used for Underground Storage of Hydrogen Utilised in meeting Peak Energy Demands. In: Ferrari, A., Laloui, L. (Eds.), Energy Geotechnics. Springer International Publishing, Cham, pp. 179–184.
Peleg, M., 2022. A New look at Models of the combined effect of Temperature, pH, Water activity, or Other Factors on Microbial Growth Rate. Food Eng. Rev. 14 (1), 31–44. https://doi.org/10.1007/s12393-021-09292-x.
Penggao, Z., 2019. Query on the viewpoint "strong stress sensitivity exists in low permeability reservoir". Special Oil & Gas Reserv. 26 (1), 163–168.
Perera, M.S.A., 2023. A review of underground hydrogen storage in depleted gas reservoirs: Insights into various rock-fluid interaction mechanisms and their impact on the process integrity. Fuel 334, 126677. https://doi.org/10.1016/j.fuel.2022.126677.
Persova, M.G., Soloveichik, Y.G., Vagin, D.V., Grif, A.M., Kiselev, D.S., Patrushev, I.I., Nasybullin, A.V., Ganiev, B.G., 2021. The design of high-viscosity oil reservoir model based on the inverse problem solution. J. Pet. Sci. Eng. 199, 108245. https://doi.org/10.1016/j.petrol.2020.108245.
Pfeiffer, W.T., Bauer, S., 2015. Subsurface Porous Media Hydrogen Storage – Scenario Development and simulation. Energy Procedia 76, 565–572. https://doi.org/10.1016/j.egypro.2015.07.872.
Pfeiffer, W.T., al Hagrey, S.A., Köhn, D., Rabbel, W., Bauer, S., 2016a. Porous media hydrogen storage at a synthetic, heterogeneous field site: numerical simulation of storage operation and geophysical monitoring. Environ. Earth Sci. 75 (16), 1177. https://doi.org/10.1007/s12665-016-5958-x.
Pfeiffer, W.T., Graupner, B., Bauer, S., 2016b. The coupled non-isothermal, multiphase-multicomponent flow and reactive transport simulator OpenGeoSys–ECLIPSE for porous media gas storage. Environ. Earth Sci. 75 (20), 1347. https://doi.org/10.1007/s12665-016-6168-2.
Pfeiffer, W.T., Beyer, C., Bauer, S., 2017. Hydrogen storage in a heterogeneous sandstone formation: dimensioning and induced hydraulic effects. Pet. Geosci. 23 (3), 315–326. https://doi.org/10.1144/petgeo2016-050.
Pirrone, M., Machicote, S., De Lisio, S., 2024. Pulsed Neutron Logging for Underground Hydrogen Storage monitoring in Depleted Reservoirs. In: SPE Europe Energy Conference and Exhibition, pp. D031S020R002.
Preisig, M., Prévost, J.H., 2011. Coupled multi-phase thermo-poromechanical effects. Case study: CO2 injection at in Salah, Algeria. Int. J. Greenh. Gas Con. 5 (4), 1055–1064. https://doi.org/10.1016/j.ijggc.2010.12.006.
Rahimi, M., Abbaspour-Fard, M.H., Rohani, A., 2021. Machine learning approaches to rediscovery and optimization of hydrogen storage on porous bio-derived carbon. J. Clean. Prod. 329, 129714. https://doi.org/10.1016/j.jclepro.2021.129714.
Rahimzadeh Kivi, I., Ameri, M., Molladavoodi, H., 2018. Shale brittleness evaluation based on energy balance analysis of stress-strain curves. J. Pet. Sci. Eng. 167, 1–19. https://doi.org/10.1016/j.petrol.2018.03.061.
Rajabi, M.M., Ataie-Ashtiani, B., Simmons, C.T., 2018. Model-data interaction in groundwater studies: Review of methods, applications and future directions. J. Hydrol. 567, 457–477. https://doi.org/10.1016/j.jhydrol.2018.09.053.
Ramesh Kumar, K., Makhmutov, A., Spiers, C.J., Hajibeygi, H., 2021. Geomechanical simulation of energy storage in salt formations. Sci. Rep. 11 (1), 19640. https://doi.org/10.1038/s41598-021-99161-8.
Ramesh Kumar, K., Honorio, H., Chandra, D., Lesueur, M., Hajibeygi, H., 2023. Comprehensive review of geomechanics of underground hydrogen storage in depleted reservoirs and salt caverns. J. Energy Storage 73, 108912. https://doi.org/10.1016/j.est.2023.108912.
Raza, A., Mahmoud, M., Alafnan, S., Arif, M., Glatz, G., 2022. H2, CO2, and CH4 Adsorption Potential of Kerogen as a Function of Pressure. Temperature, and Maturity. Int. J. Mol. Sci. 23 (21), 12767. https://doi.org/10.3390/ijms232112767.
Ren, F., Zhu, C., Yuan, Z., Karakus, M., Tang, S., He, M., 2023. Recognition of shear and tension signals based on acoustic emission parameters and waveform using machine learning methods. Int. J. Rock Mech. Min. Sci. 171, 105578. https://doi.org/10.1016/j.ijrmms.2023.105578.
Rivolta, G., Maniglio, M., Elgendy, A., Panfili, P., Cominelli, A., 2024. Evaluating the Impact of Biochemical Reactions on H2 Storage in Depleted Gas Fields. SPE J. 29 (08), 4494–4509. https://doi.org/10.2118/215142-PA.
Roa Pinto, J.S., Bachaud, P., Fargetton, T., Ferrando, N., Jeannin, L., Louvet, F., 2021. Modeling phase equilibrium of hydrogen and natural gas in brines: Application to storage in salt caverns. Int. J. Hydrog. Energy 46 (5), 4229–4240. https://doi.org/10.1016/j.ijhydene.2020.10.242.
Rosman, A., Hamdi, Z., Ali, M., Bataee, M., 2023. Mitigating Global Warming with Underground Hydrogen Storage: Impacts of H2S Generation, SPE Offshore Europe Conference & Exhibition, pp. D031S013R005.
Ruiz Maraggi, L.M., Moscardelli, L.G., 2023. Modeling hydrogen storage capacities, injection and withdrawal cycles in salt caverns: introducing the GeoH2 salt storage and cycling app. Int. J. Hydrog. Energy 48 (69), 26921–26936. https://doi.org/10.1016/j.ijhydene.2023.03.293.
Saeed, M., Jadhawar, P., 2023. Evaluating the Performance of Various Cushion Gas Types for Underground Hydrogen Storage in an Aquifer, 1st International Conference on Green Hydrogen for Global Decarbonisation: ICGHGD-2023.
Saeed, M., Jadhawar, P., 2024a. Modelling underground hydrogen storage: A state-of-the-art review of fundamental approaches and findings. Gas Sci. Eng. 121, 205196. https://doi.org/10.1016/j.jgsce.2023.205196.
Saeed, M., Jadhawar, P., 2024b. Optimizing underground hydrogen storage in aquifers: the impact of cushion gas type. Int. J. Hydrog. Energy 52, 1537–1549. https://doi.org/10.1016/j.ijhydene.2023.08.352.
Saeed, M., Jadhawar, P., Bagala, S., 2023. Geochemical Effects on Storage gases and Reservoir Rock during Underground Hydrogen Storage: A Depleted North Sea Oil Reservoir Case Study. Hydrogen 323–337.
Saeibehrouzi, A., Holtzman, R., Denissenko, P., Abolfathi, S., 2024. Solute transport in unsaturated porous media with spatially correlated disorder. Adv. Water Resour. 191, 104773. https://doi.org/10.1016/j.advwatres.2024.104773.
Safari, A., Zeng, L., Nguele, R., Sugai, Y., Sarmadivaleh, M., 2023. Review on using the depleted gas reservoirs for the underground H2 storage: A case study in Niigata prefecture, Japan. Int. J. Hydrog. Energy 48 (28), 10579–10602. https://doi.org/10.1016/j.ijhydene.2022.12.108.
Sainz-Garcia, A., Abarca, E., Rubi, V., Grandia, F., 2017. Assessment of feasible strategies for seasonal underground hydrogen storage in a saline aquifer. Int. J. Hydrog. Energy 42 (26), 16657–16666. https://doi.org/10.1016/j.ijhydene.2017.05.076.
Scafidi, J., Wilkinson, M., Gilfillan, S.M.V., Heinemann, N., Haszeldine, R.S., 2021. A quantitative assessment of the hydrogen storage capacity of the UK continental shelf. Int. J. Hydrog. Energy 46 (12), 8629–8639. https://doi.org/10.1016/j.ijhydene.2020.12.106.
Scheibe, T.D., Murphy, E.M., Chen, X., Rice, A.K., Carroll, K.C., Palmer, B.J., Tartakovsky, A.M., Battiato, I., Wood, B.D., 2015. An Analysis Platform for Multiscale Hydrogeologic Modeling with Emphasis on Hybrid Multiscale Methods. Groundwater 53 (1), 38–56. https://doi.org/10.1111/gwat.12179.
Schöpping, P., Rossen, B., 2019. Feasibility of Seasonal Storage of Green Gas in Dutch Geological Formations.
Sekar, L.K., Okoroafor, E.R., 2025. A novel data-driven machine learning model to predict maximum hydrogen column height for saline aquifers. Int. J. Hydrog. Energy 142, 98–108. https://doi.org/10.1016/j.ijhydene.2025.05.342.
Seyed Alizadeh, S.M., Parhizi, Z., Alibak, A.H., Vaferi, B., Hosseini, S., 2022. Predicting the hydrogen uptake ability of a wide range of zeolites utilizing supervised machine learning methods. Int. J. Hydrog. Energy 47 (51), 21782–21793. https://doi.org/10.1016/j.ijhydene.2022.05.038.
Sharafisafa, M., Shen, L., Xu, Q., 2018. Characterisation of mechanical behaviour of 3D printed rock-like material with digital image correlation. Int. J. Rock Mech. Min. Sci. 112, 122–138. https://doi.org/10.1016/j.ijrmms.2018.10.012.
Shi, H., Zhu, Q., Chen, Z., Li, J., Feng, D., Zhang, S., Ye, J., Wu, K., 2023. Pore-scale modeling of water–gas flow in heterogeneous porous media. Phys. Fluids 35 (7), 072114. https://doi.org/10.1063/5.0157655.
Shojaee, A., Ghanbari, S., Wang, G., Mackay, E., 2024. Interplay between microbial activity and geochemical reactions during underground hydrogen storage in a seawater-rich formation. Int. J. Hydrog. Energy 50, 1529–1541. https://doi.org/10.1016/j.ijhydene.2023.10.061.
Sibson, R.H., 1990. Rupture nucleation on unfavorably oriented faults. Bull. Seismol. Soc. Am. 80 (6A), 1580–1604. https://doi.org/10.1785/BSSA08006A1580.

Sidorenko, M., Orlov, D., Ebadi, M., Koroteev, D., 2021. Deep learning in denoising of micro-computed tomography images of rock samples. Comput. Geosci. 151, 104716. https://doi.org/10.1016/j.cageo.2021.104716.
Silverii, F., Maccaferri, F., Richter, G., Gonzalez Cansado, B., Wang, R., Hainzl, S., Dahm, T., 2021. Poroelastic model in a vertically sealed gas storage: a case study from cyclic injection/production in a carbonate aquifer. Geophys. J. Int. 227 (2), 1322–1338. https://doi.org/10.1093/gji/ggab268.
Singh, S.K., 1989. Fatigue and strain hardening behaviour of graywacke from the flagstaff formation, New South Wales. Eng. Geol. 26 (2), 171–179. https://doi.org/10.1016/0013-7952(89)90005-7.
Singh, R., Altaee, A., Gautam, S., 2020. Nanomaterials in the advancement of hydrogen energy storage. Heliyon 6 (7). https://doi.org/10.1016/j.heliyon.2020.e04487.
Song, R., Song, Y., Liu, J., Yang, C., 2024. Multiscale experimental and numerical study on hydrogen diffusivity in salt rocks and interlayers of salt cavern hydrogen storage. Int. J. Hydrog. Energy 79, 319–334. https://doi.org/10.1016/j.ijhydene.2024.06.418.
Song, X., Wu, W., Zhang, H., He, L., Fu, X., Wang, G., Cui, J., 2026. A differential-ratio neutron logging method for high-precision monitoring of hydrogen storage in depleted gas reservoirs. Int. J. Hydrog. Energy 197, 152697. https://doi.org/10.1016/j.ijhydene.2025.152697.
Standardization, I.O.f, 2017. Carbon dioxide capture, transportation and geological storage — geological storage, ISO/TC 265, 27914. ISO, p. 2017.
Sun, Q., Tang, H., Ruan, H., Tang, X., Zhang, M., 2023. The use of a gravity-assisted-storage-extraction protocol for hydrogen storage in saline aquifers. J. Clean. Prod. 413, 137408. https://doi.org/10.1016/j.jclepro.2023.137408.
Sun, K., Liu, H., Leung, J.Y., Wang, J., Feng, Y., Liu, R., Kang, Z., Zhang, Y., 2024a. Impact of effective stress on permeability for carbonate fractured-vuggy rocks. J. Rock Mech. Geotech. Eng. 16 (3), 942–960. https://doi.org/10.1016/j.jrmge.2023.04.007.
Sun, Q., Zhang, M., Ertekin, T., 2024b. The Design of Hydrogen Saline Aquifer Storage Processes Using a Machine-Learning Assisted Multiobjective Optimization Protocol. SPE J. 29 (04), 2086–2105. https://doi.org/10.2118/218405-PA.
Sun, B., Zhang, M., Sun, Q., Zhong, J., Shao, G., 2025. Review on natural hydrogen wells safety. Nat. Commun. 16 (1), 369. https://doi.org/10.1038/s41467-024-55773-y.
Suresh, S., 1998. Fatigue of Materials. Cambridge University Press.
Tabiai, I., 2018. 3D Full Field Displacement and Strain Measurements at the Microscale in Fiber Reinforced Composites under Transverse Load Using Digital Image Correlation. Ecole Polytechnique, Montreal (Canada).
Tackie-Otoo, B.N., Haq, M.B., 2024. A comprehensive review on geo-storage of H2 in salt caverns: Prospect and research advances. Fuel 356, 129609. https://doi.org/10.1016/j.fuel.2023.129609.
Tang, H.-D., 2020. Multi-scale crack propagation and damage acceleration during uniaxial compression of marble. Int. J. Rock Mech. Min. Sci. 131, 104330. https://doi.org/10.1016/j.ijrmms.2020.104330.
Tarkowski, R., 2019. Underground hydrogen storage: Characteristics and prospects. Renew. Sust. Energ. Rev. 105, 86–94. https://doi.org/10.1016/j.rser.2019.01.051.
Tenthorey, E., Hsiao, W.M., Puspitasari, R., Giddins, M.A., Pallikathekathil, Z.J., Dandekar, R., Suriyanto, O., Feitz, A.J., 2024. Geomechanics of hydrogen storage in a depleted gas field. Int. J. Hydrog. Energy 60, 636–649. https://doi.org/10.1016/j.ijhydene.2024.02.189.
Terzaghi, K., 1943. Theoretical Soil Mechanics.
Thaysen, E.M., McMahon, S., Strobel, G.J., Butler, I.B., Ngwenya, B.T., Heinemann, N., Wilkinson, M., Hassanpouryouzband, A., McDermott, C.I., Edlmann, K., 2021. Estimating microbial growth and hydrogen consumption in hydrogen storage in porous media. Renew. Sust. Energ. Rev. 151, 111481. https://doi.org/10.1016/j.rser.2021.111481.
Tian, D., Song, Z., Khaledi, K., Yang, Z., Amann, F., 2024. Experimental and numerical analyses of creep-fatigue behavior in sandstone for energy storage applications. J. Energy Storage 101, 113879. https://doi.org/10.1016/j.est.2024.113879.
Tietze, V., Stolten, D., 2015. Comparison of hydrogen and methane storage by means of a thermodynamic analysis. Int. J. Hydrog. Energy 40 (35), 11530–11537. https://doi.org/10.1016/j.ijhydene.2015.04.154.
Tremosa, J., Jakobsen, R., Le Gallo, Y., 2023. Assessing and modeling hydrogen reactivity in underground hydrogen storage: A review and models simulating the Lobodice town gas storage. Front. Energy Res. 11, 1145978. https://doi.org/10.3389/fenrg.2023.1145978.
Truche, L., Berger, G., Destrigneville, C., Guillaume, D., Giffaut, E., 2010. Kinetics of pyrite to pyrrhotite reduction by hydrogen in calcite buffered solutions between 90 and 180°C: Implications for nuclear waste disposal. Geochim. Cosmochim. Acta 74 (10), 2894–2914. https://doi.org/10.1016/j.gca.2010.02.027.
Verdon, J.P., Kendall, J.M., Stork, A.L., Chadwick, R.A., White, D.J., Bissell, R.C., 2013. Comparison of geomechanical deformation induced by megatonne-scale CO2 storage at Sleipner, Weyburn, and in Salah. Proc. Natl. Acad. Sci. 110 (30), E2762–E2771. https://doi.org/10.1073/pnas.1302156110.
Viswanathan, H.S., Ajo-Franklin, J., Birkholzer, J.T., Carey, J.W., Guglielmi, Y., Hyman, J.D., Karra, S., Pyrak-Nolte, L.J., Rajaram, H., Srinivasan, G., Tartakovsky, D.M., 2022. From Fluid Flow to coupled Processes in Fractured Rock: recent advances and New Frontiers. Rev. Geophys. 60 (1), e2021RG000744. https://doi.org/10.1029/2021RG000744.
Vo Thanh, H., 2025. Interpretable knowledge-guided machine learning for prediction wettability hydrogen-rocks/minerals-brine system in underground hydrogen storage project. Int. J. Hydrog. Energy 177, 151462. https://doi.org/10.1016/j.ijhydene.2025.151462.
Vo Thanh, H., 2026. Physics informed machine learning for prediction hydrogen solubility in aqueous solution to implication for underground hydrogen storage formations. Renew. Energy 256, 124460. https://doi.org/10.1016/j.renene.2025.124460.
Vo Thanh, H., Rahimi, M., Dai, Z., Zhang, H., Zhang, T., 2023. Predicting the wettability rocks/minerals-brine-hydrogen system for hydrogen storage: Re-evaluation approach by multi-machine learning scheme. Fuel 345, 128183. https://doi.org/10.1016/j.fuel.2023.128183.
Vo Thanh, H., Dai, Z., Du, Z., Yin, H., Yan, B., Soltanian, M.R., Xiao, T., McPherson, B., Abualigah, L., 2024a. Artificial intelligence-based prediction of hydrogen adsorption in various kerogen types: Implications for underground hydrogen storage and cleaner production. Int. J. Hydrog. Energy 57, 1000–1009. https://doi.org/10.1016/j.ijhydene.2024.01.115.
Vo Thanh, H., Zhang, H., Dai, Z., Zhang, T., Tangparitkul, S., Min, B., 2024b. Data-driven machine learning models for the prediction of hydrogen solubility in aqueous systems of varying salinity: Implications for underground hydrogen storage. Int. J. Hydrog. Energy 55, 1422–1433. https://doi.org/10.1016/j.ijhydene.2023.12.131.
W. G. P, K. and P.G, R, 2023. An overview of underground hydrogen storage with prospects and challenges for the Australian context. Geoenerg. Sci. Eng. 231, 212354. https://doi.org/10.1016/j.geoen.2023.212354.
Wang, B., Zhou, Y.-S., 2017. Review:fault Hydrogen mechanism and its interrelation with seismic activity. Prog. Geophys. 32 (5), 1921–1929. https://doi.org/10.6038/pg20170508.
Wang, G., Pickup, G., Sorbie, K., Mackay, E., 2022a. Numerical modelling of H2 storage with cushion gas of CO2 in subsurface porous media: Filter effects of CO2 solubility. Int. J. Hydrog. Energy 47 (67), 28956–28968. https://doi.org/10.1016/j.ijhydene.2022.06.201.
Wang, G., Pickup, G., Sorbie, K., Mackay, E., 2022b. Scaling analysis of hydrogen flow with carbon dioxide cushion gas in subsurface heterogeneous porous media. Int. J. Hydrog. Energy 47 (3), 1752–1764. https://doi.org/10.1016/j.ijhydene.2021.10.224.
Wang, Q., Xu, S., He, M., Jiang, B., Wei, H., Wang, Y., 2022c. Dynamic mechanical characteristics and application of constant resistance energy-absorbing supporting material. Int. J. Min. Sci. Technol. 32 (3), 447–458. https://doi.org/10.1016/j.ijmst.2022.03.005.
Wang, J., Wu, R., Wei, M., Bai, B., Xie, J., Li, Y., 2023a. A comprehensive review of site selection, experiment and numerical simulation for underground hydrogen storage. Gas Sci. Eng. 118, 205105. https://doi.org/10.1016/j.jgsce.2023.205105.
Wang, J., Yang, Y., Cai, S., Yao, J., Xie, Q., 2023b. Pore-scale modelling on hydrogen transport in porous media: Implications for hydrogen storage in saline aquifers. Int. J. Hydrog. Energy 48 (37), 13922–13933. https://doi.org/10.1016/j.ijhydene.2022.11.299.
Wang, Y., Yan, M., Song, W., 2023c. The effect of cyclic stress amplitude on macro-meso failure of rock under triaxial confining pressure unloading. Fatigue Fract. Eng. Mater. Struct. 46 (6), 2212–2228. https://doi.org/10.1111/ffe.13993.
Wang, G., Pickup, G., Sorbie, K., de Rezende, J.R., Zarei, F., Mackay, E., 2024a. Bioreaction coupled flow simulations: Impacts of methanogenesis on seasonal underground hydrogen storage. Int. J. Hydrog. Energy 55, 921–931. https://doi.org/10.1016/j.ijhydene.2023.11.035.
Wang, H., Chen, S., Deng, P., Wang, M., Xu, Z., 2024b. Pore-Scale Investigation of Caprock Integrity in Underground Hydrogen Storage. In: SPE Canadian Energy Technology Conference and Exhibition, pp. D021S026R005.
Wang, H., Jie, Y., Zhou, D., Ma, X., 2024c. Underground hydrogen storage in depleted gas reservoirs with hydraulic fractures: Numerical modeling and simulation. J. Energy Storage 97, 112777. https://doi.org/10.1016/j.est.2024.112777.
Wang, L., Chen, W., Sui, Q., 2024d. Study of hydro-mechanical behaviours of rough rock fracture with shear dilatancy and asperities using shear-flow model. J. Rock Mech. Geotech. Eng. 16 (10), 4004–4016. https://doi.org/10.1016/j.jrmge.2023.11.020.
Wang, Y., Sun, Q., Chen, F., Wang, M., 2024e. Multiscale Model for Hydrogen Transport and Storage in Shale Reservoirs. SPE J. 29 (06), 3238–3264. https://doi.org/10.2118/219472-PA.
Wang, Z., Hu, M., Steefel, C., 2024f. Pore-Scale Modeling of Reactive Transport with coupled Mineral Dissolution and Precipitation. Water Resour. Res. 60 (6), e2023WR036122. https://doi.org/10.1029/2023WR036122.
Wang, Z., Zhang, Y., Liu, Z., Li, S., Qiu, K., 2024g. Investigation of the effects of hydrogen injection and withdrawal frequency on stability and tightness of the salt cavern based on a novel coupled thermal-hydro-mechanical model. Int. J. Hydrog. Energy 82, 1238–1251. https://doi.org/10.1016/j.ijhydene.2024.08.034.
Wang, J., Hu, Z., Yan, X., Yao, J., Sun, H., Yang, Y., Zhang, L., Zhong, J., 2025a. Gradient-boosted spatiotemporal neural network for simulating underground hydrogen storage in aquifers. J. Comput. Phys. 521, 113557. https://doi.org/10.1016/j.jcp.2024.113557.
Wang, Y., Vo Thanh, H., Zhang, H., Rahimi, M., Dai, Z., Abualigah, L., 2025b. Low-carbon advancement through cleaner production: A machine learning approach for enhanced hydrogen storage predictions in coal seams. Renew. Energy 241, 122342. https://doi.org/10.1016/j.renene.2025.122342.
Wen, C., Jia, S., Fu, X., Wu, G., Wang, B., Sun, J., He, H., Zeng, X., 2024a. Semi-analytical assessment of dynamic sealing capacity of underground gas storage: A case of Songliao Basin, Northeastern China. J. Rock Mech. Geotech. Eng. https://doi.org/10.1016/j.jrmge.2024.06.007.
Wen, M., Wang, Q., Busch, A., 2024b. Evolution of poro-mechanical and transport properties of sandstones under different cyclic stress paths: Implications for underground hydrogen storage. In: European Geosciences Union General Assembly 2024 (EGU24): 19226.
WMO, 2024. WMO Greenhouse Gas Bulletin No. 20–28 October 2024: The State of Greenhouse Gases in the Atmosphere Based on Global Observations through 2023, Geneva.

Wu, L., Hou, Z., Luo, Z., Huang, L., Xiong, Y., Mehmood, F., Liu, J., Sun, W., Xie, Y., 2023. Efficiency assessment of underground biomethanation with hydrogen and carbon dioxide in depleted gas reservoirs: A biogeochemical simulation. Energy 283, 128539. https://doi.org/10.1016/j.energy.2023.128539.

Wu, L., Hou, Z.-M., Luo, Z.-F., Fang, Y.-L., Huang, L.-C., Wu, X.-N., Chen, Q.-J., Wang, Q.-C., 2024. Impacts of microbial interactions on underground hydrogen storage in porous media: A comprehensive review of experimental, numerical, and field studies. Pet. Sci. 21 (6), 4067–4099. https://doi.org/10.1016/j.petsci.2024.08.015.

Xu, M., Qi, X., Geng, D., 2024. Application of improved and efficient image repair algorithm in rock damage experimental research. Sci. Rep. 14 (1), 14849. https://doi.org/10.1038/s41598-024-65790-y.

Xue, F., Lin, Z., Wang, T., 2024. Experimental study on effects of cyclic loading paths on cracking behavior and fracture characteristics of granite. Eng. Fract. Mech. 295, 109761. https://doi.org/10.1016/j.engfracmech.2023.109761.

Yang, G., Shen, Y., Jia, H., Wei, Y., Zhang, H., Liu, H., 2018. Research progress and tendency in characteristics of multi-scale damage mechanics of rock under freezing-thawing. Chin. J. Rock Mech. Eng. 37 (3), 545–563.

Yang, Y., Wu, Y., Lu, Y., Shi, M., Chen, W., 2021. Microorganisms and their metabolic activities affect seepage through porous media in groundwater artificial recharge systems: A review. J. Hydrol. 598, 126256. https://doi.org/10.1016/j.jhydrol.2021.126256.

Yang, J., He, X., Wang, S., Chen, H., 2024a. Monitoring underground hydrogen storage migration and distribution using time-lapse acoustic waveform inversion. Int. J. Hydrog. Energy 69, 272–281. https://doi.org/10.1016/j.ijhydene.2024.05.002.

Yang, S., Hu, S., Qi, Z., Li, J., Yan, W., Huang, X., Ao, X., Yuan, Y., 2024b. Stability evaluation of fault in hydrocarbon reservoir-based underground gas storage: A case study of W gas storage. Fuel 357, 129657. https://doi.org/10.1016/j.fuel.2023.129657.

Yang, Z., Fan, J., Chen, J., Jiang, D., Suo, J., Li, Z., 2024c. Dilatancy and Acoustic Emission Characteristics of Rock Salt in Variable-Frequency Fatigue Tests. Rock Mech. Rock. Eng. 57 (12), 10877–10894. https://doi.org/10.1007/s00603-024-04119-7.

Yekta, A.E., Pichavant, M., Audigane, P., 2018. Evaluation of geochemical reactivity of hydrogen in sandstone: Application to geological storage. Appl. Geochem. 95, 182–194. https://doi.org/10.1016/j.apgeochem.2018.05.021.

Yin, Y., Ren, Q., Lei, S., Zhou, J., Xu, L., Wang, T., 2024. Mesoscopic crack pattern fractal dimension-based concrete damage identification. Eng. Fract. Mech. 296, 109829. https://doi.org/10.1016/j.engfracmech.2023.109829.

Young, W.C., Budynas, R.G., Sadegh, A.M., 2002. Roark's Formulas for Stress and Strain, 7. McGraw-Hill New York.

Zaid, J., Hannah, M., Andreas, B., Sebastian, G., Tom, B., Helen, L., Kamaljit, S., 2023. Pore-scale visualization of hydrogen storage in a sandstone at subsurface pressure and temperature conditions: Trapping, dissolution and wettability. J. Colloid Interface Sci. 629, 316–325. https://doi.org/10.1016/j.jcis.2022.09.082.

Zamehrian, M., Sedaee, B., 2022. Underground hydrogen storage in a naturally fractured gas reservoir: the role of fracture. Int. J. Hydrog. Energy 47 (93), 39606–39618. https://doi.org/10.1016/j.ijhydene.2022.09.116.

Zeng, L., Hosseini, M., Keshavarz, A., Iglauer, S., Lu, Y., Xie, Q., 2022a. Hydrogen wettability in carbonate reservoirs: Implication for underground hydrogen storage from geochemical perspective. Int. J. Hydrog. Energy 47 (60), 25357–25366. https://doi.org/10.1016/j.ijhydene.2022.05.289.

Zeng, L., Keshavarz, A., Xie, Q., Iglauer, S., 2022b. Hydrogen storage in Majiagou carbonate reservoir in China: Geochemical modelling on carbonate dissolution and hydrogen loss. Int. J. Hydrog. Energy 47 (59), 24861–24870. https://doi.org/10.1016/j.ijhydene.2022.05.247.

Zeng, L., Vialle, S., Ennis-King, J., Esteban, L., Sarmadivaleh, M., Sarout, J., Dautriat, J., Giwelli, A., Xie, Q., 2023. Role of geochemical reactions on caprock integrity during underground hydrogen storage. J. Energy Storage 65, 107414. https://doi.org/10.1016/j.est.2023.107414.

Zhan, C., Dai, Z., Samper, J., Yin, S., Ershadnia, R., Zhang, X., Wang, Y., Yang, Z., Luan, X., Soltanian, M.R., 2022a. An integrated inversion framework for heterogeneous aquifer structure identification with single-sample generative adversarial network. J. Hydrol. 610, 127844. https://doi.org/10.1016/j.jhydrol.2022.127844.

Zhan, C., Dai, Z., Soltanian, M.R., de Barros, F.P., 2022b. Data-worth analysis for heterogeneous subsurface structure identification with a stochastic deep learning framework. Water Resour. Res. 58 (11), e2022WR033241. https://doi.org/10.1029/2022WR033241.

Zhan, S., Zeng, L., Al-Yaseri, A., Sarmadivaleh, M., Xie, Q., 2024. Geochemical modelling on the role of redox reactions during hydrogen underground storage in porous media. Int. J. Hydrog. Energy 50, 19–35. https://doi.org/10.1016/j.ijhydene.2023.06.153.

Zhang, X., Knapp, R.M., McLnerney, M.J., 1992. A Mathematical Model for Microbially Enhanced Oil Recovery Process, SPE/DOE Enhanced Oil Recovery Symposium, pp. SPE-24202-MS.

Zhang, J., Li, Y., Huang, G., Chen, X., Bao, A., 2016. Assessment of parameter uncertainty in hydrological model using a Markov-Chain-Monte-Carlo-based multilevel-factorial-analysis method. J. Hydrol. 538, 471–486. https://doi.org/10.1016/j.jhydrol.2016.04.044.

Zhang, S., Wu, S., Duan, K., 2019. Study on the deformation and strength characteristics of hard rock under true triaxial stress state using bonded-particle model. Comput. Geotech. 112, 1–16. https://doi.org/10.1016/j.compgeo.2019.04.005.

Zhang, Z., Borhani, T.N., Olabi, A.G., 2020. Status and perspective of CO2 absorption process. Energy 205, 118057. https://doi.org/10.1016/j.energy.2020.118057.

Zhang, J., Clennell, M.B., Sagotra, A., Pascual, R., 2023a. Molecular dynamics simulation and machine learning for predicting hydrogen solubility in water: Effects of temperature, pressure, finite system size and choice of molecular force fields. Chem. Phys. 564, 111725. https://doi.org/10.1016/j.chemphys.2022.111725.

Zhang, Y., Yang, L., Huang, W., 2023b. Study on Hydrogen Flow and Heat transfer in Underground Salt Cavern Hydrogen Storage. J. Phys. Conf. Ser. 2599 (1), 012017. https://doi.org/10.1088/1742-6596/2599/1/012017.

Zhang, D., Zhang, L., Wang, Z., Meng, F., Wen, J., Gao, L., 2024a. Multi-level loading of the seepage pressure in filled cracked sandstone: Seepage-creep mechanical characteristics and crack initiation mechanism. Eng. Fract. Mech. 300, 109991. https://doi.org/10.1016/j.engfracmech.2024.109991.

Zhang, M., Yang, Y., Pan, B., Liu, Z., Jin, Z., Iglauer, S., 2024b. Molecular simulation on H2 adsorption in nanopores and effects of cushion gas: Implications for underground hydrogen storage in shale reservoirs. Fuel 361, 130621. https://doi.org/10.1016/j.fuel.2023.130621.

Zhang, X., Guo, P., Gao, X., Zou, C., Wang, K., Hu, J., Sun, Y., Lei, L., 2025. Crack and failure behaviors of sandstone subjected to dynamic loads visualized by micro-computed tomography. J. Rock Mech. Geotech. Eng. 17 (3), 1459–1473. https://doi.org/10.1016/j.jrmge.2024.05.001.

Zhao, Y., Gong, M., Zhou, Y., Dong, X., Shen, J., 2019. Thermodynamics analysis of hydrogen storage based on compressed gaseous hydrogen, liquid hydrogen and cryo-compressed hydrogen. Int. J. Hydrog. Energy 44 (31), 16833–16840. https://doi.org/10.1016/j.ijhydene.2019.04.207.

Zhao, C., Li, M., Wang, X., Liu, B., Pan, X., Fang, H., 2022a. Improving the accuracy of nonpoint-source pollution estimates in inland waters with coupled satellite-UAV data. Water Res. 225, 119208. https://doi.org/10.1016/j.watres.2022.119208.

Zhao, J., Yong, R., Hu, D., She, C., Fu, Y., Wu, J., Jiang, T., Ren, L., Zhou, B., Lin, R., 2024. Deep and ultra-deep shale gas fracturing in China: problems, challenges and directions. Acta Pet. Sin. 45 (1), 295–311. https://doi.org/10.7623/syxb202401017.

Zhao, C., Zhang, Z., Wang, S., Lei, Q., 2022b. Effects of fracture network distribution on excavation-induced coupled responses of pore pressure perturbation and rock mass deformation. Comput. Geotech. 145, 104670. https://doi.org/10.1016/j.compgeo.2022.104670.

Zhao, Q., Wang, H., Chen, C., 2024a. Underground hydrogen storage: A recovery prediction using pore network modeling and machine learning. Fuel 357, 130051. https://doi.org/10.1016/j.fuel.2023.130051.

Zhao, Q., Wang, Y., Chen, C., 2024b. Numerical simulation of the impact of different cushion gases on underground hydrogen storage in aquifers based on an experimentally-benchmarked equation-of-state. Int. J. Hydrog. Energy 50, 495–511. https://doi.org/10.1016/j.ijhydene.2023.07.262.

Zhao, W., Mao, S., Mehana, M., 2025. Techno-economic analysis and site screening for underground hydrogen storage in Intermountain-West region, United States. Int. J. Hydrog. Energy 109, 275–286. https://doi.org/10.1016/j.ijhydene.2025.02.095.

Zhong, Z., Xu, C., Hu, Y., Zhang, F., Wu, F., Li, B., 2024. Frictional strength and sliding behaviors of an analogue rock-fault structure: A laboratory study. Int. J. Rock Mech. Min. Sci. 174, 105665. https://doi.org/10.1016/j.ijrmms.2024.105665.

Zhou, Y., Sheng, Q., Li, N., Fu, X., 2020. Numerical analysis of the mechanical properties of rock materials under tiered and multi-level cyclic load regimes. Soil Dyn. Earthq. Eng. 135, 106186. https://doi.org/10.1016/j.soildyn.2020.106186.

Zhou, J., Deng, G., Tian, S., Xian, X., Yang, K., Zhang, C., Dong, Z., 2023. Experimental study on the permeability variation of sandstone at cyclic stress: Implication for underground gas storage. J. Energy Storage 60, 106677. https://doi.org/10.1016/j.est.2023.106677.

Zhu, Y., Wang, H., Vano, K., 2022. Applying the wavelet neural network to estimate hydrogen dissolution in underground sodium chloride solutions. Int. J. Hydrog. Energy 47 (54), 22720–22730. https://doi.org/10.1016/j.ijhydene.2022.05.130.

Zhuang, X., Wang, W., Su, Y., Yan, B., Li, Y., Li, L., Hao, Y., 2024. Multi-objective optimization of reservoir development strategy with hybrid artificial intelligence method. Expert Syst. Appl. 241, 122707. https://doi.org/10.1016/j.eswa.2023.122707.

Zivar, D., Kumar, S., Foroozesh, J., 2021. Underground hydrogen storage: A comprehensive review. Int. J. Hydrog. Energy 46 (45), 23436–23462. https://doi.org/10.1016/j.ijhydene.2020.08.138.